Human Argonaute proteins:

Analysis of endonucleolytic activity and endogenous phosphorylation sites

DISSERTATION

zur Erlangung des Doktorgrades der Naturwissenschaften (Dr. rer. nat.)

der Fakultät für Biologie und Vorklinische Medizin

der Universität Regensburg

vorgelegt von Judith Hauptmann

aus Plauen

im Jahr 2014

Das Promotionsgesuch wurde eingereicht am:
19.12.2014

Die Arbeit wurde angeleitet von:
Prof. Dr. Gunter Meister

Unterschrift:

Weisheit hört auf, Weisheit zu sein,
wenn sie zu stolz wird um zu weinen,
zu ernst um zu lachen,
und zu sehr von sich eingenommen,
um anderes zu sehen als sich selbst.

Khalil Gibran

Abstract

Argonaute (Ago) proteins interact with small non-coding RNAs, which guide them to complementary target RNAs to mediate gene silencing. The domain organization of Ago proteins clearly reflects their function. The ends of the small RNA are bound by the Mid and PAZ domains and the structure of the PIWI domain closely resembles that of the endonuclease RNase H. Indeed, some Ago proteins can cleave perfectly complementary target RNAs. Here, the endonucleolytically inactive human Ago proteins Ago1, Ago3, and Ago4 were mutated to yield minimally changed, catalytically active proteins. The generation of these mutants revealed several features that are important for Ago cleavage activity, in particular two regions in the N-terminal domain and two structural elements in the catalytic domain. The identification of these structural requirements contributes essentially to our understanding of Ago-mediated silencing activity.

Ago proteins not only cleave their targets. In case of partial complementarity between small RNA and target RNA, they recruit additional factors to mediate gene silencing. Here, predominant mechanisms are translational repression and reduction of target stability. Considering the wide spectrum of gene regulation emanating from Ago proteins, it is important to understand how the proteins are regulated themselves. Here, post-translational modifications, in particular phosphorylations, of Ago proteins were analyzed by mass spectrometry. Multiple endogenous phosphorylation sites of Ago2 and its paralogues were detected. Among them are sites, which are organized in phosphorylation clusters. The data generated in this thesis represents a valuable resource for future analyses of Ago proteins and their modifying enzymes, which will provide insights into the interplay of small RNA-guided gene silencing and signaling pathways.

The phosphorylation sites analyzed here were identified on endogenous Ago proteins. To provide large amounts of endogenous protein, a novel, peptide-based purification strategy was established. Ago Affinity Purification by Peptides (Ago-APP) is based on the interaction of Ago proteins with a conserved binding partner, a member of the GW182 protein family. Therefore, the approach purifies all four human Ago proteins and can even be applied species-independently. Ago-APP represents a powerful tool for the characterization of diverse Ago complexes at the levels of protein, small RNA, and target RNA.

Zusammenfassung

Argonaute-(Ago-)Proteine interagieren mit kleinen, nicht-codierenden RNAs, welche sie zu komplementären Ziel-RNAs leiten, um Genrepression zu vermitteln. Die Domänenorganisation von Ago-Proteinen spiegelt deren Funktion deutlich wider. Die Enden der kleinen RNA werden durch die Mid- und PAZ-Domänen gebunden und die Struktur der PIWI-Domäne ähnelt stark der der Endonuklease RNase H. Tatsächlich können einige Ago-Proteine perfekt komplementäre Ziel-RNAs schneiden. Hier wurden Mutationen in die endonukleolytisch inaktiven humanen Ago-Proteine Ago1, Ago3 und Ago4 eingeführt, um minimal veränderte, katalytisch aktive Proteine zu erhalten. Mit Hilfe dieser Mutanten wurden mehrere strukturelle Merkmale identifiziert, die wichtig für die Spalt-Aktivität der Proteine sind, insbesondere zwei Regionen in der N-terminalen Domäne und zwei strukturelle Elemente in der katalytischen Domäne. Die Identifikation dieser strukturellen Voraussetzungen trägt essentiell zu unserem Verständnis der durch Ago-Proteine vermittelten Genrepressions-Aktivität bei.

Ago-Proteine spalten ihre Ziel-RNAs nicht nur. Im Falle teilweiser Komplementarität zwischen kleiner RNA und Ziel-RNA rekrutieren sie zusätzliche Faktoren, um die Genexpression negativ zu beeinflussen. Vorherrschende Mechanismen sind hierbei translationale Repression und die Verminderung der mRNA-Stabilität. Angesichts des breiten Spektrums Ago-vermittelter Genregulation ist es wichtig zu verstehen, wie diese Proteine selbst reguliert werden. Hier wurden massenspektrometrische Methoden angewendet, um post-translationale Modifikationen, speziell Phosphorylierungen, von Ago-Proteinen zu untersuchen. Zahlreiche endogene Phosphorylierungsstellen von Ago2 und seinen Paralogen wurden detektiert. Darunter befinden sich Modifikationsstellen, welche in Phosphorylierungs-Clustern organisiert sind. Die im Rahmen dieser Arbeit gewonnenen Daten sind eine wertvolle Informationsquelle für zukünftige Analysen von Ago-Proteinen und deren modifizierenden Enzymen, welche Einblicke in das Zusammenspiel der durch kleine RNAs vermittelten Genrepression mit Signalwegen geben werden.

Die hier analysierten Phosphorylierungsstellen wurden in endogenen Ago-Proteinen identifiziert. Um große Mengen endogener Proteine bereitzustellen, wurde eine neuartige, Peptid-basierte Aufreinigungsstrategie etabliert. *Ago Affinity Purification by Peptides* (Ago-APP, 'Ago-Affinitätsreinigung durch Peptide') basiert auf der Interaktion von Ago-Proteinen mit einem konservier-

ten Bindungpartner, einem Mitglied der GW182-Proteinfamilie. Daher reichert die beschriebene Aufreinigungsmethode alle vier humanen Ago-Proteine an und kann darüber hinaus Spezies-unabhängig angewendet werden. Ago-APP stellt ein leistungsfähiges Hilfsmittel für die Charakterisierung verschiedener Ago-Komplexe auf den Ebenen von Protein, kleiner RNA und Ziel-RNA dar.

Publications and Presentations

Parts of this thesis have been published in the following articles:

J. Hauptmann, A. Dueck, S. Harlander, J. Pfaff, R. Merkl and G. Meister. Turning catalytically inactive human Argonaute proteins into active slicer enzymes. Nature Structural and Molecular Biology, 20(7):814-7, 2013

J. Hauptmann, L. Kater, P. Löffler, R. Merkl and G. Meister. Generation of catalytic human Ago4 identifies structural elements important for RNA cleavage. RNA, 20(10):1532-8, 2014

Parts of this thesis constitute a manuscript in preparation:

J. Hauptmann, A. Bruckmann, D. Schraivogel, S. Manickavel, L. Jakob, J. Pfaff, M. Hafner, R. Deutzmann and G. Meister. Ago-APP: A GW peptide-based Argonaute affinity capture strategy.

Additionally, I contributed to the following Preview:

J. Hauptmann and G. Meister. Argonaute regulation: two roads to the same destination. Developmental Cell, 25(6):553-4, 2013

Parts of this thesis have been presented at international conferences:

J. Hauptmann, S. Harlander, R. Merkl and G. Meister. Turning catalytically inactive human Argonaute proteins into active slicer enzymes. Oral presentation. 8th Microsymposium on small RNAs, May 2013, Vienna, Austria.

J. Hauptmann, L. Kater, S. Harlander, P. Löffler, R. Merkl and G. Meister. Turning catalytically inactive human Argonaute proteins into active slicer enzymes. Oral presentation. 19th Annual Meeting of the RNA Society, June 2014, Quebec, Canada.

Contents

1 Introduction 1

1.1 Argonaute proteins . . . 1
1.1.1 Biogenesis of small RNAs . . . 2
1.1.2 Assembly of the RNA-induced silencing complex . . . 2
1.1.3 The structure of Argonaute proteins . . . 2
1.1.4 RNA-binding and endonucleolytic activity . . . 3
1.1.4.1 Guide and target binding . . . 3
1.1.4.2 Structural rearrangements during ternary complex formation . . . 4
1.1.5 Individual functions of human Ago proteins . . . 5
1.1.5.1 The role of Argonaute cleavage activity in mammalia . . . 5
1.1.5.2 Paralogue-specific expression defines Ago protein function . . . 6
1.1.5.3 Sorting of small RNAs into Ago proteins . . . 6
1.1.6 Expression levels of human Ago1-4 . . . 7
1.1.6.1 The interdependence of Ago protein and small RNA levels . . . 7
1.1.6.2 Dynamic changes of Ago protein expression . . . 8

1.2 Argonaute and GW182 proteins . . . 8
1.2.1 Mechanisms of GW182-mediated repression . . . 9
1.2.2 The molecular basis of tryptophan-mediated GW182 interactions . . . 9

1.3 Regulation by post-translational modifications . . . 10
1.3.1 Post-translational modifications of miRNA biogenesis components . . . 10
1.3.2 Post-translational modifications of Argonaute proteins . . . 11
1.3.2.1 Phosphorylation of human Ago proteins . . . 11
1.3.2.2 Modifying enzymes and signaling pathways . . . 13

2 Results 17

2.1 Analysis of human Argonaute cleavage activity . . . 17
2.1.1 The Argonaute N domain affects cleavage activity . . . 17

2.1.2 Cluster 2 is a PIWI domain feature that defines cleavage activity 18
2.1.3 An additional insertion in the Ago4 PIWI domain prevents slicing function 19
2.1.4 The N-terminal domain affects cleavage activity of Ago1 and Ago4 22
2.1.5 Ago cleavage mutants can unwind miRNA duplexes 22
2.1.6 Catalytically active human Agos rescue miR-451 processing in Ago2-deficient mouse embryonic fibroblasts 24
2.2 Ago-APP: Ago Affinity Purification by Peptides 26
2.2.1 A short TNRC6B peptide precipitates Ago proteins 26
2.2.2 Ago-APP precipitates Argonaute proteins from different species 28
2.2.3 Ago-APP co-precipitates small RNAs 29
2.2.4 Analysis of target RNA enrichment by Ago-APP 29
2.2.5 Competition of T6B peptide and endogenous TNRC6B 30
2.2.6 Quantification of Ago1–4 protein amounts in different tissues 31
2.3 Phosphorylation of endogenous Argonaute proteins 35
2.3.1 Purification of human Ago proteins 35
2.3.2 Detection of endogenous phosphorylation sites of human Ago2 36
2.3.3 Detection of endogenous phosphorylation sites of human Ago1–4 38
2.3.4 Characterization of Ago2 phosphomutants 39
2.3.4.1 Location and conservation of potential Ago2 phosphorylation sites . 39
2.3.4.2 Analysis of miRNA binding and cleavage activity of a subset of Ago2 phosphomutants 41

3 Discussion 43
3.1 Catalytic activation of human Ago proteins 44
3.1.1 The Ago N domain affects cleavage activity 44
3.1.2 Structural elements in the PIWI domain define cleavage function 46
3.1.2.1 Cluster 2 46
3.1.2.2 The Ago4-specific insertion 46
3.1.3 Human slicers provide new insights into Ago function 47
3.2 Ago-APP: a novel purification strategy for Ago proteins 48
3.2.1 Evolutionary conservation of tryptophan-mediated interactions 48
3.2.1.1 The specificity of Ago-APP 48
3.2.1.2 Tryptophan-mediated protein interactions: a common theme 49
3.2.2 Ago-APP co-depletes Ago proteins and miRNAs 50
3.2.3 Efficient target binding requires full length GW182 proteins 50
3.2.4 Establishment of an Ago1–4 quantification method 51
3.2.5 Ago-APP: A novel tool for the characterization of Ago complexes 51
3.3 Endogenous phosphorylation sites of human Ago proteins 53
3.3.1 Endogenous phosphorylation sites of human Ago2 53
3.3.1.1 Phosphorylation clusters and multiply phosphorylated peptides of human Ago2 53
3.3.2 Phosphorylation sites of human Ago1, Ago3, and Ago4 55

3.3.3 Characterization of selected Ago2 phosphomutants . . . 55
3.3.4 Phosphorylation of Ago proteins—an outlook . . . 56

4 Material and Methods 57

4.1 Material . . . 57
4.1.1 Consumables and chemicals . . . 57
4.1.2 Bacterial strains and cell lines . . . 57
4.1.3 Vectors, oligonucleotides, and cloned constructs . . . 58
4.1.3.1 Vectors . . . 58
4.1.3.2 Constructs . . . 58
4.1.3.3 Oligonucleotides . . . 59
4.1.4 Antibodies . . . 63
4.1.5 Exactly quantifiable heavy peptides for SRM measurements . . . 63
4.1.6 Technical equipment . . . 64

4.2 Generation of DNA constructs . . . 65
4.2.1 Polymerase Chain Reaction (PCR), restriction digests, and ligation . . . 65
4.2.2 Site-directed mutagenesis ('QuikChange') . . . 65
4.2.3 Generation of Chimeras . . . 66
4.2.4 Mutagenesis by 3-way blunt end ligation . . . 66
4.2.5 Transformation of *E. coli* . . . 66
4.2.6 Extraction of plasmid DNA from *E. coli* . . . 66
4.2.7 Sequencing . . . 67

4.3 Protein-based methods . . . 67
4.3.1 Expression and purification of recombinant protein . . . 67
4.3.2 Cell culture . . . 68
4.3.2.1 Transfection by calcium phosphate . . . 68
4.3.2.2 Transfection by Lipofectamine LTX and PLUS Reagent . . . 68
4.3.3 Lysate preparation . . . 69
4.3.3.1 Lysate preparation from cell culture samples . . . 69
4.3.3.2 Lysate preparation from tissues . . . 69
4.3.4 Immunoprecipitation (IP) . . . 69
4.3.5 Ago-APP (Ago Affinity Purification by Peptides) . . . 70
4.3.6 SDS-PAGE, Western Blot, and Coomassie staining . . . 71
4.3.7 Mass-spectrometric analyses . . . 71
4.3.7.1 MS sample preparation . . . 72
4.3.7.2 Mass spectrometers . . . 72
4.3.7.3 Mass-spectrometric measurements . . . 73
4.3.7.4 MS data analysis . . . 73

4.4 RNA-based methods . . . 73
4.4.1 RNA isolation . . . 73
4.4.2 Quantitative real time PCR (qRT-PCR) . . . 74
4.4.3 RNA separation by urea PAGE and Northern Blotting . . . 74

4.4.4 RISC cleavage assays 75
4.4.4.1 *In vitro* transcription 75
4.4.4.2 Cap-labeling of the target RNA 75
4.4.4.3 RISC cleavage assay 76
4.4.4.4 Autoradiographic sequencing gels 76
4.5 Bioinformatic analyses 77
4.5.1 Sequence retrieval and alignments 77
4.5.2 Homology models 77

A Appendix 79

Bibliography 87

List of Figures

1.1 The structure of human Ago2 . . . 3
1.2 The function of Ago2 cleavage activity . . . 5
1.3 Interdependence of Ago and small RNA levels . . . 8
1.4 Post-translational modifications of human Ago2 . . . 12
1.5 Known phosphorylation sites of human Ago2 . . . 14

2.1 The Ago3 N domain affects cleavage function . . . 18
2.2 Cleavage activity of Ago3 N-terminal mutants . . . 19
2.3 Cleavage activity of the Ago1 PIWI domain . . . 20
2.4 Cleavage activity of the Ago4 PIWI domain . . . 21
2.5 Comparison of the catalytic centers of Ago1, 2, and 4 . . . 22
2.6 The N-terminal domain affects Ago1 and Ago4 cleavage activity . . . 23
2.7 Ago cleavage mutants bind miR-19b . . . 24
2.8 Rescue of miR-451 processing by catalytically active Agos . . . 25
2.9 Identification of a strong Ago-binding region in human TNRC6B . . . 26
2.10 GST-T6B precipitates human Ago1–4. . . . 27
2.11 Ago-APP precipitates Argonaute proteins from different species . . . 28
2.12 miRNA isolation and depletion by Ago-APP . . . 29
2.13 Co-precipitation of target RNAs in Ago-APPs . . . 30
2.14 T6B peptide competes with full length TNRC6B . . . 31
2.15 Ago1–4 quantification in different human cell lines . . . 32
2.16 Quantification of Ago1–4 in different mouse tissues . . . 33
2.17 Purification of endogenous Ago proteins . . . 35
2.18 Detection of potential phosphorylation sites in endogenous Ago2 . . . 37
2.19 Phosphorylation of human Ago1–4 . . . 39
2.20 Location and conservation of potential Ago2 phosphorylation sites . . . 40
2.21 miRNA binding of Ago phosphomutants . . . 41
2.22 Cleavage activity of Ago2 phosphomutants . . . 42

3.1 Cleavage-defining elements of human Ago1–4 44
3.2 Comparison of residues that form tryptophan binding pockets in Ago proteins . 49

List of Tables

1.1 Overview of Ago2 phosphorylations 13

4.1 Bacterial strains 57
4.2 Cell lines 58
4.3 Vectors 58
4.4 Oligonucleotides for Northern Blotting, quantitative real time PCR, sequencing, and *in vitro* transcription scale up PCRs 59
4.5 Oligonucleotides for cloning 60
4.6 Antibodies 63
4.7 Stable isotope-labeled peptides 63

A.1 Phosphopeptides: Ago2-IP I 79
A.2 Phosphopeptides: Ago2-IP II 80
A.3 Phosphopeptides: TNRC6A–C Co-IP I 80
A.4 Phosphopeptides: TNRC6A–C Co-IP II 80
A.5 Phosphopeptides: Ago-APP I 81
A.6 Phosphopeptides: Ago-APP II 82
A.7 Phosphopeptides of Ago1–4 83
A.8 Phosphopeptides of Ago1–4 (PhosphoSitePlus) 85

List of Abbreviations

Units were abbreviated according to the International System of Units. Chemical names not indicated below were abbreviated according to the IUPAC (International Union of Pure and Applied Chemistry) recommendations.

aa	amino acid
AEBSF	4-(2-aminoethyl) benzenesulfonyl fluoride hydrochloride
Amp	ampicillin
Ago-APP	Ago affinity purification by peptides
APS	ammonium persulphate
ATP	adenosine triphosphate
BAT	brown adipose tissue
bp	base pair(s)
Bis	N,N'-methylene bisacrylamide
cDNA	complementary DNA
CDS	coding sequence
CID	collision-induced dissociation
C-P4H(I)	collagen prolyl-4-hydroxylase type I
CTD	C-terminal domain
cv	column volume
DCL-3	Dicer-like 3
DMEM	Dulbecco's Modified Eagle's Medium
DNA	deoxyribonucleic acid
ds	double-stranded
DSSP	define secondary structure of proteins
DTT	dithiothreitol
dNTP	deoxynucleoside triphosphate
EDC	1-ethyl-3-(3-dimethyl-aminopropyl)-carbodiimid
EDTA	ethylenediaminetetraacetic acid
EGFR	epithelial growth factor receptor
eIF	eukaryotic initiation factor
ERK	extracellular signal–regulated protein kinases
EtBr	ethidium bromide
FBS	fetal bovie serum
FDR	false discovery rate

FRET	Förster resonance energy transfer
GAPDH	glyceraldehyde 3-phosphate dehydrogenase
GFP	green fluorescent protein
GSH	glutathione
GSK3β	glycogen synthase kinase 3β
GST	glutahione-S-transferase
GTP	guanosine triphosphate
HA	hemagglutinin
HEK 293T	human embryonic kidney 293T
HEPES	4-(2-hydroxyethyl)-1-piperazineethanesulfonic acid
HMGA2	high mobility group AT hook 2
HSP90	heat shock protein 90
IDA	iminodiacetate
IP	immunoprecipitation
IPTG	isopropyl β-D-1-thiogalactopyranoside
Kana	kanamycin
kb	kilobase
LB	lysogeny broth
MAPK	MAP (mitogen-activated protein) kinase
MAPKAPK2	MAP-activated protein kinase 2
mHESM	miRNAs regulated by hypoxia-dependent EGFR-suppressed maturation
MKK	MAPK kinase
mRNA	messenger RNA
MS	mass spectrometry, mass-spectrometric
Neo	neomycine
NMR	nuclear magnetic resonance
nt	nucleotides(s)
OD	optical density
PABP	poly(A)-binding protein
PACT	protein activator of the interferon-induced protein kinase
PAGE	polyacrylamide gel electrophoresis
PAM2	PABP interacting motif 2
PAN2/3	PAB-dependent poly(A)-specific ribonuclease subunit 2/3
PAR-CLIP	Photoactivatable-Ribonucleoside-Enhanced Crosslinking and Immunoprecipitation
PAZ	PIWI-Argonaute-Zwille
PBS(-T)	phosphate-buffered saline (containing Tween 20)
PCR	polymerase chain reaction
piRNA	PIWI-interacting RNA
PIWI	P-element-induced wimpy testes
PNK	polynucleotide kinase
PTM	post-translational modification
PTP1B	protein tyrosine phosphatase 1B
RAS	rat sarcoma
RdDM	RNA-dependent DNA methylation
RdRP	RNA-dependent RNA polymerase
RIPA	radioimmunoprecipitation assay
RISC	RNA-induced silencing complex
RNA	ribonucleic acid
ROS	reactive oxygen species

RRM	RNA recognition motif
sDMA	symmetric dimethyl arginine
SDS	sodium dodecyl sulfate
siRNA	small interfering RNA
SRM	selected reaction monitoring
ss	single-stranded
SSC	saline-sodium citrate buffer
TBS(-T)	Tris-buffered saline (containing Tween 20)
TEMED	tetramethylethylenediamine
TRBP	transactivating response RNA binding protein
TRIM71	tripartite motif-containing protein 71
UBA	ubiquitin-associated
UTR	untranslated region
YAP	Yes-associated protein

1. Introduction

1.1 Argonaute proteins

Argonaute proteins are central components of small RNA-mediated gene silencing. They associate with different classes of small RNA and mediate gene silencing by various means, including post-transcriptional as well as transcriptional mechanisms. The small RNA-binding modules are found in many phyla where they have adopted to specific functions. The number of different Argonaute proteins varies between one in *Schizosaccharomyces pombe*, five in *Drosophila melanogaster* (Drosophila), eight in mammalia, ten in *Arabidopsis thaliana* (Arabidopsis), and reaches twenty-six in *Caenorhabditis elegans* (*C. elegans*) [1].

Argonaute proteins subdivide into the clades of Ago-like proteins ('Ago proteins', named after Arabidopsis Ago1), PIWI-like proteins ('PIWI proteins', named after the Drosophila protein PIWI), and worm-specific WAGO proteins [2–4].

The members of the first clade, Ago proteins, are ubiquitously expressed. They are essential components of small RNA-guided gene silencing and mediate target repression by mechanisms such as endonucleolytic cleavage or recruitment of additional factors that ultimately affect translation efficiency and mRNA stability [5, 6]. Besides these cytoplasmic functions, Ago proteins are also present in the nucleus, where they were found to act at transcriptional level [7–9]. Ago-mediated epigenetic silencing is commonly observed in *Schizosaccharomyces pombe*, nematodes, and plants [10]. It involves specialized machineries, that ensure for example small RNA production and DNA methylation [10].

PIWI proteins are predominantly expressed in the germline and protect the genome from mobile genetic elements through post-transcriptional repression as well as transcriptional silencing of transposon sequences [11–13].

Additionally to the Ago and PIWI protein families, *C. elegans* comprises the third clade of worm-specific Argonaute proteins, termed 'WAGO' proteins [2]. These Argonaute proteins associate for example with secondary small RNAs that arise from the action of RNA-dependent RNA polymerases and fulfill widespread functions [14–16].

Notably, Argonaute proteins are also present in archaea and prokaryotes. Several Argonaute proteins of these organism associate preferentially with single-stranded DNA rather than with RNA. Their target molecules can be DNA and RNA [17]. It is currently assumed that such 'ancestral Argonautes' protect against mobile genetic elements and represent one of the earliest innate immune strategies [18, 19].

Mammalian Ago proteins associate with microRNAs (miRNAs) or small-interfering RNAs (siRNAs), which are typically 21–24 nt in length. In contrast, PIWI proteins bind the slightly longer PIWI-interacting RNAs (piRNAs). The following section describes the biogenesis of these different small RNA species.

1.1.1 Biogenesis of small RNAs

miRNAs and siRNAs. Most miRNAs are encoded by miRNA genes that are transcribed by RNA polymerase II [20, 21]. Primary miRNA transcripts (pri-miRNAs) are often polycistronic and characterized by hairpin structures, which are flanked by single-stranded 3' and 5' extensions [22]. The microprocessor complex, which contains the endonuclease Drosha and its cofactor DGCR8 (DiGeorge Syndrome Critical Syndrome Region 8), cleaves these transcripts near the basis of the hairpins [23–26]. The resulting miRNA precursor (pre-miRNA) is then exported to the cytoplasm by exportin 5 [27–29]. There, the hairpin loop is removed by the endonuclease Dicer [30, 31], which is associated with the double-stranded (ds) RNA-binding proteins TRBP (TAR RNA binding protein) and PACT (protein activator of the interferon-induced protein kinase) [32–34].

siRNAs enter the small RNA biogenesis pathway at the step of Dicer cleavage and typically arise from long dsRNA [35, 36]. DsRNA can be of exogenous or endogenous sources, for example originating from viral infections, transposon expression, bidirectional or pseudogene transcription, or from long hairpin structures [37]. In mammals, long dsRNA is usually targeted by the interferon response system. Here, endogenous siRNAs (endo-siRNAs) have so far only been observed in mouse oocytes [38–40] and embryonic stem cells [41].

piRNAs. piRNAs are transcribed from distinct piRNA clusters which commonly represent an immense fundus of diverse transposon sequences [13]. piRNA biogenesis is fundamentally different from miRNA or siRNA biogenesis as it does not involve double-stranded precursors and Dicer processing [42]. For piRNA production, endonucleolytic cleavage of a single-stranded precursor seems to play a role, but the exact mechanism is still unknown [43–45]. Noteworthy, piRNA-mediated silencing comprises an amplification mechanism where the intertwined action of endonucleolytically active PIWI proteins facilitates a directed response to actively transcribed transposons, known as the 'ping pong cycle' [46, 47]. Given their role in antiviral response and protection from mobile genetic elements, the function of mammalian piRNAs does partly overlap with that of endo-siRNAs [13].

1.1.2 Assembly of the RNA-induced silencing complex

After Dicer processing, the resulting dsRNA is loaded into Ago proteins in an energy-dependent process that requires chaperons [48]. One of the strands (termed 'miRNA*' or siRNA 'passenger strand') is removed and degraded. The other strand, the siRNA 'guide strand', is bound to Ago in an RNA-induced silencing (RISC) complex and confers specificity for post-transcriptional gene silencing. It was shown that endonucleolytically active Argonaute proteins can cleave the passenger strand and can therefore accelerate the loading process [49–51]. Additionally, it was proposed that the non-catalytic human Ago1 can cleave passenger strands [52]. However, unwinding and passenger strand removal do not strictly depend on endonucleolytic activity and non-slicing Argonautes are able to load single-stranded RNAs as well [53, 54]. Due to the high duplex stability of uncleaved siRNAs, loading of non-catalytic Ago proteins is a slower process [53]. It is not yet known whether duplex unwinding requires an external helicase since Ago proteins have been reported to play a role in duplex unwinding themselves [55].

1.1.3 The structure of Argonaute proteins

Argonaute proteins consist of four functional domains that are structurally organized within two lobes [56–62] (Fig. 1.1).

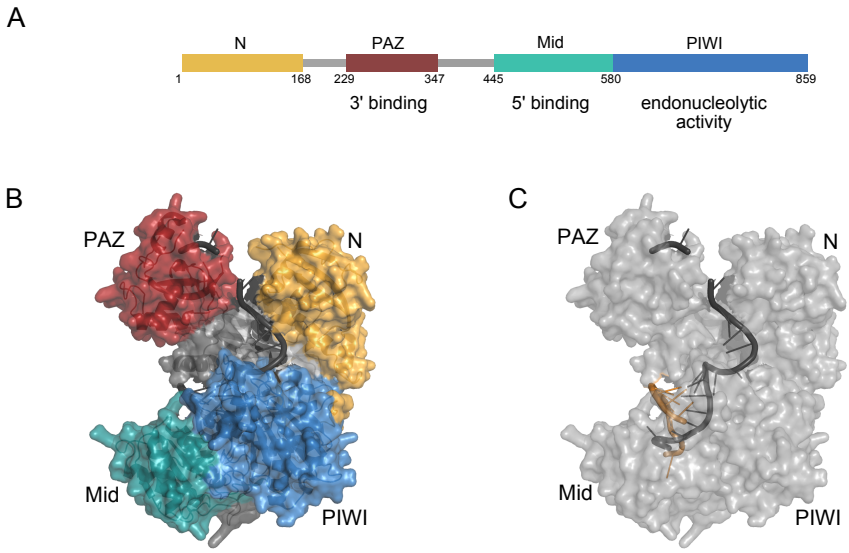

Figure 1.1: The structure of human Ago2 (A) Domain organization of human Ago2 with the functions of the PAZ, Mid, and PIWI domains indicated. (B) The structure of human Ago2 (PDB 4W5O, [74]) with domains colored as in (A). (C) The bound miRNA of 21 nt length is shown in gray. A co-crystallized short target RNA that pairs from nt 2–9 is depicted in orange.

The Mid domain comprises a binding pocket that can accommodate the 5' end of the small RNA [63–67]. The 3' end of the RNA is anchored in the PAZ (Piwi-Agonaute-Zwille) domain [68–70].

The PIWI domain resembles an RNAse-H fold and some Argonautes are indeed able to cleave their targets endonucleolytically [3]. This slicing activity is thought to rely on the presence of a catalytic triad [56, 71]. Recent structural studies of a yeast Argonaute showed that an additional residue is involved in catalysis, extending the catalytic center to a tetrade of Asp-Glu-Asp-His [60]. These residues are conserved in human Ago proteins [60]. Of the human Ago family members, only Ago2 is able to cleave its targets [72, 73]. The required catalytic tetrade is also present in human Ago3, suggesting that other protein features affect cleavage activity as well. Additionally to its endonucleolytic function, the PIWI domain exhibits two binding pockets for the tryptophan-mediated interaction with GW182 proteins [58].

The N-terminal domain is the region with highest sequence variability of the otherwise very conserved Ago proteins. There has not been a characteristically assigned function of the Argonaute N domain for a long time—until it was suggested to facilitate duplex unwinding and passenger strand removal by its so-called 'wedging function' [55].

1.1.4 RNA-binding and endonucleolytic activity

1.1.4.1 Guide and target binding

Ago proteins bind small RNAs via their phosphate-sugar backbone, allowing the bases of the guide RNA to protrude into the nucleic acid binding channel [58, 65]. Furthermore, the 5' part of the bound single-stranded RNA is organized in a preformed A-form helix, ready to accept complementary bases of the target RNA via Watson-Crick base pairing [58, 65].

An extrinsic requirement for the cleavage function of Ago proteins is the perfect or near-perfect complementarity of the target RNA. The minimal base pairing requirements have been studied at the DNA-binding Argonaute protein of *Thermus thermophilus* [75]. Crystallization studies with target DNAs of different lengths showed that base pairing of the guide strand positions 4 to 16 is necessary for target DNA cleavage. Depending on their number and position, mismatches and bulges are also tolerated. If mismatches occur between positions 2–8, substrate cleavage is reduced. Mismatches at the cleavage site abolish slicing function [75]. Additionally to this positional effect, bulges are more likely to be tolerated in the target strand. This strand has a higher capacity to compensate for non-perfect base pairing because it does not contact the Ago protein. The only contacts are via Watson-Crick base pairing interactions with the guide RNA [65].

Human Ago2 is optimized to accommodate partially paired duplexes [74]. Vertebrate miRNAs bind predominantly to partially complementary target sites. This interaction relies on binding of so-called 'seed sequences', i.e. duplex formation of the nucleotides 2 to 8 [76]. Human Ago2 is adapted to recognize these sites. It comprises a binding pocket for the first nucleotide of the target RNA, preferentially an adenine. Outgoing from there, the protein is shaped to meet the minor groove of the guide:target duplex. Beyond the ninth nucleotide, duplex formation is energetically unfavorable and most likely requires conformational changes [74].

1.1.4.2 Structural rearrangements during ternary complex formation

A loaded Argonaute does not represent a rigid complex. The two-state model postulates that an Ago-bound single-stranded nucleic acid is initially anchored at both ends. When duplex formation propagates to the guide 3' end, this end is released from the PAZ domain [77]. Several observations support this model and hint at global rearrangements taking place upon binding of perfectly as well as partially complementary targets.

Already the modeling of a duplex into one of the first structurally resolved Argonautes, the *Aquifex aeolicus* Argonaute, indicated that conformational changes have to take place to accommodate the nucleic acids [56]. This was expected to include an opening of the nucleic acid binding channel and movement of the PAZ domain [56]. Both presumptions were experimentally verified by structural studies of the Argonaute protein from *Thermus thermophilus* [57, 65, 75]. A comparison of a binary complex with a ternary complex containing a partially complementary target showed that the N and PAZ domains are indeed moved apart from the Mid-PIWI lobe and ensure opening of the binding channel and accommodation of the double strand [57, 65]. Furthermore, the guide DNA in a binary complex is kinked between nt 10 and nt 11. Upon duplex formation, it binds in a different trajectory and an unobstructed helix is formed [57, 65]. These studies were extended by a detailed structural analysis of cleavage-deficient *Thermus thermophilus* Ago bound to perfectly complementary target RNAs of different lengths [75]. In this case, extended duplex formation releases the guide 3' end from the PAZ domain [75]. Remarkably, the N domain was observed to block base pairing of the terminal three bases [75].

Similarly, the guide RNA bound in a human binary Ago complex is also kinked [58]. This kink is introduced by Ile-365 which inserts between guide nucleotides 6 and 7 [58]. Upon binding of a partially complementary target, the Ile-365-accommodating helix moves and allows for another step of duplex propagation before it stabilizes the newly-formed conformation [74]. Simultaneously, repositioning of the PAZ domain and widening of the binding channel seem to be initiated by this helix movement [74].

Additionally to structural studies, kinetic analyses and FRET (Förster Resonance Energy Transfer) measurements of Ago proteins confirmed the two-state model [78, 79]. FRET experiments used an archaeal Ago where fluorescent dyes were incorporated into different positions of the protein and guide DNA. The strongest FRET shift upon ternary complex formation was detected for a reporter located in the PAZ do-

main and a guide DNA labeled close to the 3' end, again favoring a release of the nucleic acid from the PAZ domain upon target binding [78].

Structural studies of Argonaute from the yeast *Kluyveromyces polysporus* identified a fourth catalytic residue necessary for target cleavage [60]. It is located on a so-called 'glutamate finger' which can adopt an active ('plugged-in') and an inactive ('plugged-out') conformation. The comparison of cleavage-incompatible and cleavage-compatible Ago conformations in *Thermus thermophilus* suggested that a 3' guide release from the PAZ domain triggers several loop rearrangements which lead to the insertion of the glutamate finger into the catalytic center [80]. However, the inactive conformation has not been identified in other eukaryotic Agos [60] and it is still unclear if this region is subject to structural rearrangements in human Ago2 [17].

1.1.5 Individual functions of human Ago proteins

1.1.5.1 The role of Argonaute cleavage activity in mammalia

In mammals, perfectly complementary miRNA targets do rarely exist. Considering the possibility to accept certain helical imperfections, target cleavage might still have an impact on miRNA-mediated gene regulation. Ago-mediated endonucleolytic activity has indeed been observed, but it occurs only for few targets [81–85]. More than miRNAs, endo-siRNAs depend on target slicing. Mammalian endo-siRNAs have so far only been detected in mouse oocytes and embryonic stem cells, where they are suggested to act as part of an ancient immunity system [38–41]. The RNAi machineries of Drosophila and *C. elegans* are functionally separated and can therefore be targeted selectively. In these model organisms, the inactivation of siRNA-mediated repression shows no phenotypic effects [86–89]. Taken together, endogenous target cleavage contributes only little to mammalian miRNA-mediated gene regulation.

However, exogenously applied siRNAs are of high interest for drug development and represent a widely used tool in molecular biology. siRNA-mediated knockdowns depend on the catalytic activity of Ago2, which is shown by the fact that Ago2-depleted mouse embryonic fibroblasts are not sensitive to RNAi treatment [73]. Still, non-catalytic Ago proteins have also been reported to contribute to siRNA-mediated knockdowns [90].

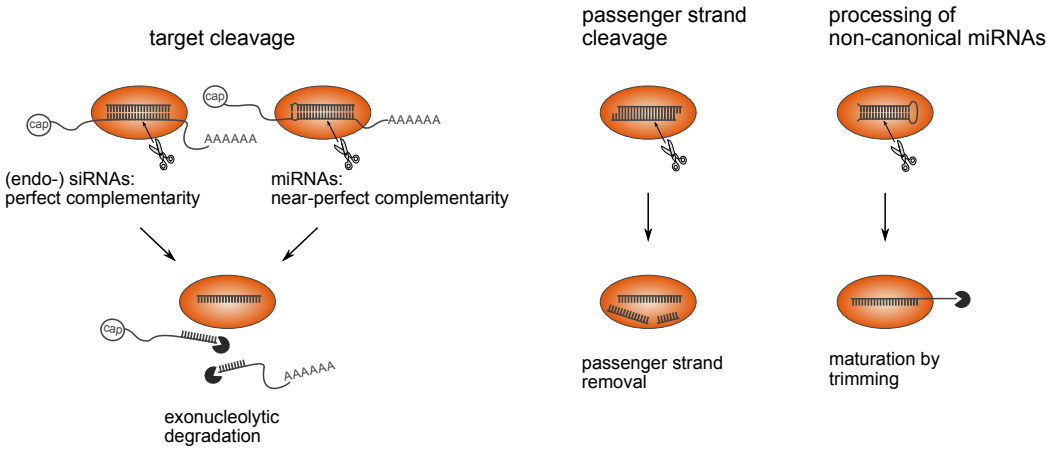

Figure 1.2: The function of Ago2 cleavage activity. Three processes that depend on endonucleolytic activity of human Ago2: target cleavage (A), passenger strand cleavage (B), and endonucleolytic processing of non-canonical miRNAs (C). The target mRNA is designated by its cap and poly(A) tail.

Additionally, Ago2 cleaves perfectly paired passenger strands like it cleaves perfectly paired targets [49–51], thereby facilitating efficient passenger strand removal and RISC formation [53].

If Ago2 does usually not cleave miRNA targets, why is its endonucleolytic activity conserved? An answer to this question is provided by engineered mice, which express non-slicing Ago2. These animals show erythropoietic defects and lack one specific miRNA, which regulates the differentiation of erythroid lineages [91]. miR-451 does not depend on Dicer processing, but is bound to Ago2, sliced, and trimmed by additional factors to yield a mature miRNA [91–96].

Taken together, the catalytic function of Ago2 plays a role in cleavage-mediated silencing of target RNAs, during RISC assembly, and during processing of non-canonical miRNAs (Fig. 1.2).

1.1.5.2 Paralogue-specific expression defines Ago protein function

Erythropoietic defects were also observed when Ago2 was specifically deleted from bone marrow (and therefore from lymphoid and erythroid lineages) [97]. Interestingly, this phenotype is independent of the catalytic activity of Ago2 [97], indicating a specific role of Ago2 in its 'non-slicing' function. A complete knockout of Ago2 is embryonic lethal, suggesting that this protein is indispensable for embryonic development [73, 98]. In contrast, Ago1, Ago3, and Ago4 knockout mice and even combinatorial Ago1/Ago3 and Ago1/Ago4 knockout mice are viable [99]. Whereas a combination of Ago1 and Ago3 was reported to play a role in flu resistance [99], male Ago4 knockout mice display fertility defects and meiotic alterations [100]. In particular, sex chromosome inactivation is perturbed in these mice and prophase I is induced prematurely [100].

Importantly, any Ago protein can mediate miRNA-mediated repression in mouse embryonic stem cells depleted of Ago1–4, indicating that mammalian Agos function redundantly in the miRNA pathway [101]. In line with that, cross-complementing expression changes (e.g. increased Ago1 expression upon Ago2 depletion) have been observed in studies that investigated Ago knockouts [100, 102]. However, assuming that human Ago proteins function redundantly, specific functions could still be conferred by the selective loading of miRNAs, termed 'sorting'.

1.1.5.3 Sorting of small RNAs into Ago proteins

Depending on the organism, small RNA sorting exists at different degrees of complexity. For example, a very strict sorting system in Drosophila targets miRNAs to Ago1 and siRNAs to Ago2. Discrimination is already applied during small RNA biogenesis, when the structurally different precursors are loaded into two different Dicer complexes [103, 104].

Arabidopsis comprises a complex processing and silencing machinery, including four Dicer and ten Ago proteins. Here, a substantial part of sorting is mediated by the identity of the small RNA 5' nucleotide [105].

In contrast, human Ago proteins interact with only one Dicer paralogue [4]. All human Ago proteins bind miRNAs and siRNAs [72, 73]. The individual Agos bind a similar spectrum of miRNAs [95, 106] and targets [106, 107], as identified by different sequencing approaches. Interestingly, after combined depletion of Ago1 and Ago2 in mouse skin, Ago3 associates with a similar set of miRNAs as Ago1 and Ago2 do in wild type samples [102]. A special case of sorting exists for miR-451, whose processing depends on an endonucleolytically active Ago protein. Pre-miR-451 is loaded to all human Ago proteins, but mature miR-451 is exclusively associated with human Ago2 [93, 94].

Taken together, there is little evidence for a role of miRNA sorting in mammals. However, among the human Ago proteins, Ago2 is clearly in a special position, but this is only partly attributable to its endonucleolytic activity. A large part of Ago2-related effects is probably related to its expression determinants.

1.1.6 Expression levels of human Ago1-4

So far, most of the studies that addressed Ago1–4 expression levels relied on mRNA-based techniques and utilized semiquantitative or quantitative PCR approaches [72, 108–111]. *Ago1–3* transcripts show a rather ubiquitous and overlapping expression in different tissues [72, 108, 109]. A comparison of expression levels reveals that in general *Ago2* is most abundant, followed by *Ago1*, *Ago3*, and *Ago4* [111]. Interestingly, the otherwise very weakly expressed *Ago4* is enriched in whole testis as well as in certain cell types corresponding to different stages of spermatogenesis [110].

At protein level, three different approaches have been used for Ago quantification.

First, the four human Ago proteins were immunopurified by monoclonal antibodies and mass-spectrometrically analyzed [53]. This strategy presupposes that the used antibodies have similar efficiencies and deplete comparable ratios of the individual Agos from the cellular extract. Such a condition is unlikely and the estimated ratios of 24:60:14:1.2 (Ago1:Ago2:Ago3:Ago4, measured in HEK 293T cells) should be interpreted carefully.

In another approach, shotgun proteomics was applied and Ago1–3 contents were quantified by the number of unique, paralogue-specific peptides that were detected [102]. Using this technique, ratios of 22:80:22 (Ago1:Ago2:Ago3, measured in a human melanoma cell line) were reported [102]. However, mammalian Agos are very similar at amino acid sequence level. Therefore, Ago peptides can often not be assigned to an Ago paralogue in mass-spectrometric measurements. Consequently, these non-assignable peptides introduce strong uncertainty.

Finally, a pulldown experiment conducted to confirm Ago binding to a specific TNRC6B fragment identified all human Agos in the ratios 26:61:12:1 (Ago1:Ago2:Ago3:Ago4, measured in HeLa cells) [112]. The interpretation of these mass-spectrometric data entailed similar uncertainties, esp. in terms of peptide assignment and mass-spectrometric intensities. However, the applied enrichment step for Ago proteins represents a valuable basis for future analysis.

A puzzling aspect of Ago expression is the codon usage in their mRNAs, especially the occurrence of more rare codons in *Ago3* and *Ago4* [111]. It is not known whether this intrinsic effect is due to the redundancy of the highly similar Ago proteins and Ago3/Ago4 progressively loosing importance, or if it serves a certain purpose and is required to fine-tune Ago expression [111].

1.1.6.1 Ago protein and small RNA levels are interdependent

Several studies conducted in different experimental systems show that miRNA and Ago levels are interdependent (Fig. 1.3). On the one hand, Ago protein levels depend on the presence of small RNAs. Unloaded Ago is not stable and is subjected to degradation [114, 115]. On the other hand, small RNAs depend on the presence of Ago proteins [116, 117]. Consequently, Ago depletion reduces the levels of mature miRNAs in several organisms [97, 118–120] and Ago overexpression increases miRNA levels [120, 121]. It is assumed that this interplay between Ago and miRNA levels depends on an Ago function during miRNA biogenesis, most likely during product release and loading after Dicer processing of the pre-miRNA [97, 122]. Tipping the sensitive equilibrium of a system with low Ago expression can have unexpected consequences, e.g. a release of endogenous target repression upon siRNA treatment [122, 123].

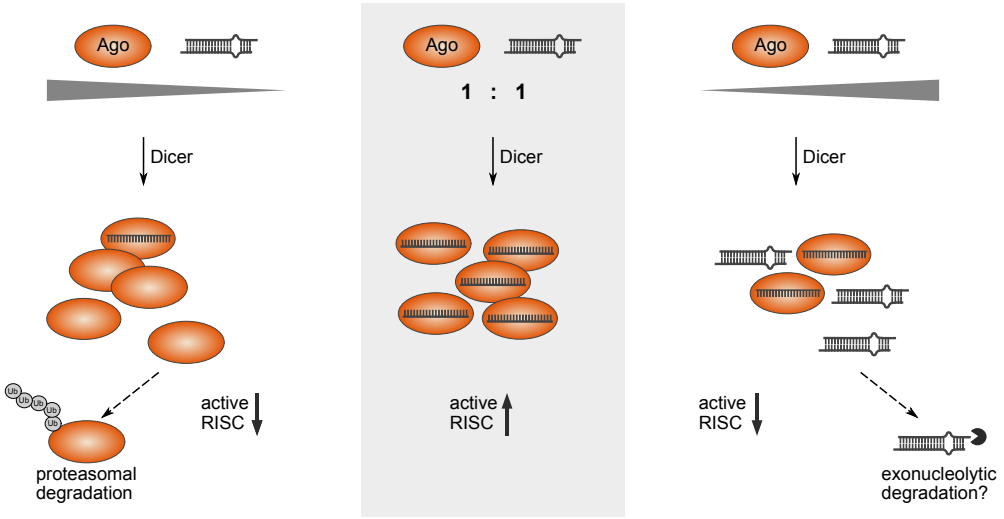

Figure 1.3: The interdependence of Ago and small RNA levels. Unloaded Ago proteins are unstable and subjected to degradation (left side), whereas small RNA levels depend on the presence of Ago proteins (right side). Partially adapted from [113].

One study attempted to determine the exact miRNA and Ago copy numbers per cell [124]. In contrast to the observed interdependency, the authors concluded that there is an about 13-fold excess of miRNA molecules over Ago molecules [124]. Another study quantitatively compared the miRNA content of immunopurified Ago2 with that of total lysate, hypothesizing that a large part of miRNAs is not RISC-associated [125]. Moreover, a third study reported that miRNAs associate with Ago proteins to different extents [126]. These reports suggest that not all miRNAs are bound to Ago [124–126].

1.1.6.2 Dynamic changes of Ago protein expression

Importantly, the described studies represent snapshots of Ago1–4 protein expression. Several observations point at Ago expression being regulated time-dependently and tissue-specifically. For example, total Ago levels can change as part of cellular reprogramming events. This has been observed during the activation of T cells, when a major part of the total Ago pool is subjected to proteasomal degradation, thus resetting the miRNA machinery and allowing to substitute a large portion of translationally repressed targets [127]. A more specific readjustment of the Ago protein levels has been observed during mouse brain development, where the initially high Ago1 levels decrease and adapt to the lower levels of Ago2 [121]. Since Ago2 exhibits 3' trimming activity towards mature miRNAs, a strongly altered Ago1:Ago2 ratio might ultimately affect miRNA isoform identity, target binding, and target repression [121].

1.2 Argonaute and GW182 proteins

Mammalian miRNA-mediated gene silencing depends only to minor parts on endonucleolytic cleavage. The major part of repression is based on translational inhibition and mRNA destabilization. To accomplish these functions, Ago proteins recruit additional effector complexes. Therefore, Ago proteins directly interact with GW182 proteins, which are termed TNRC6A, B, and C (trinucleotide repeat-containing protein 6 A, B, and C) in humans [128, 129]. These proteins are core components of the effector complexes and are required for miRNA-mediated repression in metazoan organisms [128, 130–133]. Importantly,

GW182 proteins alone can silence reporter mRNAs when they are artificially bound to them [134]. The exact mechanism of silencing is still under investigation, but it is becoming clear that it involves both mechanisms of target destabilization and translational repression [6].

1.2.1 Mechanisms of GW182-mediated repression

For miRNA-mediated gene silencing, deadenylation of the target RNA plays a crucial role [134–136]. GW182 proteins recruit the deadenylation complexes CCR4-NOT and PAN2-PAN3 [6, 137–139]. Besides deadenylation, decapping and 5'–3' decay also contribute to target destabilization [6]. Importantly, several translation factors were reported to dissociate from decapped and/or deadenylated target RNAs, suggesting that target destabilization and translational inhibition are coupled [140].

However, deadenylation- and decapping-independent repression has also been observed [138, 141] and such active mechanisms of translational repression are currently discussed. One line of evidence is provided by the interaction of GW182 proteins with the poly(A) binding protein (PABP) [142, 143]. One of the first models for GW182-mediated translational repression suggested that GW182 and eIF4G (a cap-binding translation initiation factor) compete for PABP binding [142, 143]. GW182 binding to PABP would therefore prevent closed-loop formation, which stimulates translation [142, 143]. However, current models favor a positive effect of the poly(A) tail and PABP on the association of RISC with the target mRNA [144]. After target binding, PABP dissociates from the complex, which simultaneously decreases translation efficiency [140, 144]. Furthermore, it was recently shown that RISC induces the dissociation of eIF4AI and eIF4AII from the mRNA, thereby preventing translation initiation [145–147]. Also recently, the translational repressor and decapping activator DDX6 was reported to bind to the CCR4-NOT complex [148, 149]. Altogether, the outlined mechanisms establish important links between CCR4-NOT recruitment and translational repression.

It has been a long-lasting debate if silencing is mediated by translational repression, destabilization of the target RNA, or a combination of both mechanisms. The contribution of these mechanisms was studied at reporter constructs [150, 151] and endogenous targets [152, 153]. These studies suggested that translational repression dominates over destabilization at the beginning of a repression event and that target destabilization prevails after a while [150–153]. Importantly, neither of the two repression modes can be ruled out and future research will reveal how they are used and if they are mechanistically coupled.

1.2.2 The molecular basis of tryptophan-mediated GW182 interactions

GW182 proteins are characterized by a C-terminal silencing domain that comprises several interaction motifs such as an ubiquitin-associated (UBA)-like domain, a glutamine (Q)-rich region, RNA recognition motifs (RRMs), or a poly(A) binding motif (PAM2). Apart from these motifs, GW182 proteins are largely unstructured proteins that contain several regions with multiple glycine/tryptophan repeats. These regions occur throughout the protein with most of them being present in the N-terminal part. Here, the GW motifs are important for Ago binding and up to three Ago binding motifs have been identified in this region [154–157].

To further analyze the molecular mechanism of Ago binding, a recent study investigated the N-terminal, GW-rich region by means of a peptide array [112]. Three binding hot spots were identified, one of which had been described before [112, 129]. This Ago-binding peptide (TNRC6B 599-683) was characterized in detail. The GW peptide is unstructured and contains five tryptophans. Mutagenesis, nuclear magnetic resonance (NMR) titration experiments, and crosslinking experiments showed that Ago binding is mediated by two of these residues, with W623 contributing the main part and W634 further enhancing binding

affinity [112]. Importantly, not all tryptophan-containing peptides that were used in the peptide array conducted by Pfaff *et al.* were able to bind Ago. The comparison of positive binders suggested that tryptophan spacing defines Ago binding [112]. This is in line with the distinct spacing of two tryptophan binding pockets that were identified in structural studies of human Ago2 [58].

Tryptophan-mediated interactions of GW182 proteins are not only essential for Ago binding, but also for interaction with the deadenylation complexes CCR4-NOT [138, 139] and PAN2-PAN3 [138, 158]. Binding of these complexes depends on an additive effect of several tryptophan residues [138]. Interestingly, even an unrelated peptide with engineered Trp-containing motifs was shown to mediate the interaction with CCR4-NOT, indicating that the exact sequence context is less important than the presence of tryptophans [138]. Similar to human Ago2, structural studies revealed also the presence of two tryptophan binding pockets in CNOT9, the main GW182-interacting subunit of CCR4-NOT [148, 149]. In contrast, only one tryptophan binding pocket is suggested to mediate the interaction of GW182 and PAN3 [158]. The pocket is located at the dimerization interface of homodimerized PAN3. Consequently, binding of the TNRC6C silencing domain was reported to depend on the dimerization of PAN3 [158]. Interestingly, this binding mode would provide the possibility to regulate the association of GW182 and PAN3 by dimerization of PAN3 [158].

Taken together, multiple interactions of GW182 proteins are mediated by tryptophans. Protein association can be determined by binding of one or multiple tryptophan residues, an influence of flanking residues, and/or an influence of tryptophan spacing. With that, GW182 are important binding platforms that connect Ago proteins to a complex machinery that mediates deadenylation and translational repression.

1.3 Regulation of small RNA-guided gene silencing by post-translational modifications

Small RNA-guided gene silencing regulates numerous cellular processes. To facilitate adequate responses, the silencing machinery itself is subject to regulation, as already exemplified by the interdependence of Ago protein and small RNA expression (section 1.1.6). Another layer of regulation is added by post-translational modifications [4]. The following section covers post-translational modifications that affect miRNA biogenesis and function. First, it gives a short overview on known modifications of components that are involved in the biogenesis of small RNAs. Thereafter, phosphorylation of Argonaute proteins is covered in detail.

1.3.1 Post-translational modifications of miRNA biogenesis components

Drosha, the endonuclease that initiates miRNA biogenesis, is a nuclear protein. Its localization is ensured by phosphorylation of two serine residues in its N-terminal region and depends on GSK3β (glycogen synthase kinase 3β) [159, 160]. Furthermore, acetylation and ubiquitination occur in the same region and were reported to affect protein stability [161].

Another miRNA biogenesis factor, the Dicer binding partner TRBP, is also phosphorylated at several sites [162]. These modifications were found to increase stability of the Dicer-TRBP complex, resulting in enhanced miRNA generation and miRNA-mediated repression. TRBP is phosphorylated by the MKK1/Erk pathway and upon pathway activation, growth-promoting miRNAs seem to be selectively upregulated [162]. However, it is not clear how this additional level of regulation is achieved.

1.3.2 Post-translational modifications of Argonaute proteins

Argonaute proteins can be post-translationally modified in many ways, e.g. by phosphorylation, ubiquitination, hydroxylation, and methylation.

PIWI proteins of Drosophila, *Xenopus laevis*, and mouse are methylated in arginine-glycine (RG)-rich regions at their N-termini [163–166]. It was reported that this symmetric dimethyl arginine (sDMA) modification of arginine residues depends on protein methyltransferase 5 (PRMT5) [164]. The modification is necessary for the interaction with Tudor-domain containing proteins. Hence, it affects fundamental PIWI-specific functions such as transposon silencing, PIWI protein localization, or the identity of the small RNAs that are loaded to the proteins [163–166].

Several post-translational modifications have been identified for human Ago proteins. Whereas ubiquitination and sumoylation decrease protein stability [167, 168], hydroxylation of Ago2 positively regulates protein stability [169] (Fig. 1.4).

Ago2 hydroxylation at P700 depends on type I collagen prolyl-4-hydroxylase [C-P4H(I)] and has been validated by mass-spectrometric analysis of the endogenous protein [169]. C-P4H(I) is activated under hypoxic conditions when also Ago2 stabilization in pulmonary artery smooth muscle cells is observed, concomitant with positive effects on the expression of certain miRNAs and RISC activity in general [170].

In contrast, Ago proteins are destabilized by ubiquitination. Until now, the only described E3 ubiquitin ligase interacting with Ago is mLin41 (also known as Trim71) [167]. Ago2 ubiquitination has been observed in mouse embryonic stem cells [167], but not in another experimental system using neural progenitor cells [171]. It remains to be seen if mLin41/Trim71 affect Ago levels by ubiquitination or if these proteins predominantly act through different mechanisms such as translational repression or complementation of miRNA-mediated repression [172, 173]. However, ubiquitination is involved in Ago turnover [114, 127, 174], although autophagy mechanisms have also been reported [115, 175].

1.3.2.1 Phosphorylation of human Ago proteins

Due to its dynamic nature and its strong involvement in signaling pathways, phosphorylation is the most investigated post-translational modification. Several sites of Ago2 have been reported to be phosphorylated and affect for example protein stability or small RNA binding (Fig. 1.4) [4, 176]. Among them is S387. Phosphorylation of this site has been shown to promote localization of Ago2 to processing bodies, cytoplasmic foci involved in RNA turnover [177]. S387 phosphorylation depends on activation of the p38 MAPK pathway, in particular on MAPKAPK2 [177]. Another study identified the kinase Akt3 and hypothesized that S387 phosphorylation decreases the amount of target cleavage compared to translational repression [178]. Irrespective of its cellular function, phosphorylation of S387 seems to be a common post-translational modification which is present under standard growth conditions and can be increased in response to cellular stresses [177].

Several phosphorylated sites were identified by mass-spectrometric analysis of overexpressed and immunopurified Ago2 [179]. Remarkably, the study by Rüdel *et al.* included already known modification sites (e.g. pS387) as well as sites that were confirmed in later investigations (e.g. pY393). Simultaneously, this work identified Y529 as a modification site and showed that phosphorylation at this position interferes with small RNA binding [179]. The same site was characterized in another study, which focused on activated mammalian macrophages [180]. Here, phosphorylation of Y529 was suggested to facilitate the dynamic exchange of Ago2-bound miRNAs, consequently relieving the repression of certain targets and enabling the expression of proinflammatory genes [180].

Finally, phosphorylation of Y393 occurs under hypoxic conditions and depends on the kinase activity of

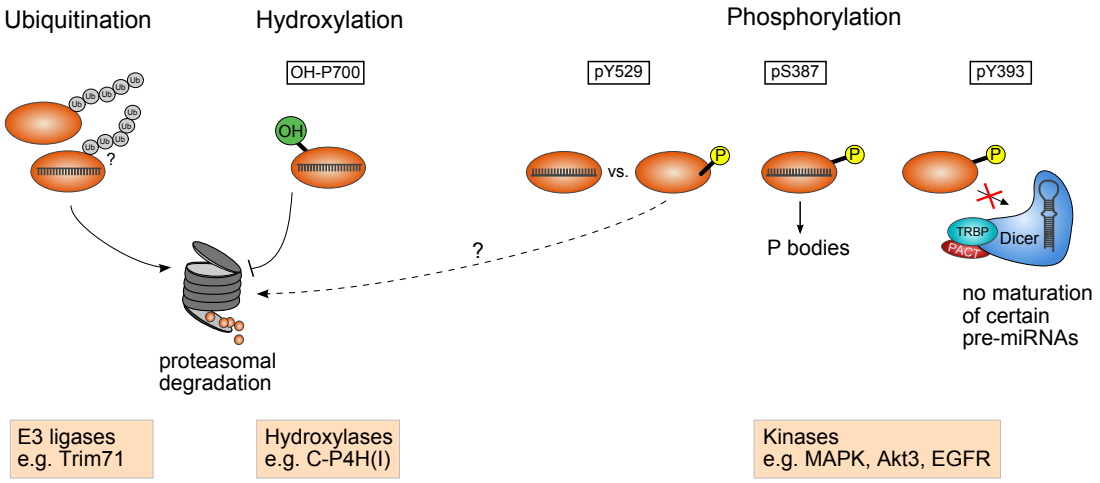

Figure 1.4: Post-translational modifications of human Ago2. Summary of ubiquitination, hydroxylation, and phosphorylation events that affect human Ago2. Proposed functions of the different modifications and modifying enzymes are indicated. Adapted from [4, 113].

EGFR [181]. Phosphorylation of this residue decreases the interaction with Dicer and affects maturation and loading of certain miRNAs termed 'mHESM' (miRNAs regulated by hypoxia-dependent EGFR-suppressed maturation) [181]. These miRNAs have tumor-suppressive function and their precursors have a large loop structure in common, suggesting that this specific feature decides on differential maturation and loading ability in a complex of Ago2 (pY393) and Dicer. Importantly, Y393 phosphorylation is enriched in hypoxic tumor areas and correlates negatively with survival rates of breast cancer patients [181].

Table 1.1 gives an overview on the described phosphorylation sites, their proposed function, and on the methods used to detect these modifications.

On the structural level, the influence of the described modification sites cannot be explained to full extent. Fig. 1.5 illustrates the position of the known and characterized phosphorylation sites. S387 and Y393 are located in the second linker region (L2), which is in close proximity to the N-terminal domain of Ago2 (Fig. 1.5 A). Since Dicer interaction is decreased in Y393 phospho-mimicking mutants, this region was suggested to be part of the binding surface. However, Dicer is known to bind to a particular region in the Ago PIWI domain termed 'PIWI box' [182] and it is structurally not clear how the Y393 modification affects this interaction, especially how it selectively inhibits maturation of longer loop precursors [181].

Y529 is located within the 5' binding pocket formed by the Mid domain (Fig. 1.5 B). The 5' nucleotide of the bound small RNA stacks to Y529. Since the hydroxyl group of this amino acid is oriented towards the 5' phosphate of the first guide nucleotide, a phosphorylation of this residue was suggested to induce electrostatic repulsion and thus prevent small RNA binding [179].

S387 and Y393 are located at the protein surface and would therefore be easily accessible by a kinase. However, Y529 is buried inside the protein in a pocket usually occupied with the small RNA (Fig. 1.5 A). It is questionable if this residue can be accessed by any kinase or if alternative phosphorylation mechanisms exist [179].

Table 1.1: Overview on known phosphorylated sites of Ago2. The position of the phosphorylated site, its proposed function, and the used detection methods are summarized.

site	ref.	proposed function	PTM identification and validation
pS387	[177]	localization	IP of FLAG/HA-Ago2 and MS analysis *in vitro* phosphorylation assay pS387-specific antibody
pS387	[179]	(localization)	IP of FLAG/HA-Ago2 and MS analysis
pS387	[178]	switch from target cleavage to translational repression	pS387-specific antibody
pY393	[179]	unknown	IP of FLAG/HA-Ago2 and MS analysis
pY393	[181]	Dicer binding, miRNA processing	IP of FLAG-Ago2 and MS analysis *in vitro* kinase assays pY393-specific antibody
pY529	[179]	miRNA binding	IP of FLAG/HA-Ago2 and MS analysis IP of endogenous Ago2 with pY-specific antibody
pY529	[180]	(miRNA binding)	IP with pY-specific antibody phospho-mimicking and non-phosphorylatable mutants
pS253, pT303, pT307, pS798	[179]	unknown	IP of FLAG/HA-Ago2 and MS analysis

1.3.2.2 Modifying enzymes and signaling pathways

There is an increasing number of studies that link post-translational modifications to cellular cues, signaling, and disease. For example, a connection between RAS-induced senescence, Ago2, and the miRNA machinery has been identified recently [183]. Here, the cysteine-containing catalytic center of protein tyrosine phosphatase 1B (PTP1B) was shown to be oxidized by RAS^{G12V}-induced ROS signaling. This results in inactivation of the phosphatase and specific enrichment of Y393-phosphorylated Ago2. Similar to the work of Shen *et al.* [181], this study could also show decreased Dicer interaction and miRNA binding of a pY393-mimicking mutant [183]. Among the less expressed miRNAs are several miRNAs targeting the oncogene p21. The authors suggest that constitutive pY393 phosphorylation results in an altered miRNA expression profile and de-repression of the senescence-mediating p21, which would provide a link between ROS signaling and senescence [183]. Interestingly, this pathway does not involve activation of a kinase, but inactivation of a phosphatase.

Signaling pathways affect the small RNA machinery not only by direct modification of its components. As an example, the Hippo pathway accounts for elevated miRNA levels in response to increased cell density via a rather indirect mechanism [184]. Hippo signaling is inactive at low cell densities. A cofactor of the Microprocessor complex, p72, interacts then with YAP (Yes-associated protein), which is retained in the nucleus. Maturation of p72-responsive miRNAs is inefficient under these conditions. After pathway activation and phosphorylation, YAP localizes to the cytoplasm. Hence, p72 is accessible for Microprocessor accessory function and miRNA processing is promoted [184]. Importantly, the interaction of p72 and YAP

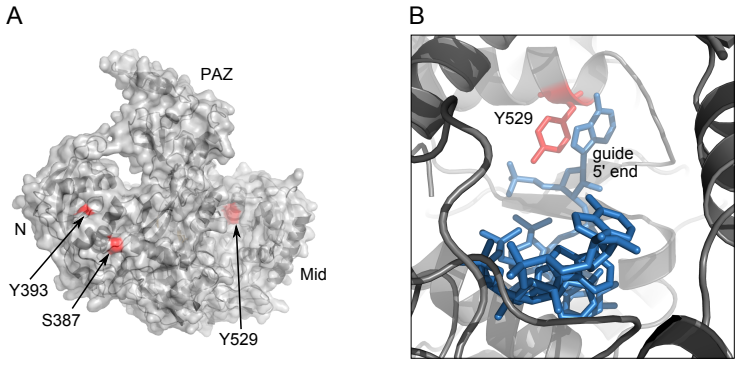

Figure 1.5: Localization of known phosphorylation sites of Ago2 (A) The position of known phosphorylation sites is shown in the structure of human Ago2 (PDB IP 4OLA, [58]). (B) Close-up view of the 5' binding pocket of human Ago2. Y529 is shown in red and the bound guide RNA is shown in blue.

is increased in YAP-dependent tumors.

Interestingly, Ago degradation during T cell activation depends on PI3K/mTOR signaling, suggesting a functional link between the phosphorylation and ubiquitination machineries [127].

Hypoxia and high cell density are extreme conditions. Numerous mechanisms may exist to adapt cells to these and other conditions, be it by fine-tuning one of the pathways described here or by exploiting completely different, yet uncharacterized post-translational modifications.

In addition, most studies so far focused on phosphorylation of human Ago2. Hardly anything is known about its paralogues Ago1, Ago3, and Ago4. Do these proteins underly similar regulation mechanisms? Or would a paralogue-specific modification confer specific functions to one of the Ago family members?

Aim of this thesis

Ago proteins take a central role in post-transcriptional gene silencing. They associate with small non-coding RNAs, which provide them with specificity and guide them to target RNAs. Some Ago proteins are endonucleolytically active and can cleave their targets. Furthermore, Ago proteins recruit additional factors and thereby mediate translational repression and target destabilization.

One requirement for Ago cleavage function is the presence of a defined catalytic tetrade in the active center of the proteins. Still, the presence of these four residues is not always sufficient to mediate endonucleolytic cleavage, as exemplified by human Ago3. By a detailed analysis of the inactive human Ago proteins (Ago1, Ago3, and Ago4), this thesis aimed at identifying additional requirements, which affect the endonucleolytic function of human Ago proteins.

Since Ago proteins are part of a powerful regulation machinery, it is essential to understand how these proteins are regulated themselves. Regulation is often achieved by post-translational modifications and also human Ago proteins are post-translationally modified. However, only few sites are known and most of these were detected using overexpressed Ago proteins. Therefore, a second focus of this thesis is the mass-spectrometric identification of endogenous post-translational modifications, in particular the identification of phosphorylations. Potential phosphorylation sites should be subjected to a first characterization in terms of accessibility, cross-species conservation, and functionality.

The mass-spectrometric analysis of post-translational modifications requires large amounts of material, which can hardly be provided by antibody-based approaches. Therefore, a better tool for the isolation of Ago proteins was to be established and characterized.

2. Results

2.1 Analysis of human Argonaute cleavage activity

Of the human Ago protein family members, Ago2 is the only protein with slicer activity. It is known that this endonucleolytic activity resides in the PIWI domain, which resembles an RNase H-like fold. It has also been shown that three catalytic residues (DDH) within this domain determine cleavage activity. Interestingly, a fourth catalytic residue was identified and extends the catalytic center to a tetrad of DEDH. Although these residues are present in the Ago3 PIWI domain, Ago3 is not an endonuclease. Here, minimal regions of human Ago3, Ago1, and Ago4 were substituted by the respective Ago2 sequences to investigate additional factors that determine cleavage activity.

2.1.1 The Argonaute N domain affects cleavage activity

First, chimeras of Ago2 and Ago3 were designed and tested for slicer activity. Therefore, FLAG/HA-tagged Ago mutants were expressed in HEK 293T cells, subjected to an α-FLAG immunoprecipitation (IP), and incubated with a radiolabeled target RNA fully complementary to endogenous miR-19b. In a first approach, increasing portions of Ago3 were fused to Ago2 and tested in the described *in vitro* assay (Fig. 2.1 A).

Interestingly, a chimera containing the Ago3 PIWI domain is able to cleave the target RNA (Fig. 2.1 B, lane 7), indicating that the factor inactivating Ago3 slicing function is located beyond the PIWI domain. Analysis of the other chimeras showed that—although MutB and MutC have weaker cleavage activities—even a mutant containing only the first 170 N-terminal amino acids of Ago2 is able to cleave the target RNA (Fig. 2.1 B, lane 12).

The amino acid sequences of human Ago1–4 are generally very similar, but their N-terminal regions show relatively high divergence. Ago3 differs from the other Agos at two main sites: first, the very N-terminal part of Ago3 is shorter than that of Ago1 or Ago2. Second, there is an Ago3-specific insertion of eight amino acids (Fig. 2.2A). To further narrow down sequence elements that affect Ago slicer activity, different Ago3 N-terminal mutants were designed and tested (Fig. 2.2B). Adjustment of the very N-terminal part to the sequence present in Ago2 did not affect cleavage function (Fig. 2.2). A combination of this mutant with a deletion of the Ago3-specific insertion did also not affect endonucleolytic activity. In the next step, both regions were extended. This systematic analysis revealed that amino acids 1-64 and 137-160 facilitate Ago3 cleavage function when substituted by the according Ago2 sequence (Fig. 2.2). Importantly, adjustment of only the first region does not suffice to render Ago3 cleavage-active (data not shown).

Hence, Ago cleavage function is not only defined by the PIWI domain, which harbors the catalytic center. Two short sequence elements in the N domains of human Ago2 and Ago3 are implicated in slicing as well.

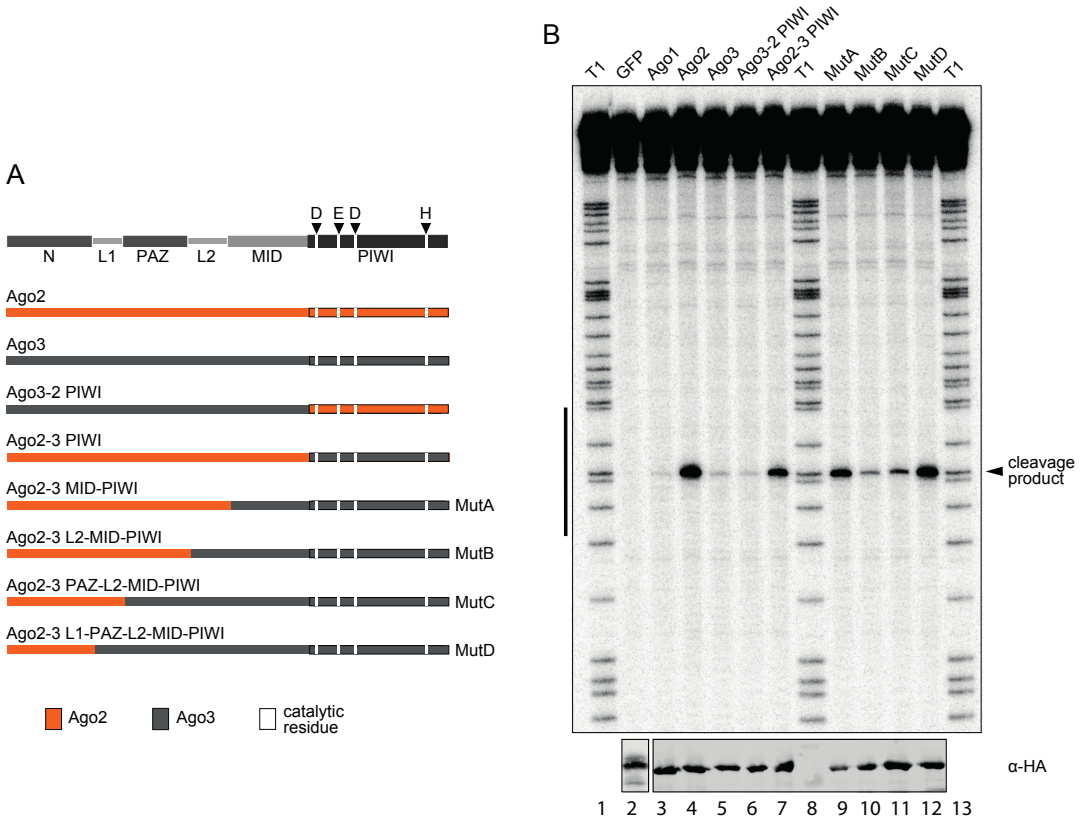

Figure 2.1: The Ago3 N domain affects cleavage function. (A) An increasing portion of Ago3 was fused to Ago2 to identify regions important for slicer function. General domain organization, location of the catalytic residues, and Ago2/Ago3 wild type features are shown on top. (B) FLAG/HA-tagged Ago1-3 wild type constructs and Ago2-3 chimeras were expressed in HEK 293T cells, immunoprecipitated, and assayed for slicer function using a radioactively labeled target RNA complementary to the co-precipitating endogenous miR-19b. 'T1' indicates a partial RNAse T1 digest of the cap-labeled target RNA. The black bar to the left represents the region of the target RNA complementary to miR-19b. The cleavage product is indicated by an arrow. A part of the immunoprecipitated proteins was used for Western Blotting to ensure equal transfection and IP efficiency.

2.1.2 Cluster 2 is an additional PIWI domain feature that defines cleavage activity

In contrast to Ago3, Ago1 does not comprise a complete catalytic tetrade in its PIWI domain (Fig. 2.3 A, B). Surprisingly, introduction of the fourth catalytic residue did not activate Ago1 cleavage function (Fig. 2.3 C, lane 3). To investigate the Ago1 PIWI domain independently of the other Ago1 domains, it was fused to the Ago2 N-PAZ-Mid module which has been shown to support slicer function (Fig. 2.1, Ago2–3 PIWI). Adjustment of the catalytic tetrade in this Ago2–1 chimera did also not affect slicer activity, suggesting that other features in the Ago1 PIWI domain interfere with slicing (Fig. 2.3 C, lane 5). The alignment of the Ago1–4 PIWI domains revealed two regions that differ from the sequences present in the cleavage-competent PIWI domains of Ago2 and Ago3, cluster 1 and cluster 2 (Fig. 2.3 A, gray). Interestingly, these regions either contain or are in close proximity to one of the catalytic residues E635 and D667 in Ago1. Whereas changing cluster 1 to the sequence present in Ago2 did not affect the chimera's cleavage activity,

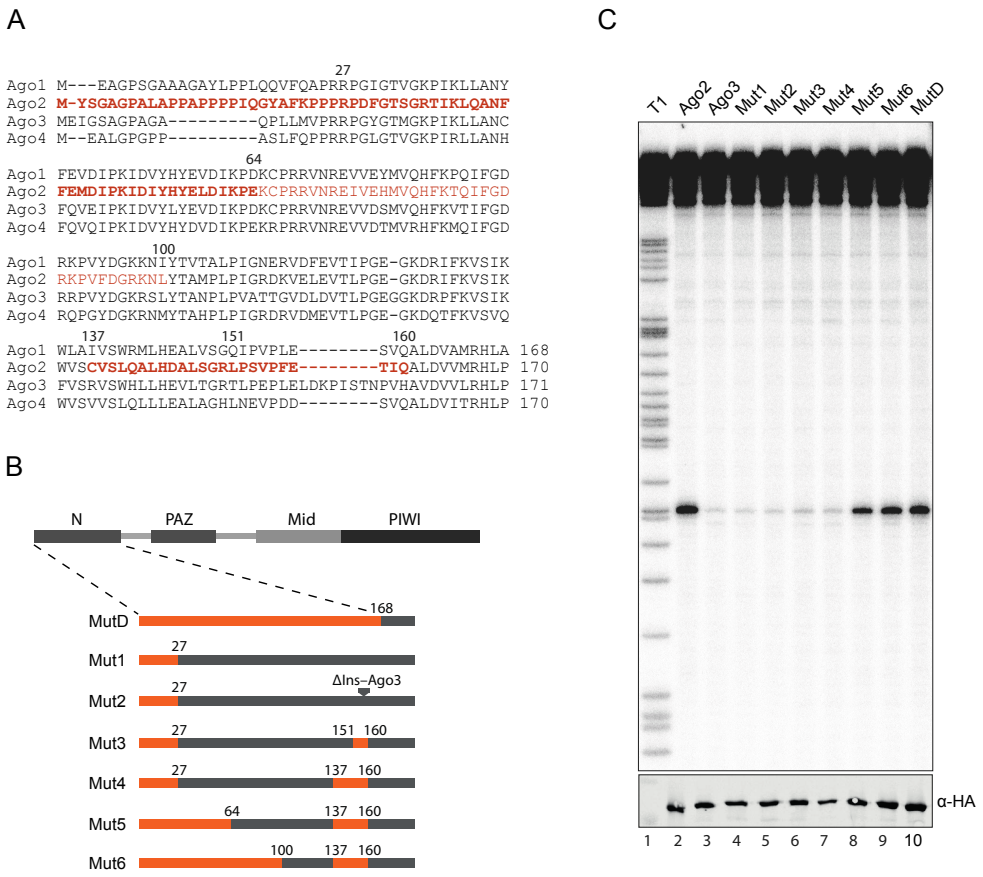

Figure 2.2: Cleavage activity of Ago3 N-terminal mutants. (A) Alignment of the N domains of Ago1–4. Chimeric borders are indicated by numbers according to the Ago2 sequence. Substituted sequences are shown in red. Minimal sequence elements defining cleavage function are shown in bold red. (B) Schematic overview of Ago3 mutants with N-terminal deletions and substitutions. Only the N-terminal parts of the protein chimeras are shown. (C) Ago3 N-terminal mutants were tested for slicer activity as described in Fig. 2.1.

alteration of cluster 2 restored it to wild type levels (Fig. 2.3).

2.1.3 An additional insertion in the Ago4 PIWI domain prevents slicing function

Ago4 shows the strongest sequence variation among the highly conserved human Agos. Instead of the catalytic tetrade DEDH, Ago4 comprises the residues DEGR (Fig. 2.4 A, B). To test whether this is the only feature obstructing its slicer activity, the Ago4 PIWI domain was fused to the N-PAZ-Mid module of Ago2 and the catalytic tetrad was restored (Fig. 2.4 B). Introduction of the catalytic residues did not activate Ago4 PIWI slicer function (Fig. 2.4 C, lane 2). At amino acid sequence level, the Ago4 PIWI domain differs from the PIWI domain of Ago2 at two more sites: first, Ago4 harbors a ten amino acids long insertion

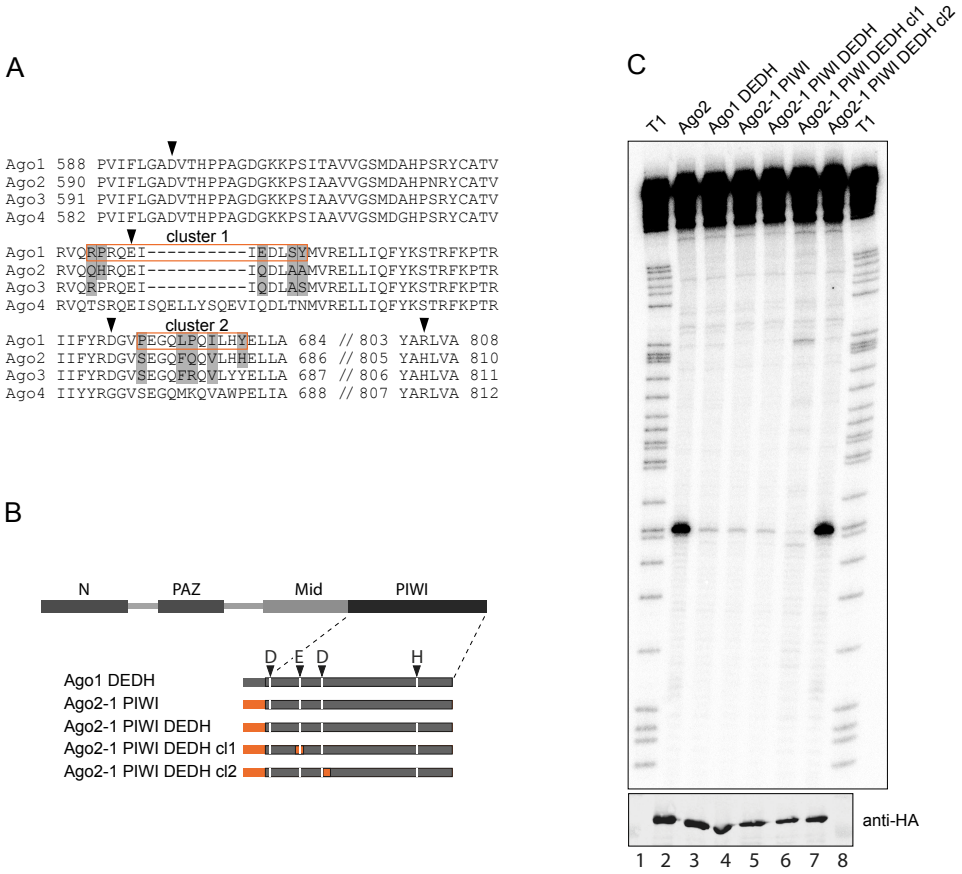

Figure 2.3: Cleavage activity of the Ago1 PIWI domain. (A) Partial alignment of the PIWI domains of Ago1–4. The positions of catalytic residues are indicated by black triangles. Clustering Ago1 residues that differ from the residues of cleavage-compatible Ago2 and Ago3 are shown in gray. Cluster 1 and cluster 2 are highlighted. (B) Schematic overview of the Ago1 PIWI mutants. Only the PIWI-containing parts of the proteins are shown. (C) Slicer function of Ago1 PIWI mutants was tested in a cleavage assay as described in Fig. 2.1

that is not present in the other Agos. Second, the Ago4 sequence at cluster 2 (which has been identified to affect Ago1 slicer function) differs also from Ago2 (Fig. 2.4 A). Deletion of the Ago4-specific insertion or adjustment of the cluster 2 sequence alone did not activate the Ago4 PIWI domain (Fig. 2.4 C, lanes 3 and 4). When both alterations were combined, cleavage activity of the Ago4 PIWI domain reached Ago2 wild type levels (Fig. 2.4 C, lane 5).

To investigate how cluster 2 and the Ago4-specific insertion might affect slicer function, homology models of Ago1 and Ago4 were built on the basis of the human Ago structures published at that respective time. For the Ago1 homology model, this included only structural information on Ago2, but Ago1 and Ago2 structures could be used for Ago4 homology modeling [58, 59, 61, 62].

A comparison of the catalytic centers of both proteins shows that Ago1 comprises a shortened helix at a position where Ago2 is characterized by a kinked helix (Fig. 2.5 A, cluster 2 of Ago1 shown in orange). This was also verified by secondary structure content analysis by means of the algorithm DSSP (Define Secondary Structure of Proteins), which uses structural information of a protein or homology model to

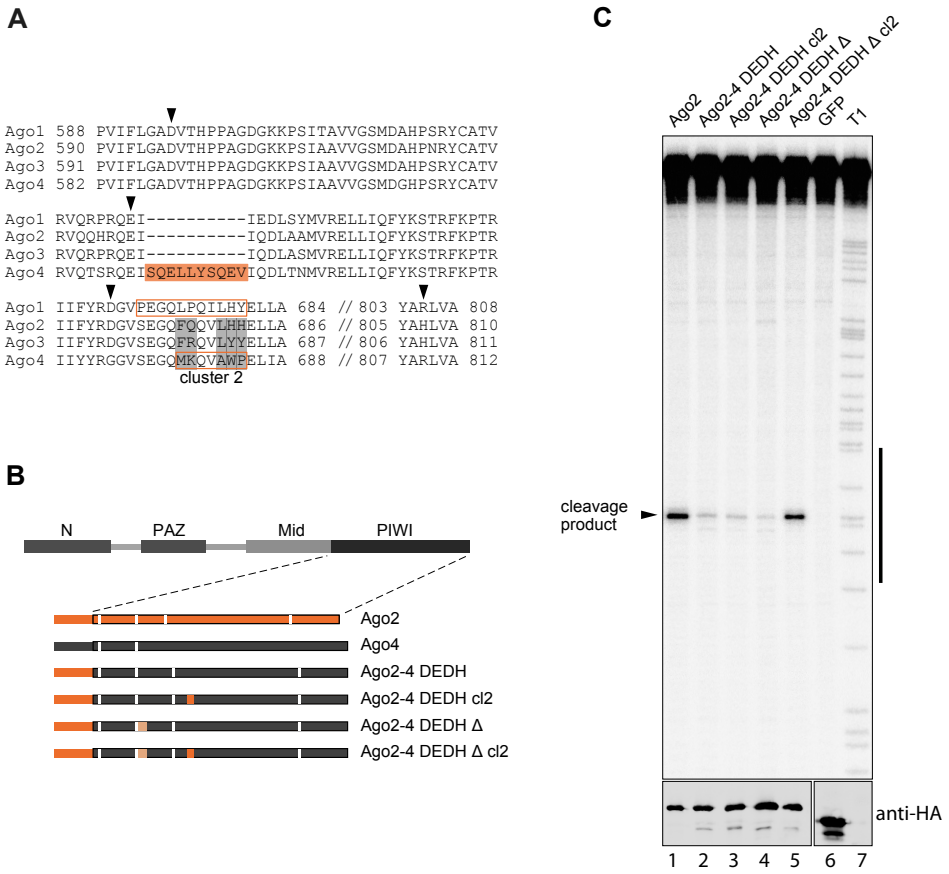

Figure 2.4: Cleavage activity of the Ago4 PIWI domain. (A) Partial alignment of the Ago1–4 PIWI domains. The positions of catalytic residues are indicated by black triangles. Ago4 comprises a specific insertion of ten amino acids, highlighted in orange. The variant region corresponding to cluster 2 of Ago1 is boxed, varying amino acids are shown in gray. (B) Schematic overview of the Ago4 PIWI mutants. Only the PIWI-containing parts of the proteins are shown. Deletions are indicated by light orange color. (C) A cleavage assay of the Ago4 PIWI mutants was conducted as described in Fig. 2.1

assign secondary structure [185][1]. Since cluster 2 is located close to the catalytic residue D669 (D667 in Ago1), it might be possible that secondary structure changes in that region induce a mis-alignment of the catalytic center and thus prevent target cleavage.

Additionally to cluster 2, the Ago4 PIWI domain bears a specific insertion of ten amino acids length that obstructs slicer function (Fig. 2.4). In this case, the homology model reveals that the insertion forms a loop adjacent to E637 (E629 in Ago4) (Fig. 2.5 B). This residue has been identified to extend the catalytic triad to a tetrade in Ago of the yeast *Kluyveromyces polysporus* and is located on a so-called 'glutamate finger' [60]. Here and in *Neurospora crassa* and *Thermus thermophilus*, the glutamate finger was shown to exist in two different conformations that depend on target binding and facilitate cleavage activity [60]. Although the inactive, 'plugged-out' conformation has not been identified in other eukaryotic Agos [60], it is most likely that the Ago4-specific insertion in this region affects positioning of the catalytic residues and/or intramolecular rearrangements upon target binding.

[1] contributed by Prof. Dr. Rainer Merkl, University of Regensburg

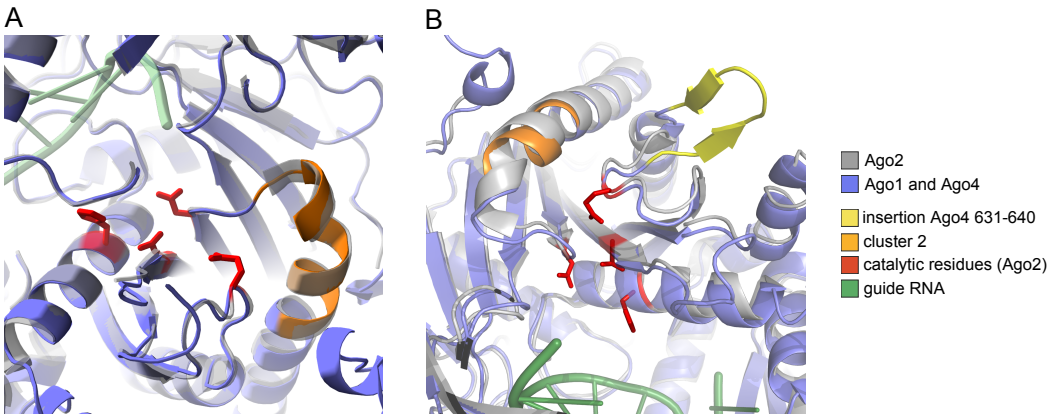

Figure 2.5: Comparison of the catalytic centers of Ago1, 2, and 4. (A) An overlay of the catalytic centers of Ago2 (based on PDB 4OLA [58]) and Ago1 is shown. For Ago1 representation, a homology model calculated on the basis of the published Ago2 structures [58, 59] was used. (B) The catalytic centers of Ago2 and Ago4 are depicted in a different view. Here, the Ago4 homology model was built on basis of all human Ago structures published by then, including structural information on Ago1 [58, 59, 61, 62].

2.1.4 The N-terminal domain affects cleavage activity of Ago1 and Ago4

Surprisingly, neither the activated Ago1 nor the activated Ago4 PIWI domain were able to cleave in the full-length context of the individual proteins [Fig. 2.6 A (lane 4) and B (lane 3)]. Since two short sequence elements in the N-terminal domain of Ago3 had been identified to influence cleavage function (Fig. 2.2), N-terminal changes were also applied to Ago1 and Ago4. In both proteins, substitution of the complete N-terminal part with the Ago2 sequence showed that this region indeed affects cleavage activity [Figs. 2.6 A (lane 5) and B (lane 6), Fig. 2.6 C]. When only the first of the two sequence elements identified in Ago3 was changed in Ago1, this activity was maintained [Figs. 2.6 A (lane 6) and 2.6 C]. This indicates that the second sequence element, mainly characterized by an Ago3-specific insertion, might also be an Ago3-specific feature (Fig. 2.6 D).

To more precisely characterize cleavage-determining regions, a set of N-terminal mutants was analyzed for Ago4 (Fig. 2.6 C). In contrast to Ago1, substitution of only the first N-terminal sequence element did not completely support cleavage function (Fig. 2.6 B, lane 7), but combination with the second sequence element raised the activity to wild type levels (lane 8). Comparable endonucleolytic activity was detected when the first N-terminal region was shortened, finally encompassing an only five amino acids long 'FFEMD' motif, which also had been shown to affect Ago3 cleavage function (lanes 8–11) [186]. Still, reduction of the second sequence element or substitution of this element alone did not completely support Ago4 endonucleolytic activity (lanes 12 and 13). Different from Ago3, Ago4 does not comprise an insertion in this region, underscoring that not the Ago3-specific insertion alone obstructs cleavage activity (Fig. 2.6 D).

2.1.5 Ago cleavage mutants can unwind miRNA duplexes

The high sequence similarity of the four human Argonaute proteins supports the creation of functional chimeras. Still, the implemented changes could affect Ago structure and function beyond endonucleolytic activity. To exclude that loss of cleavage activity is caused by altered miRNA binding, the individual mutants were tested for their miRNA binding ability. Therefore, FLAG/HA-tagged Ago mutants were

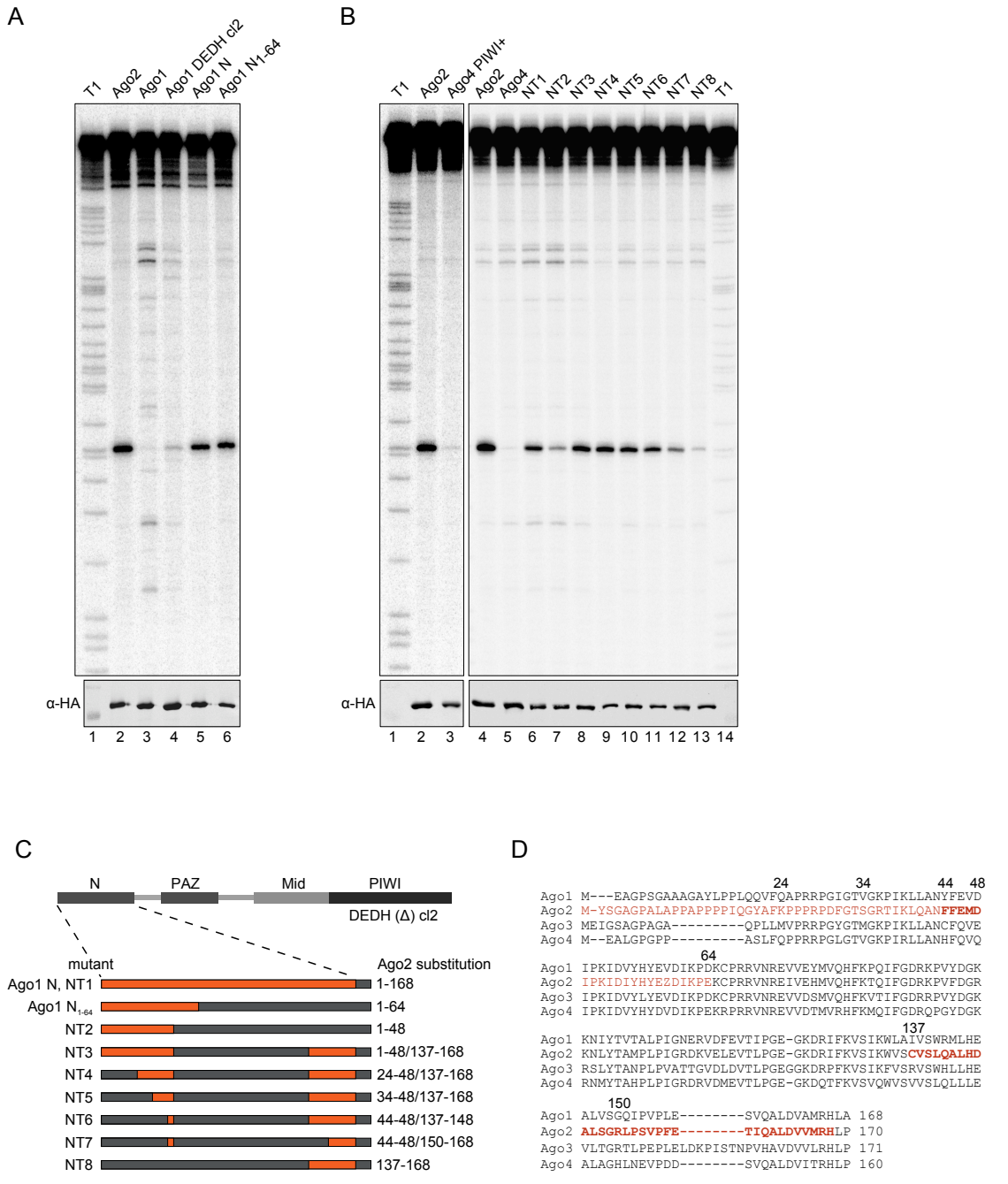

Figure 2.6: The N-terminal domain affects Ago1 and Ago4 cleavage activity. (A, B) Full length Ago1 (A) and Ago4 (B) mutants harboring cleavage-compatible PIWI domains were tested for cleavage activity as described in Fig. 2.1. The activated PIWI domains of Ago2-1 PIWI DEDH cl2 (for Ago1, cf. Fig. 2.3) and Ago2-4 DEDH Δ cl2 (for Ago4, cf. Fig. 2.4) were used. (C) Schematic overview of Ago1 and Ago4 N-terminal mutants. Only the N-terminal parts of the chimeric proteins are shown. (D) Alignment of the Ago1–Ago4 N-terminal domains. Substituted sequences are highlighted in red within the Ago2 sequence. The minimal substitutions necessary for Ago4 activation are shown in bold red. Numbering of the substitution borders is based on the Ago2 sequence.

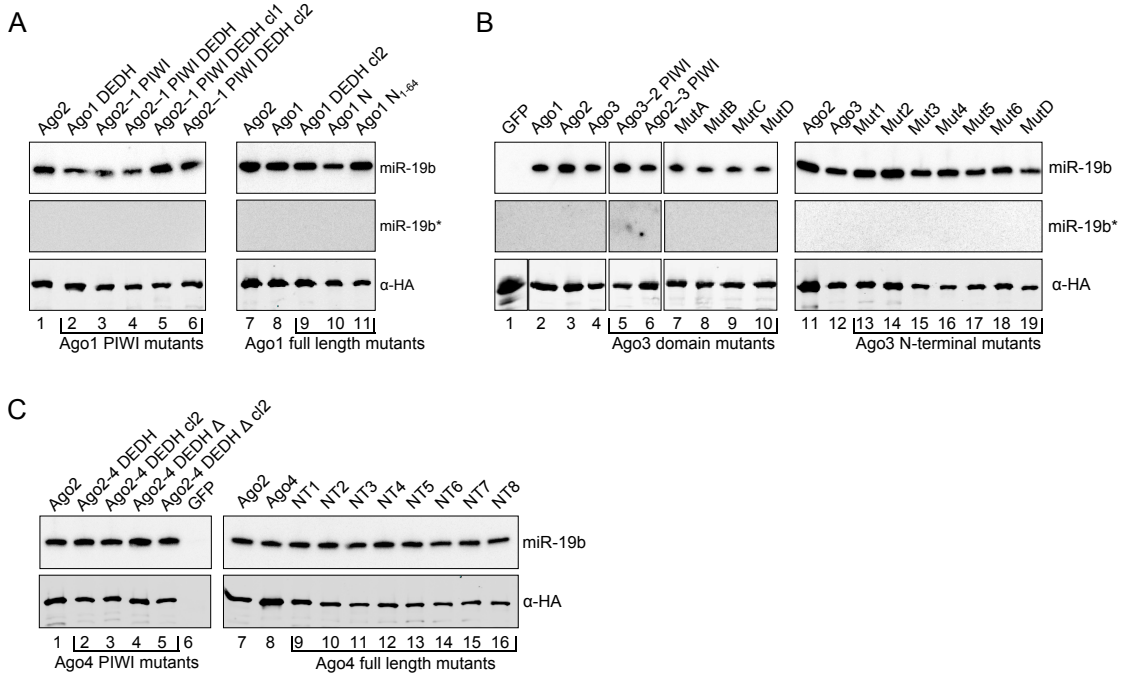

Figure 2.7: All Ago cleavage mutants bind miR-19b. FLAG/HA-tagged Ago mutants were transfected into HEK 293T cells and immunopurified by FLAG-IP. Co-purifying endogenous miR-19b and miR-19b* were analyzed by Northern Blotting. Protein expression and IP efficiency were controlled for by Western Blotting. (A) miRNA binding of the Ago1 PIWI and full length mutants shown in Figs. 2.3 and 2.6. (B) miRNA binding of the Ago3 domain and N-terminal mutants shown in Figs. 2.1 and 2.2. (C) miRNA binding of the Ago4 PIWI and N-terminal mutants shown in Figs. 2.4 and 2.6.

expressed in HEK 293T cells and immunopurified. Associated RNA was isolated and analyzed by Northern Blotting. As cleavage assays had been conducted with endogenously co-precipitating miR-19b, this miRNA was also detected here. Importantly, all Ago mutants associate with miR-19b (Fig. 2.7). miR-19b* was not detectable in any of the analyzed Ago IPs (Fig. 2.7 A and B), showing that the cleavage-inactive mutants are also able to unwind the loaded RNA duplex.

2.1.6 Catalytically active human Agos rescue miR-451 processing in Ago2-deficient mouse embryonic fibroblasts

One major function of human Ago2 is the processing of non-canonical miR-451. To test whether any catalytically active Ago protein can fulfill this function or whether a specific function of Ago2 is required, catalytically activated Ago1, 3, and 4 (Fig. 2.8 A) were assayed for miR-451 processing in Ago2-deficient mouse embryonic fibroblasts (MEF Ago2 $^{-/-}$). The cells were co-transfected with miR-451 and the different Ago constructs. The mutants 'Ago1 N_{1-64}' (Fig. 2.6 A), 'Mut5' (Fig. 2.2 C), and 'NT6' (Fig. 2.6 B) were used as catalytically active Ago1, 3, and 4. Total RNA was extracted and analyzed for miR-451 processing by Northern Blotting (Fig. 2.8 B). These experiments demonstrate that all cleavage-active Ago proteins can

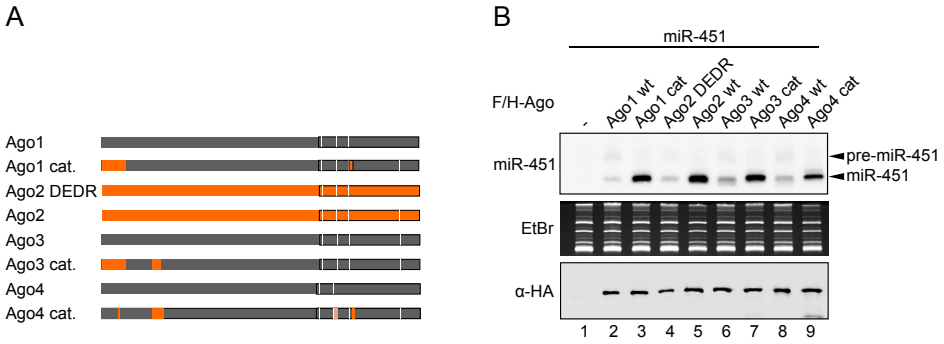

Figure 2.8: Catalytically active Ago proteins rescue miR-451 processing in Ago2-deficient MEFs. (A) Schematic overview of catalytically active and inactive Ago proteins. (B) MEF Ago2 $^{-/-}$ were co-transfected with miR-451 and FLAG/HA-tagged Ago constructs, total RNA was isolated and assayed for miR-451 processing by Northern Blotting. RNA loading and quality was controlled by Ethidium Bromide (EtBr) staining. Equal transfection efficiency and protein expression was verified by immunopurification of the FLAG-tagged Agos and Western Blotting from the same samples.

process pre-miR-451 (Fig. 2.8 B, lanes 3, 5, 7, and 9). The signal of mature miR-451 cannot be detected for wild type Ago1, 3, and 4, which are catalytically inactive (lanes 2, 6, and 8). Mature miR-451 is also not detectable in engineered cleavage-deficient Ago2, which has an incomplete catalytic tetrad (lane 4). The detection of weak bands at the height of mature miR-451 in non-slicer samples is most likely due to Ago overexpression effects as it is not present without co-transfected protein (lane 1). These results indicate that slicer function alone is sufficient for miR-451 processing.

Here, it was shown that catalytically inactive human Ago proteins can be turned into endonucleolytic enzymes by sequence changes in their N domain (Ago3) or in their N and PIWI domains (Ago1 and Ago4). This illustrates how paralogous proteins can adopt different functions on basis of their amino acid sequence. However, functionalization is also possible at the post-translational level. It is well known that post-translational modifications can influence protein properties, thereby enabling one protein to fulfill different functions. In the context of characterizing human Ago proteins, the endogenous proteins were analyzed for post-translational modifications. As part of that, a new Ago purification strategy was established and emerged as a powerful tool for the general characterization of Ago proteins. This novel approach is characterized in the following section.

2.2 Ago-APP: Ago Affinity Purification by Peptides

The binding of Ago to the human GW182 proteins TNRC6A, -B, and -C relies on interactions with tryptophans in the N-terminal half of the GW182 protein (cf. section 1.2). The exact region of Ago binding was investigated by means of a peptide screen, which assayed overlapping peptides of the TNRC6B N-terminal part for binding to human Ago2 [112]. This screen identified three major regions as interaction hot spots (Fig. 2.9, [112]). Ago2 interacted strongly with a peptide containing one of these high affinity binding sites, TNRC6B$_{599\text{-}683}$ (termed 'T6B'). This raised the question whether recombinant, GST-tagged T6B could precipitate endogenous Ago proteins. The interaction of Ago and GW proteins is conserved within and across species, implying that such a peptide purification strategy could be used as a multi-functional tool.

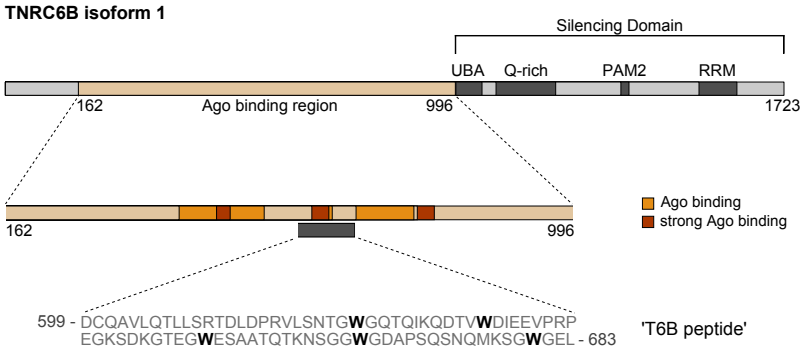

Figure 2.9: Identification of a strong Ago-binding region in human TNRC6B. A peptide screen identified several regions in the TNRC6B N-terminal half that mediate Ago binding [112]. The amino acid sequence of the best Ago-interacting peptide (TNRC6B$_{599\text{-}683}$, 'T6B') is shown and tryptophans are set bold.

2.2.1 A short TNRC6B peptide precipitates Ago proteins

In a first approach, a conventional immunopurification of endogenous Ago2 was compared to a GST pull down that used recombinant GST-tagged T6B with gluatathione sepharose beads. Indeed, the peptide-based approach precipitates endogenous Ago2 as efficiently as an Ago2-IP does (Fig. 2.10 A). Different from an Ago2-IP, also a substantial amount of endogenous Ago1 is precipitated (Fig. 2.10 A).

To be able to apply standard tools that are based on α-FLAG purifications, an N-terminal FLAG tag was fused to GST-tagged T6B. FLAG-GST-T6B can be used with either FLAG or glutathione beads and precipitates endogenous Ago2 as well as the GST-tagged peptide does (Fig. 2.10 B, compare lanes 8, 10, and 11). A mutant version of the peptide, which lacks all tryptophan residues ('T6B mutant') cannot precipitate Ago2 (lanes 7 and 9). Notably, the electrophoretic mobility of wild type and mutant T6B differs a lot, although the proteins vary only slightly in their molecular weights (compare FLAG signal in lanes 7 and 8).

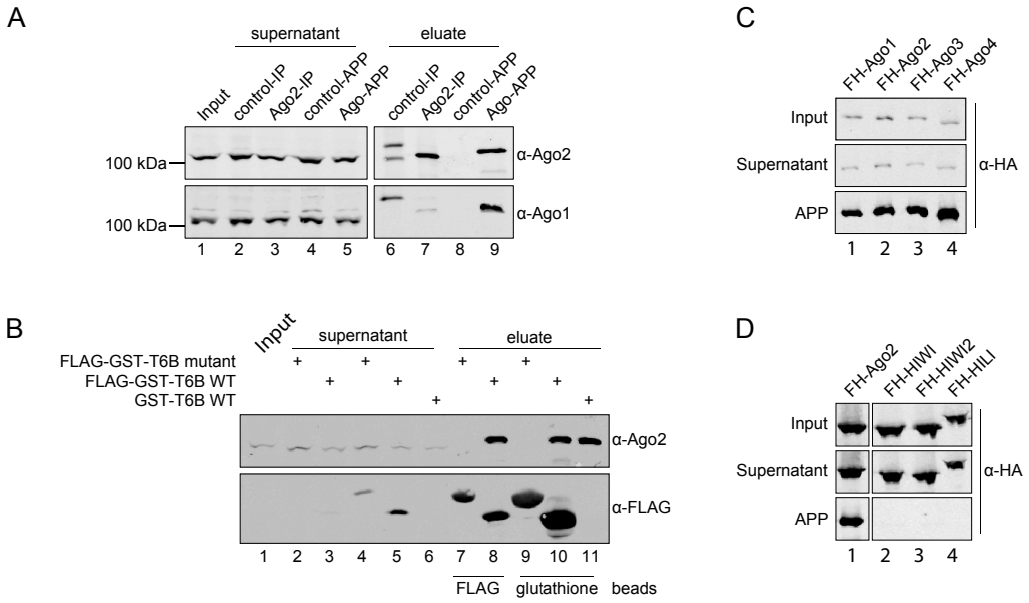

Figure 2.10: GST-T6B precipitates human Ago1–4. (A) Comparison of Ago2-IP and Ago-APP. A monoclonal antibody against human Ago2 was coupled to Protein G Sepharose beads and a recombinant GST-T6B peptide was coupled to glutathione beads. An unrelated antibody against Rmc and recombinant GST were used for control-IP and -APP. The coupled beads were washed to remove excess antibody and peptide, incubated with HeLa cell extract prepared in NET buffer, and eluted with Laemmli buffer. Ago1 and Ago2 were detected by immunoblotting. (B) Ago-APP and immunoblotting using a FLAG-GST-T6B peptide and a control peptide where all tryptophans were mutated to alanines ('T6B mutant'). FLAG- and glutathione beads were used and GST-T6B was included as a control. (C) Ago-APP from HEK 293T cells overexpressing FLAG/HA-tagged Ago1–4. Different amounts of the extracts were used to compensate for differential Ago expression. (D) Ago-APP from HEK 293T cells overexpressing the FLAG/HA-tagged human PIWI proteins HIWI, HIWI2, and HILI. Ago2 was included as a positive control.

Next, the interaction of GST-T6B with all human Ago proteins was investigated. Therefore, FLAG/HA-tagged Ago and PIWI proteins were expressed in HEK 293T cells and precipitated by the peptide purification approach. Differential expression of Ago1–4 was compensated for by using different amounts of lysate. Indeed, human Ago1–4 can be precipitated by GST-T6B (Fig. 2.10 C). Notably, all four proteins seem to be enriched to the same extend, suggesting that the T6B interaction is well-conserved and does not discriminate between different Agos. In contrast to that, human PIWI proteins are not precipitated by Ago-APP (Fig. 2.10 D).

The novel Ago purification strategy introduced here represents a favorable alternative to antibody-based approaches. Hereafter, it is referred to as 'Ago Affinity Purification by Peptides' ('Ago-APP').

A

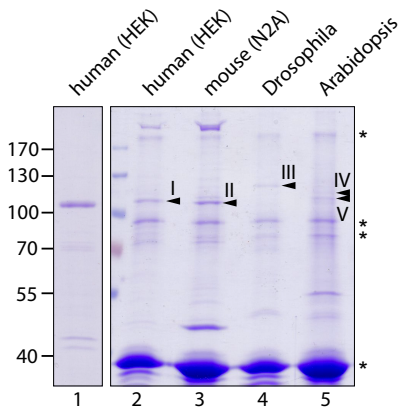

B

		score	sequence coverage [%]
I	Hs_Ago1	2330	54
	Hs_Ago2	2950	57
	Hs_Ago3	1610	37
	Hs_Ago4	1090	23
II	Mm_Ago1	1600	42
	Mm_Ago2	3500	68
	Mm_Ago3	1160	32
	Mm_Ago4	760	18
III	Dm_Ago1	540	23
IV	At_Ago4	875	36
V	At_Ago9	645	27

Figure 2.11: Ago-APP precipitates Argonaute proteins from different species (A) Protein extracts from different sources were subjected to Ago-APP, separated by SDS-PAGE, and Coomassie-stained. The protein composition of potential Ago bands was analyzed by mass spectrometry. Lane 1 shows an Ago-APP eluate that was obtained from elution with PreScission protease. The samples in lanes 2–5 were eluted with Laemmli buffer, which simultaneously eluted GST-T6B and aggregates of it (indicated by asterisks). Drosophila: *Drosophila melanogaster* embryonic extract, Arabidopsis: *Arabidopsis thaliana* Landsberg erecta PSB-D extract. (B) Summary of the mass-spectrometric results. Importantly, scores and sequence coverage shown here rely on the MASCOT search parameters and do also take into account non-unique peptides, i.e. peptides that cannot be assigned to one Ago paralogue. Hs, *Homo sapiens*; Mm, *Mus musculus*; Dm, *Drosophila melanogaster*; At, *Arabidopsis thaliana*.

2.2.2 Ago-APP precipitates Argonaute proteins from different species

Since overexpressed and endogenous Ago proteins from Ago-APPs could easily be detected by Western Blotting, the peptide-based approach was tested for large-scale purifications with subsequent Coomassie staining. Therefore, the amount of peptide-coupled beads was increased and total protein inputs were scaled up to about 20 mg. Using HEK 293T cell extracts, a distinct Coomassie-stained band of about 100 kDa can be detected (Fig. 2.11 A, lanes 1 and 2). Two alternative elution methods were used in this case—either the elution with PreScission protease, which cleaves off the peptide from its GST-tag and provides high specificity (lane 1), or the elution with Laemmli buffer, which is not specific (lane 2). The differences in specificity are obvious when comparing lanes 1 and 2.

Ago-APP purifies endogenous Ago proteins in quantities that can be clearly visualized by Coomassie staining. Consequently, the enriched Ago proteins can be analyzed by mass-spectrometric methods that require large amounts of material, as is the case for the detection of phosphorylated residues. Furthermore, the strong enrichment of Ago proteins by Ago-APP facilitates the analysis of these proteins without Western Blotting, i.e. without antibodies.

This was exploited when lysates of different origins were subjected to Ago-APP. For the murine neuronal cell line N2A, the respective Coomassie band is as intense as the band observed in human samples (lane 3). Ago-APPs from Drosophila and Arabidopsis extracts result in fainter bands (lanes 4 and 5). The mass-spectrometric analysis of these bands revealed that Ago-APP indeed purifies Ago proteins from different species, i.e. from human, murine, and Drosophila material and even from Arabidopsis extracts (Fig. 2.11 B). Importantly, band patterns that re-occur in these very different samples and cannot be detected in the PreScission-eluted sample are due to peptide aggregates (Fig. 2.11, asterisks).

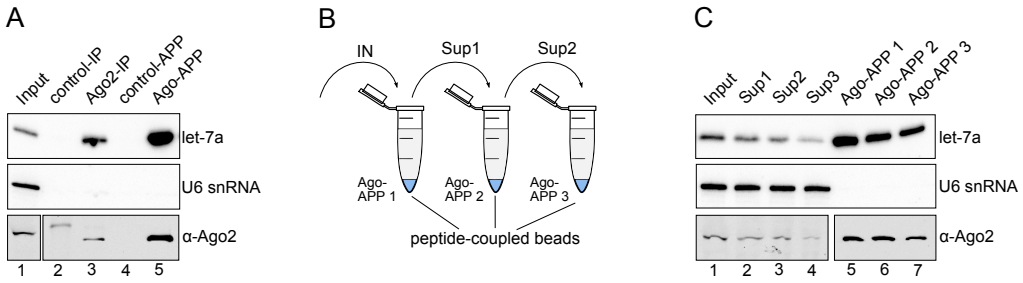

Figure 2.12: Ago-APP facilitates miRNA isolation and depletion. (A) Ago2-IP and Ago-APP from HeLa cell extracts were compared in terms of co-precipitating miRNAs. Therefore, protein and RNA samples from both purification strategies were analyzed by Western and Northern Blotting. Rmc-coupled Protein G beads and GST-coupled glutathione beads were used as negative controls. IP and APP efficiencies were controlled for by immunoblotting for Ago2. A probe against let-7a was used to detect co-precipitating miRNAs. (B) Schematic overview of an Ago- and miRNA depletion experiment. Peptide-coupled glutathione beads were incubated with HeLa cell extracts and the supernatant of this reaction was transferred to a second and a third aliquot of peptide-coupled beads. Protein and RNA samples of the lysates were taken before and after the incubation steps (IN, Sup). 'Ago-APP' represents elutions of the affinity-purified samples. (C) Western and Northern Blot analysis of the depletion experiment described in (B), immunoblotting and probes as in (A). A probe against U6 snRNA was used to control for equal RNA loading in input and supernatant samples.

2.2.3 Analysis of co-precipitating small RNAs

To further characterize the T6B interaction with Ago proteins, miRNAs co-precipitating with Ago-APPs were analyzed. A comparison with an Ago2-IP shows that Ago-APP purifies loaded Ago proteins from HeLa extracts (Fig. 2.12 A). It was shown in former Ago-APPs that the lysate cannot be depleted from Ago by a single Ago-APP and that a certain amount of Ago remains in the supernatant (Fig. 2.10 A–D). To follow up on this, a stepwise depletion experiment was conducted (Fig. 2.12 B, C). Therefore, the supernatant of a first Ago-APP was incubated with fresh peptide-coupled glutathione beads and the supernatant of this purification was again incubated with fresh peptide-coupled glutathione beads. A part of each of these 'input'/'supernatant' and 'APP' samples was analyzed by SDS-PAGE and Western Blotting. Ago2 as the highest expressed human Ago protein was detected. The remaining part was used for RNA extraction and Northern Blotting. Here, the exemplary miRNA let-7a was detected.

A stepwise decrease of Ago protein content can be observed both in APP and in input samples (Fig. 2.12 C), implying that a constant ratio of Ago proteins is engaged in the peptide interaction and that the peptide-based purification relies on an equilibrium, most likely affected by the competition with full length TNRC6B and by peptide binding itself. After the third purification step, Ago signals in the supernatant are very low and the lysate is nearly depleted from Ago proteins. Interestingly, these observations are reflected in the miRNA analysis. As Ago2 levels decrease, let7a levels do also decrease (Fig. 2.12 C). This correlation strongly suggests that neither free Ago proteins nor free miRNAs do exist.

2.2.4 Analysis of co-precipitating target RNAs

Since the peptide-based affinity approach can be used to co-purify Ago-associated miRNAs, its potential to enrich for co-precipitating target RNAs was investigated in the next step. Therefore, Ago-APP was again compared to a conventional Ago2-IP, which is known to enrich the let7 target HMGA2. One part of the affinity purifications was used for Western Blotting, where Ago2 can be detected both in Ago2-IP

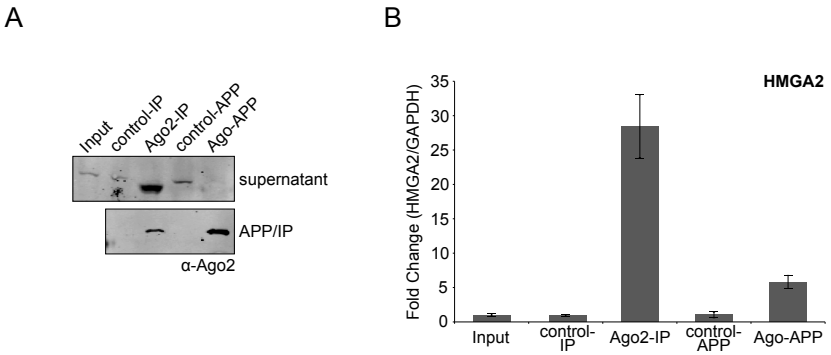

Figure 2.13: Comparison of target RNA enrichment in Ago2-IPs and Ago-APPs. (A) Immunodetection of Ago2 in Ago2-IPs and Ago-APPs of HeLa cell extracts. (B) The enrichment of the let7 target RNA HMGA2 was compared in Ago2-IPs and Ago-APPs. Therefore, RNA was extracted from an input sample and after the affinity purification, reverse-transcribed, and GAPDH and HMGA2 levels were determined by quantitative real time PCR. Affinity purifications with an antibody against Rmc and with recombinant GST were used as negative controls.

and in Ago-APP (Fig. 2.13 A). RNA was extracted from the remaining part of the purifications, reverse-transcribed, and analyzed for HMGA2 enrichment by quantitative real time PCR. Therefore, HMGA2 levels were related to unspecifically copurifying GAPDH mRNA and compared to HMGA2 levels in an input sample. A strong enrichment of HMGA2 mRNA can be detected in Ago2-IPs, whereas this mRNA is only slightly enriched in Ago-APPs (Fig. 2.13 B). Importantly, a control-IP and a control-APP did not enrich HMGA2. Hence, Ago-APP enriches miRNA targets only weakly, suggesting that full length TNRC6B is necessary to efficiently bind target RNAs.

2.2.5 Competition of T6B peptide and endogenous TNRC6B

If the weak target enrichment by Ago-APP is due to the absence of additional domains of the GW182 protein, this would suggest that the binding of T6B peptide to Ago replaces full length TNRC6B.

To investigate this possibility, a competition experiment of endogenous TNRC6B and recombinant GST-T6B was performed. Therefore, Ago2 was immunopurified from HEK 293T lysates containing overexpressed FLAG/HA-TNRC6B and from untreated lysates. First, an excess of GST-T6B was added to the IPs. TNRC6B is co-immunopurified in Ago2-IPs without peptide, but the interaction is completely lost when GST-T6B is added (Fig. 2.14 A, B).

Next, different amounts of GST-tagged peptide were incubated with the Ago2-IPs. The interaction of Ago2 and full length TNRC6B is lost when increasing amounts of GST-T6B are added (Fig. 2.14 C and D). The slightly different competition efficiencies in the FLAG/HA-TNRC6B-overexpressing and the endogenous setup are most likely due to higher amounts of full length TNRC6B being present in overexpressing lysates. Additionally, three times more total protein was used in these experiments. Importantly, TNRC6B does still co-purify with Ago2 when a GST-tagged peptide lacking all tryptophans is used (Fig. 2.14 C and D, 'Ctrl').

These experiments show that GST-T6B competes for Ago binding with full length TNRC6B. Importantly, addition of GST-T6B might be used as a strategy to specifically elute GW182 proteins and associated components from immunopurified samples.

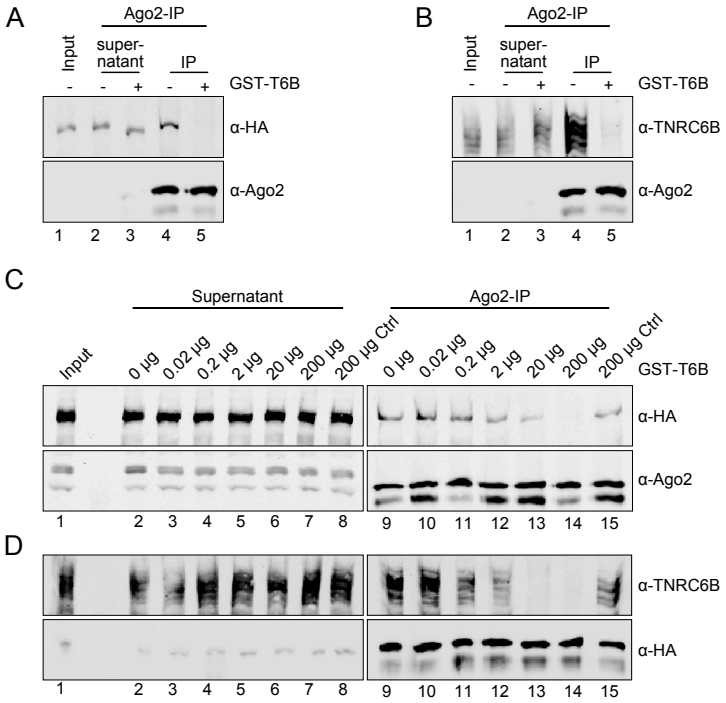

Figure 2.14: T6B peptide competes with full length TNRC6B. (A, B) Ago2-IPs were conducted in the presence or absence of an excess of GST-tagged T6B in the lysate, using either HEK 293T extracts with overexpressed FLAG/HA-tagged TNRC6B (A) or untransfected HEK 293T extracts (B). (C, D) Ago2-IPs were conducted with different amounts of GST-T6B present in the lysate, using again HEK 293T extracts with overexpressed FLAG/HA-tagged TNRC6B (C) or untransfected HEK 293T extracts (D). A GST-tagged peptide lacking all five tryptophans was included as negative control ('Ctrl'). A monoclonal antibody against TNRC6B (clone 6G3) was used for TNRC6B detection in endogenous Co-IPs (B, D).

2.2.6 Quantification of Ago1–4 protein amounts in different tissues

Ago-APP allows to purify all human and murine Agos by using the same experimental tool. Until now, most studies addressing cellular Ago1–4 levels relied on quantitative real time PCR data. Quantification of protein levels was either based on IPs of the individual Agos by different monoclonal antibodies or on shotgun proteomics [53, 102]. Since mammalian Agos show high sequence similarity, the assignment of peptide masses can be ambiguous. Furthermore, slightly different peptides can show large differences in their mass-spectrometric properties (e.g. ionization and flight behavior), leading to potential technical errors.

Here, the established peptide purification approach was used in combination with an MS-based selected reaction monitoring (SRM) approach to reliably measure the relative quantities of human and murine Agos from cell culture and tissue samples. During SRM, certain precursor ions are selected for fragmentation and certain product ions are detected. This approach can be used for peptide quantification when a known amount of a stable isotope-labeled, proteotypic peptide is spiked into the sample. The synthetic and the sample peptide will be detected at similar retention times and can still be distinguished by their isotopic mass difference.

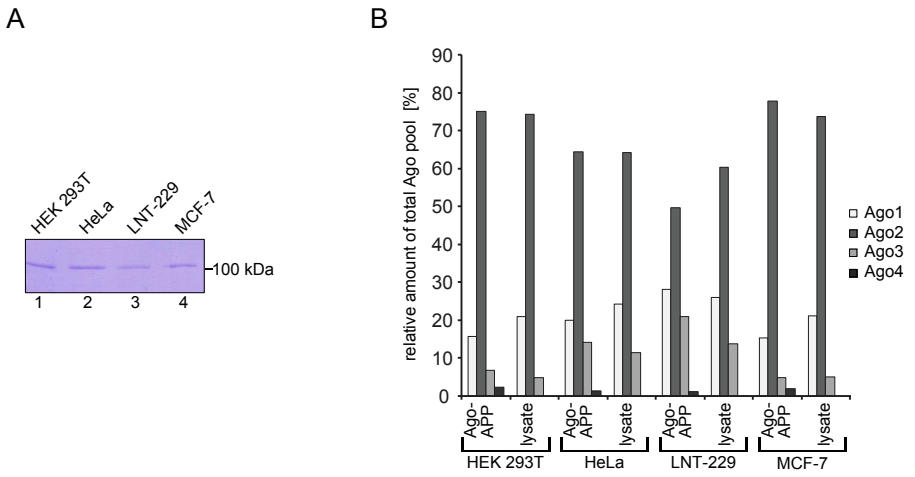

Figure 2.15: Ago1–4 quantification from Ago-APPs and lysates of different human cell lines (A) Endogenous Ago1–4 were purified from different human cell lines using Ago-APP. The eluates were separated by SDS-PAGE, Coomassie-stained, and subjected to mass-spectrometric analysis. (B) Mass-spectrometric measurements (selected reaction monitoring, SRM) of Ago-APPs and cell lysates that were not subjected to Ago-APP. The latter were also separated by SDS-PAGE, Coomassie-stained, and the gel region corresponding to the expected Ago size was cut and processed. Exactly known amounts of synthetic, isotope-labeled peptides were spiked into the tryptic digests to allow for quantification of the four Ago proteins (one isotope-labeled peptide per paralogue).

Several considerations were included during the selection of stable isotope-labeled peptides for Ago1–4: First, the chosen peptide had to be unique for the individual Ago. Second, the peptide should be reliably ionized and detected in MS analyses. And third, it would be advantageous if the same peptides could be used for analysis of human and murine samples.

For quantitative measurements, Ago-APP was used to purify Ago1–4 from different human cell lines. The eluates were separated by SDS-PAGE and stained with Coomassie Blue (Fig. 2.15 A). The Ago bands were cut from the gel and prepared for in-gel tryptic digest. Defined amounts of the stable isotope-labeled peptides were spiked into the tryptic digest, thereby facilitating quantification of the sample peptides from the measured heavy:light ratios at a given retention time. To exclude any bias of Ago-APP towards one of the four Ago proteins, a second set of samples was prepared by SDS-PAGE separation of lysate samples without previous enrichment by Ago-APP.

The measured Ago amounts reflect the published data well [53, 102, 112]. In all used cell lines, Ago2 is the most abundant protein and contributes 50–80 % of the total Ago pool, followed by Ago1 (10–30 %) and Ago3 (5–20 %). Ago4 is detected at very low quantities (1–2 %) (Fig. 2.15 B). The measured Ago ratios are approximately the same in lysate samples. Again, Ago2 is most abundant, followed by Ago1 and Ago3. The weakly expressed Ago4 cannot be detected directly from the lysate, indicating that previous enrichment by Ago-APP is a necessary step, which increases reliability of the results.

Next, the relative Ago levels in different murine tissues were determined (Fig. 2.16 A and B). For these measurements, an additional set of paralogue-specific synthetic peptides was used. Again, the measured quantities reflect the published data and the previous results well. Ago2 is most expressed in all analyzed samples. The exact amounts of Ago1, Ago2, and Ago3 vary between the different tissues. These variation range from low Ago1 expression in muscle (ca. 5 %) to high Ago1 expression in brain (ca. 35 %). In contrast, Ago3 expression varies only betwen 5 and 15 %. Ago4 is expressed in very low amounts in all tissues ex-

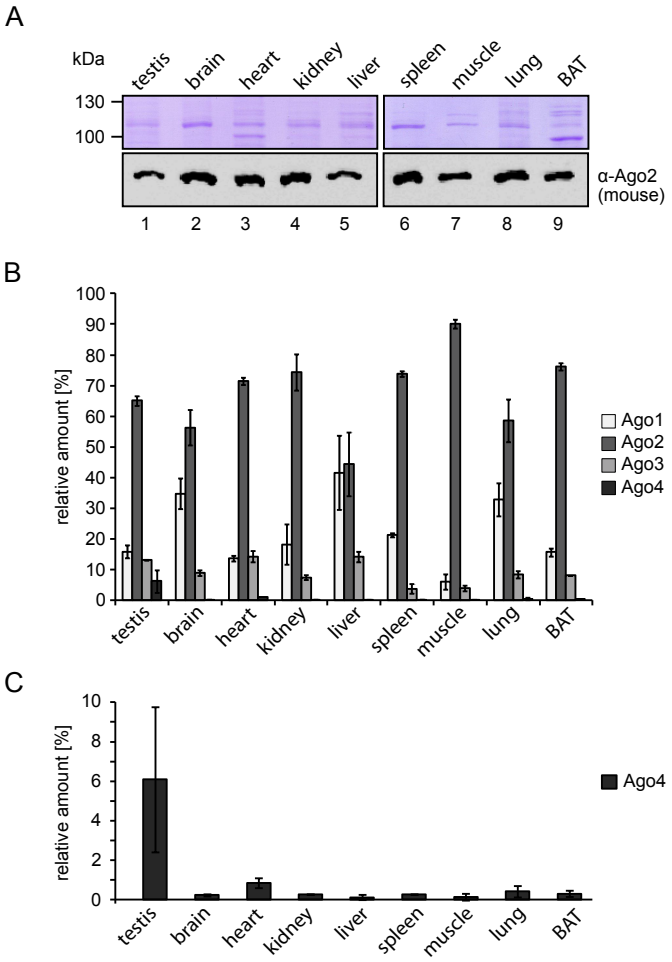

Figure 2.16: Quantification of Ago1–4 in different mouse tissues (A) Endogenous Ago1–4 were purified from different murine tissues using Ago-APP. The eluates were separated by SDS-PAGE, Coomassie-stained, and mass-spectrometrically analyzed. BAT, brown adipose tissue. (B) Ago1–4 quantification by SRM measurements with stable isotope-labeled peptides (two synthetic peptides per paralogue). The relative amount of one Ago paralogue related to the total Ago pool is shown. Error bars represent the standard deviation of identical samples that were quantified with two different paralogue-specific peptides. (C) The relative amounts of Ago4 in different mouse tissues. Data were derived from the experiment shown in (A) and (B).

cept of testis, where it contributes ca. 6 % of the total Ago pool (Fig. 2.16 C). This is in line with previously reported quantitative real time PCR measurements and the Ago4 knockout phenotype observed in mouse testes (Fig. 2.16 C) [100, 110].

Taken together, the advantages of Ago-APP, i.e. its pan-Ago properties and its cross-species applicability, are of high value and open up numerous application possibilities. Moreover, Ago-APP is based on a high-affinity interaction and thereby facilitates the enrichment of large amounts of endogenous Ago proteins for mass-spectrometric characterization. Therefore, the use of Ago-APP represents a strong foundation for the mass-spectrometric detection of phosphorylation sites on Ago proteins.

2.3 Phosphorylation of endogenous Argonaute proteins

Ago proteins are key components of a machinery that post-transcriptionally regulates protein expression. How are then Ago proteins regulated themselves?

Agos are post-translationally modified and the biological function of a few sites is known (section 1.3.2.1). However, a substantial part of the studies that investigated Ago2 phosphorylation relied on overexpressed Ago proteins. This has been necessary since the mass-spectrometric detection of phosphorylated peptides is technically challenging and depends on large amounts of material. Here, different strategies were established and optimized to purify large amounts of endogenous Ago proteins for the subsequent detection of phosphorylation sites.

2.3.1 Purification of human Ago proteins

All extracts used for phosphorylation analyses contained the phosphatase inhibitors sodium fluoride (a serine and threonine phosphatase inhibitor) and sodium orthovanadate (a tyrosine phosphatase inhibitor). First, Ago-APP, the newly established method described in 2.2, was used to purify Ago proteins. Therefore, the GST-tagged, Ago-binding TNRC6B peptide (GST-T6B) was coupled to glutathione sepharose, excess peptide was removed, and the peptide-coupled affinity matrix was incubated with cell extracts. To shorten incubation times as much as possible, the samples were eluted with Laemmli sample buffer (Fig. 2.17 A). A second purification approach used covalent binding of a monoclonal antibody against human Ago2 to Co^{2+} iminodiacetate (IDA-Co) sepharose. HEK 293T cell extracts were first precipitated by ammonium sulfate, resuspended in PBS, and then incubated with the IDA-Co matrix. After elution, the

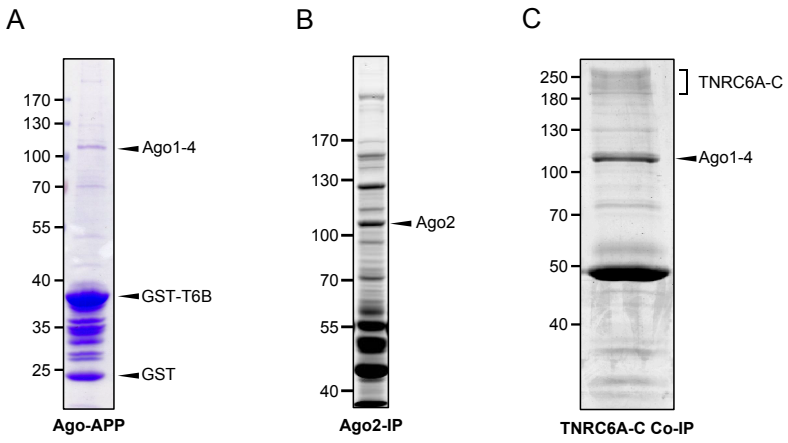

Figure 2.17: Purification of endogenous Ago proteins. (A) Purification of human Ago1–4 by Ago-APP. GST-T6B was coupled to glutathione sepharose and incubated with HEK 293T cell extracts. The samples were eluted with Laemmli buffer, separated by SDS-PAGE, and stained with Coomassie Blue. (B) Coomassie-stained SDS gel of an Ago2-IP. A monoclonal antibody against human Ago2 [187] was covalently immobilized to Co^{2+} iminodiacetate (IDA) sepharose and incubated with HEK 293T lysate (Robert Hett, Biochemistry I, University of Regensburg). (C) Co-immunopurification of human Ago1–4 with a TNRC6A–C IP. A monoclonal antibody specific for human TNRC6A, -B, and -C was coupled to Protein G Sepharose and incubated with HEK 293T lysates (Johannes Danner, Biochemistry I, University of Regensburg).

samples were separated by SDS-PAGE[2] (Fig. 2.17 B). Finally, a third purification approach used the interaction of endogenous TNRC6A, -B, and -C with Ago proteins. Here, monoclonal antibodies against human TNRC6A–C were coupled to Protein G Sepharose and incubated with HEK 293T cell extracts in a classical IP. Purified proteins were eluted with Laemmli sample buffer and separated by SDS-PAGE[3] (Fig. 2.17 B). All three purification strategies yield a distinct Ago band (Fig. 2.17 A–C). Importantly, Ago1, Ago3, and Ago4 co-purify in the Ago-APP as well as in the TNRC6A–C Co-IP approach (Fig. 2.17 A and C).

2.3.2 Detection of endogenous phosphorylation sites of human Ago2

Samples obtained from the different affinity purifications were mass-spectrometrically analyzed for post-translational modifications. Thereby, the focus was on the detection of phosphorylations. Fig. 2.18 summarizes the results of different measurements and detailed data are listed in the Appendix (tables A.1–A.6). For reasons of clarity, only potential phosphosites of Ago2 are shown. These were retrieved from unique peptides as well as from non-unique peptides, i.e. peptides that cannot be clearly assigned to one of the Agos because of the high sequence similarity of human Ago proteins. Non-unique peptides that could originate from Ago2 were included into the analysis because of the generally high expression levels of human Ago2. Furthermore, only phosphorylated peptides with Mascot scores higher than 15 and expectation values lower than 0.1 are shown. For comparison, Fig. 2.18 E represents published phosphorylation sites of Ago2 as listed at PhosphoSitePlus® (`www.phosphosite.org`) (extended data in Tab. A.8).

The following part will point out several key aspects of the obtained phosphorylation data.

Confirmation of known phosphorylation sites and detection of new phosphorylation sites. Generally, potential phosphorylation sites of Ago2 can be detected in all samples and are distributed over the whole protein. The potential phosphopeptides of the analyses conducted here overlap partially with already published phosphosites (compare Fig. 2.18 B–D to E). Importantly, one of the best-characterized phosphorylated residues, S387, was detected in five out of six analyses. Several phosphorylated residues around amino acid 830 were also repeatedly detected. However, many residues have not been found to be phosphorylated before and were reproducibly detected in the analyses presented here, e.g. residues around amino acids 360, 540, or 560. These 'new' phosphorylation sites represent interesting candidates for further characterization.

Dependence of phosphosite detection on the Ago purification method. Importantly, many of the detected phosphorylation sites overlap between different analyses. These sites occur in two mass-spectrometric measurements of the same purification strategy (cf. Fig. 2.18 C) and in analyses of different purification approaches. Based on the different purification approaches, one could speculate to enrich different Ago pools by Ago2-IP and by TNRC6A–C Co-IP/Ago-APP. Indeed, S136, T337, and S776 are only detected in TNRC6 Co-IPs, whereas T409 is only detected in Ago2-IPs.

Multiply phosphorylated peptides. In several cases, multiple phosphorylation sites were detected within a short sequence region. These 'phosphorylation clusters' occur for example in the regions around aa 360, aa 560, and, most prominent, around aa 830 (Fig. 2.18 B–D). The extended data show that two- to fourfold-phosphorylated peptides of these cluster regions were detected (A.1–A.6).

[2] purification conducted by Robert Hett, Biochemistry I, University of Regensburg
[3] purification conducted by Johannes Danner, Biochemistry I, University of Regensburg

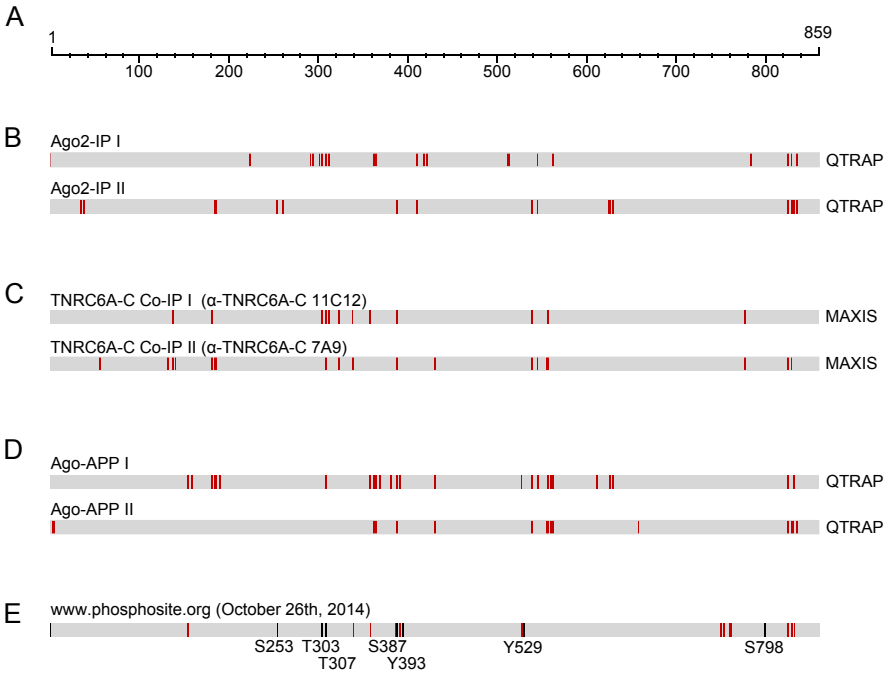

Figure 2.18: Detection of potential phosphorylation sites in endogenous Ago2. (A) Length scheme of Ago2 with one unit corresponding to one amino acid. (B–D) Overview of potential phosphorylation sites that were detected by mass-spectrometric analyses of differently purified Ago samples [(B) Co^{2+}-IDA IP, (C) TNRC6A–C Co-IP, (D) Ago-APP]. The gray bar represents Ago2 and potential phosphorylation sites are indicated in red. Phosphopeptides with scores higher than 15 and expectation values lower that 0.1 were included. Only data of Ago2 are shown, but information of non-unique peptides were included. Extended data are shown in tables A.1–A.6. The mass spectrometers used for the individual measurements are indicated on the right. (E) Published phosphorylation sites of Ago2 as listed at PhosphoSitePlus®, data representation as in (B–D). Black bars and labeled residues represent phosphorylation sites that were confirmed by Ago-specific methods, red bars indicate phosphorylation sites that were detected by proteomic screening methods only. Extended data are listed in Tab. A.8.

The data representation chosen here is simplified and exclusively based on the false discovery rate (FDR) thresholds of database search engines. Therefore, it needs to be combined with (a) information on the individual peptides (data listed in tables A.1–A.6) and (b) manual validation of the fragment ion spectra. As for the individual scores and expectation values of the detected phophopeptides, data quality varies a lot between different analyses (A.1–A.6). The applied cutoff values are not very restrictive, allowing for comparison of low-confidence phosphosites between different analyses. On the one hand, data quality depends on the amount of protein that was available for mass-spectrometric analysis, i.e. input amounts and efficiency of the purification strategy. On the other hand, the used mass spectrometers have different technical properties and analyses with the high mass accuracy MAXIS spectrometer yielded most reliable data. Notably, the absence of a specific phosphosite in this representation (Fig. 2.18) can also be caused by low sequence coverage of the respective region, a feature that is not represented here.

2.3.3 Detection of endogenous phosphorylation sites of human Ago1–4

TNRC6A–C Co-IPs and Ago-APPs purify not only Ago2, but also Ago1, Ago3, and Ago4 (Fig. 2.17 A and C). Potential phosphorylation sites of all human Ago proteins, the contribution of unique and non-unique peptides, and sequence coverage were analyzed on the basis of the best obtained data set (Fig. 2.19 A–C, Tab. A.7). Several key findings of this analysis are summarized in the following subsection.

Unique and non-unique peptides. Most phosphorylated unique peptides were detected for Ago2. The sequence coverage, which is based on several technical replicates and includes non-unique peptides, is also highest here. Surprisingly, only a small part of all potential Ago2 phosphorylation sites is derived from non-unique peptides (Fig. 2.19 B and C). Fewer phosphorylated unique peptides were detected for Ago1, Ago3, and Ago4. The observed differences in the number of phosphorylation sites are most likely due to the different Ago expression levels and emphasize the dependence of MS-based phosphoanalytic measurements on high protein quantities.

Paralogue-specific and -conserved phosphorylation sites. For both Ago1 and Ago3, paralogue-specific phosphorylation sites were detected in the N-terminal region, the region with highest sequence variability in human Ago proteins (Fig. 2.19 B). Furthermore, multiple phosphorylation sites in the region of aa 820–840 could be identified for Ago1, 3, and 4 and are completely based on unique peptides (Fig. 2.19 B). One set of phosphorylations around aa 560 is detected as unique Ago2 peptide and as non-unique Ago1/3/4 peptide, showing that at least two paralogues are modified at these sites (Fig. 2.19 B and C). Finally, the phosphorylation sites corresponding to Y322, T337, and Y338 in Ago2 are derived from peptides that are completely conserved in human Ago1–4 and can therefore not be assigned to one of the paralogues.

Detection of novel phosphorylation sites in human Ago1, Ago3, and Ago4. A comparison of Ago1, 3, and 4 phosphorylation data from this specific analysis with phosphorylation sites listed at PhosphoSitePlus® shows that only little overlap exists between the sites (Fig. 2.19 D, extended data in Tab. A.8). The most prominent example of re-occurring phosphosites is again the cluster located around aa 830.

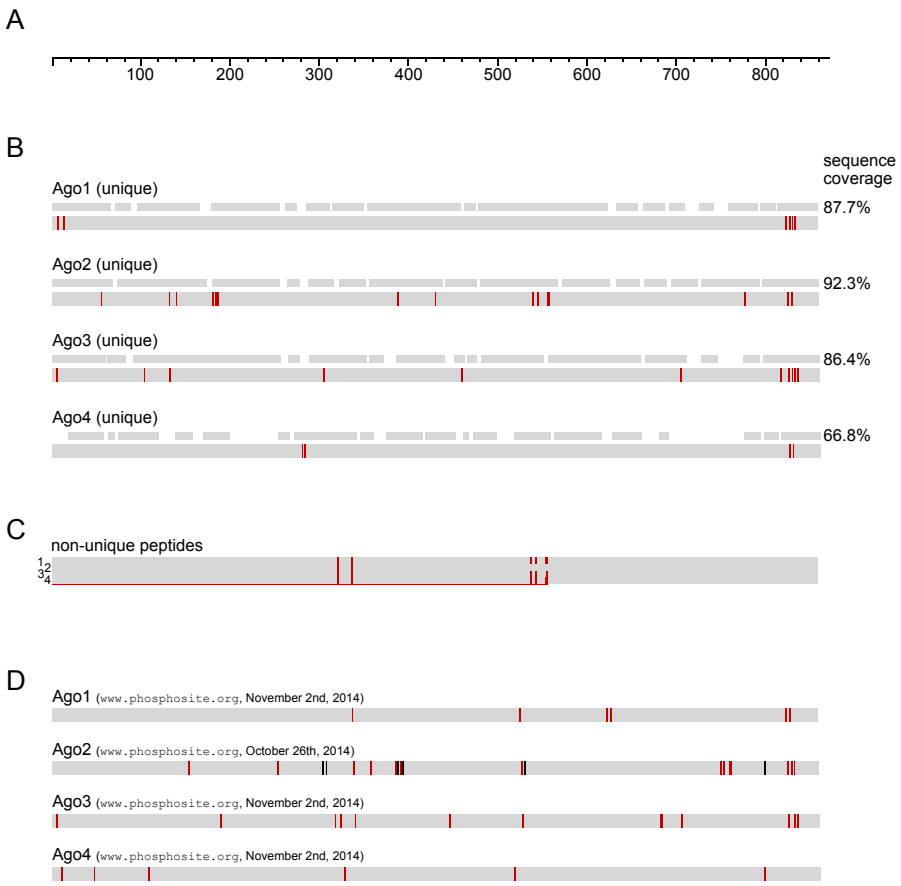

Figure 2.19: Phosphorylation of human Ago1–4 (A) Length scheme for human Agos with one unit corresponding to one amino acid. (B) Representation of phosphorylation sites derived from unique phosphopeptides of Ago1–4. These were detected in a phosphosite analysis of Ago proteins from a TNRC6A–C Co-IP (according to 'TNRC6A–C Co-IP II' in Fig. 2.18). Data were retrieved from several technical replicates and unified. The sequence coverage of the individual Ago proteins is shown on top of the phosphosite representation and takes unique and non-unique peptides into account. (C) Representation of phosphorylation sites detected from non-unique peptides of the same mass-spectrometric analysis. Site positions are based on the Ago1 sequence. Assignment to Ago1–4 is indicated at the left. (D) Ago1–4 phosphorylation sites as listed at PhosphoSitePlus®. Data representation as in Fig. 2.18 E, extended data are listed in Tab. A.8.

2.3.4 Characterization of Ago2 phosphomutants

2.3.4.1 Location and conservation of potential Ago2 phosphorylation sites

From the obtained data, an initial set of several potential phosphorylation sites was chosen for further analysis (Fig. 2.20 A). These sites were primarily chosen because they are part of certain 'phosphorylation clusters', i.e. short sequence parts with a high number of detected phosphorylations. Whereas the clusters Phos1 and Phos4 are located in linker regions of human Ago2, Phos2 is part of the Mid domain and Phos3 is located at the C-terminal end of the PIWI domain (Fig. 2.20 A).

The phosphorylation clusters Phos1–4 are well conserved among the human Ago proteins, but also among Ago proteins of different species (Fig. 2.20 B).

Structurally, these potential phosphorylation sites are either located at the surface of Ago2 (residues of Phos1, Phos2, and Phos3) or in the small RNA binding channel (residues of Phos4) (Fig. 2.20 C). With that, the investigated residues should be accessible for kinases, although this might be questionable in case of the binding channel. Notably, some sites are located in probably very flexible regions of the protein. This is the case for Phos3 (Figs. 2.20 A and C)—this region is not resolved in the crystal structures of human Ago2 and assignment of the potential phosphorylation sites is based on template-free homology modeling.

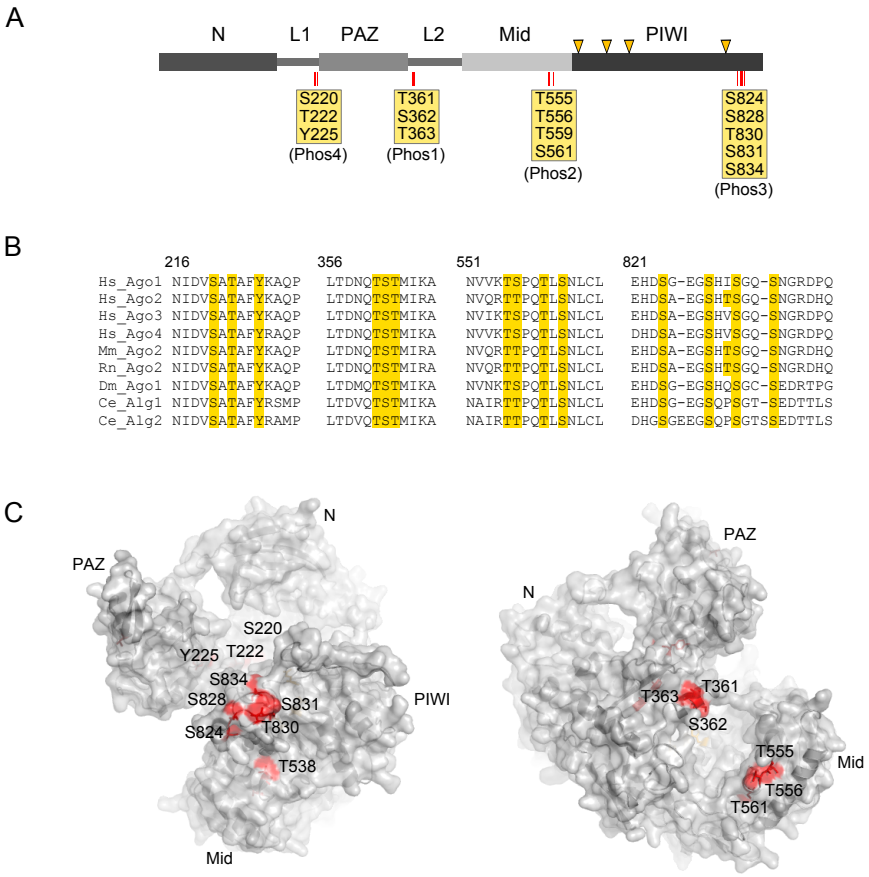

Figure 2.20: Location and conservation of potential Ago2 phosphorylation sites. (A) Schematic representation of the Ago2 domain organization. The positions of identified phosphorylation sites are indicated by red bars. The phosphorylation clusters Phos1–4 are highlighted by yellow boxes. (B) Alignment of human Ago1–4 and Ago protein sequences from different species. The regions of the phosphorylation clusters are shown and potentially phosphorylated residues are highlighted. Amino acids are numbered according to the Ago2 sequence. Hs, *Homo sapiens*; Mm, *Mus musculus*; Rn, *Rattus norvegicus*; Dm, *Drosophila melanogaster*; Ce, *Caenorhabditis elegans*. (C) Location of the identified sites within the protein. An Ago2 homology model based on PDB 4OLA [58] was used to visualize residues that belong to flexible regions and are not resolved in the Ago2 structures. Two views of the protein are shown, domains are labeled, and the positions of potential phosphorylation sites are shown in red.

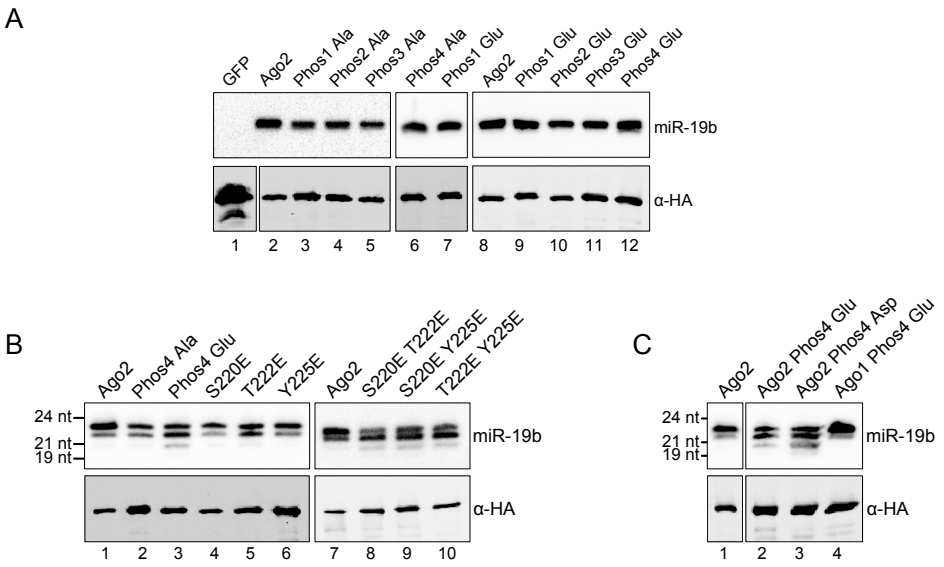

Figure 2.21: miRNA binding of non-phosphorylatable and phospho-mimicking Ago mutants. FLAG/HA-tagged Ago mutants were overexpressed in HEK 293T cells, immunopurified, and co-precipitating RNA was analyzed by Northern Blotting. miRNA association was analyzed of: (A) non-phosphorylatable and phospho-mimicking Ago2 mutants of the identified phosphorylation clusters Phos1–4, where all phosphorylatable residues were substituted by Ala or Glu (12 % urea PAGE). (B) the phospho-mimicking triple, single, and double mutants of the cluster Phos4 (18 % urea PAGE). (C) an Asp-containing Ago2 triple mutant and a Glu-containing Ago1 triple mutant of the cluster Phos4 (18 % urea PAGE). A part of the immunopurified proteins was analyzed by Western blotting to ensure equal loading.

2.3.4.2 Analysis of miRNA binding and cleavage activity of a subset of Ago2 phosphomutants

One method to investigate the functional importance of phosphorylation sites is the analysis of non-phosphorylatable and phospho-mimicking mutants. For that purpose, alanine and glutamate substitutions are typically used.

An analysis of miRNA binding potential of the cluster phosphomutants showed that all non-phosphorylatable mutants can bind miR-19b, indicating that Ago2 is still functional (Fig. 2.21 A, lanes 3–6). The phospho-mimicking mutants do also bind miR-19b (Fig. 2.21 A, lanes 9–12), although a slight shift can be observed for Phos4 Glu.

The shift observed for Phos4 Glu was investigated by higher resolution gel separation and indeed, shorter miRNA species are bound to this mutant (Fig. 2.21 B, lanes 1–3). To investigate if this is an additive effect of the three mutated sites, single and double mutants were assayed as well. The miR-19b length distribution of all single mutants resembles that of wild type Ago2 (Fig. 2.21 B, lanes 4–6), however, all double mutants are associated with miR-19b of the lengths found in the triple mutant (Fig. 2.21 B, lanes 8–10). This indicates that the observed miR-19b shortening is rather charge-dependent than site-specific. S220, T222, and Y225 are located in the small RNA binding channel (Fig. 2.20 C). Two models would explain the effect: either the channel is opened up by structural rearrangements depending on the introduction of negative charges, or the small RNA itself is repelled. Both scenarios would result in an increased accessibility of the small RNA and, potentially, in 3' trimming by a certain exonuclease or exonucleases in general.

To verify one of the proposed models, an aspartate triple mutant was tested (Fig. 2.21 C, lane 3). The

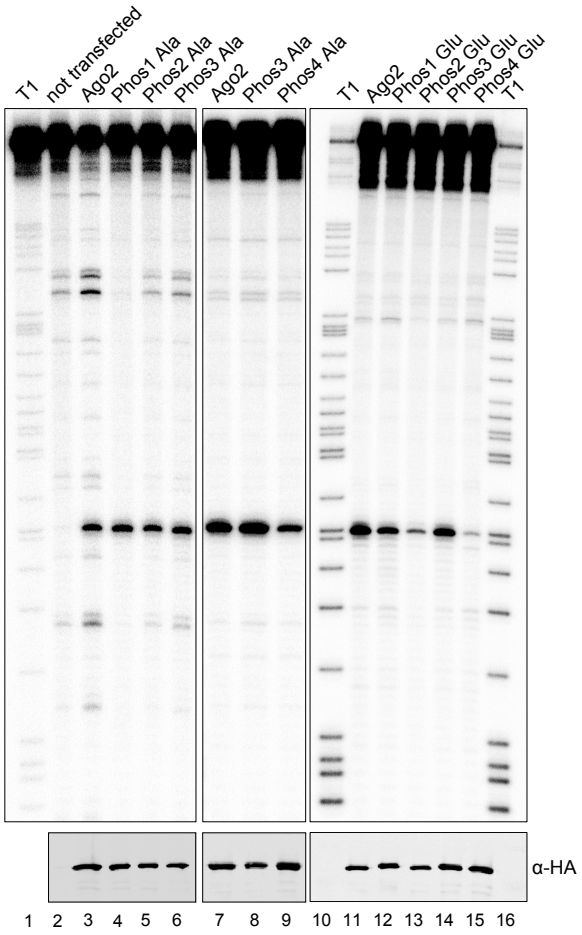

Figure 2.22: Cleavage activity of non-phosphorylatable and phospho-mimicking Ago2 mutants. FLAG/HA-tagged Ago mutants were overexpressed in HEK 293T cells, immunopurified, and incubated with a radiolabeled substrate perfectly complementary to the endogenously coprecipitating miR-19b. RNA was extracted and resolved on a sequencing gel. 'T1' indicates a partial digest of the radiolabeled substrate by RNase T1. A part of the immunopurified protein was analyzed by Western Blotting.

shorter aspartate side chain would reduce miRNA shortening in case of a direct interaction with the small RNA. In contrast, enhanced miR-19b shortening was observed (Fig. 2.21 C, lane 3), suggesting that protein-protein interactions might be affected. In fact, a charge located deeper in a protein might induce a stronger opening. Furthermore, a phospho-mimicking mutant of Ago1 Phos4 was tested. Surprisingly, this triple mutant does not show any shortening of associated miR-19b (Fig. 2.21 C, lane 4).

After having confirmed miRNA binding, the chosen Ago2 mutants were tested for cleavage activity (Fig. 2.22). All non-phosphorylatable mutants can cleave a radiolabeled target complementary to endogenous miR-19b (Fig. 2.22, lanes 4–9). In contrast, two of the phospho-mimicking mutants, Phos2 Glu and Phos4 Glu, show markedly reduced cleavage activity (Fig. 2.22, lanes 12–15). A Western blot analysis confirms equal IP efficiency of the individual proteins and miRNA binding of these mutants has been validated as well (Fig. 2.21 A). Interestingly, a miRNA shortening effect was observed in one of the cleavage-compromised mutants (Phos4 Glu). One can speculate that the introduced negative charges also affect the position of the target RNA.

These initial analyses of phosphomutants are based on few particular modification sites, which were identified by extensive phosphosite analysis of endogenous Ago2. They provide a starting point and clearly, more detailed characterization of these and other phosphomutants is necessary to integrate the obtained information into Ago regulation and cellular signaling networks.

3. Discussion

Some Argonaute proteins are endonucleolytically active. Their enzymatic activity resides in the PIWI domain and depends on the presence of four catalytic residues. However, the presence of this catalytic tetrade is not sufficient for slicer function, as exemplified by human Ago3 [3, 72, 73]. This work analyzed the human non-slicers Ago1, Ago3, and Ago4. Thereby, minimally changed, catalytically active Ago1, Ago3, and Ago4 mutants were created and tested for catalytic activity. Several structural elements that affect cleavage activity were identified. The first part of this chapter is devoted to the newly identified elements, their structural properties, and their possible functions during slicing.

Apart from the analysis of the slicer function of human Ago proteins, the present work addresses the regulation of these proteins by phosphorylation. Therefore, modification sites were supposed to be detected by mass spectrometry. Since phosphorylations often occur in substoichiometric amounts, their mass-spectrometric analysis requires large amounts of protein. In the course of purification optimization, a novel, peptide-based purification method was established. Ago-APP provides a powerful tool for the species-independent analysis of Ago complexes in terms of associated RNAs and proteins. The second part of this chapter discusses several key aspects of Ago-APP, whereas the third part summarizes and discusses data obtained from different phosphorylation analyses.

3.1 Turning catalytically inactive human Argonaute proteins into active slicer enzymes

The analysis of human Ago1–4 in terms of their endonucleolytic activity identified several structural features that influence slicer function. First and most obvious, a complete catalytic tetrad consistent of DEDH is required. These residues are present in both Ago2 and Ago3, but the catalytic center is not complete in Ago1 and Ago4 (Fig. 3.1, black/red). Second, two distinct regions in the N domain affect Ago cleavage. While Ago1 only differs in the first sequence element, Ago3 and Ago4 vary in both regions NTI and NTII (Fig. 3.1, orange). Finally, two elements within the PIWI domain were identified. A region termed 'cluster 2' is changed in both Ago1 and Ago4 (Fig. 3.1, blue), and an Ago4-specific insertion was found to additionally prevent cleavage activity (Fig. 3.1, yellow).

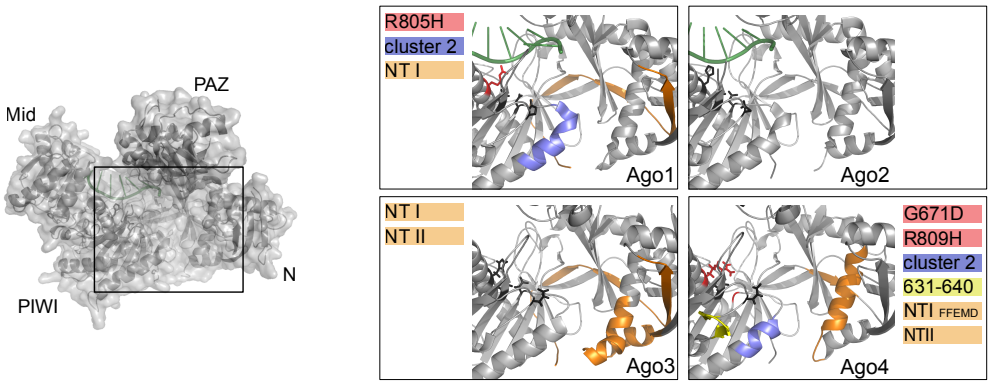

Figure 3.1: Cleavage-defining elements of human Ago1–4 Overview of the four human Argonaute proteins and the alterations, which turned them into catalytically active enzymes. For Ago1 and Ago2, the X-ray structures (PDB IDs 4KXT and 4OLA)[58, 62] are shown. Ago3 and Ago4 are depicted by homology models built on the published Ago1 and Ago2 structures. All changes needed to turn the individual Ago proteins into slicer enzymes are highlighted. The bound guide RNA is shown in green.

3.1.1 The Ago N domain affects cleavage activity

The finding that the Ago3 N domain affects cleavage activity was unexpected since the catalytic activity of Argonaute proteins was known to reside in the PIWI domain. However, deletion mutants of Drosophila Ago1 and Ago2 lacking N and PAZ domains were reported to be better slicers, suggesting that the N-PAZ lobe affects slicer function [188].

The present study used manually created Ago chimeras to identify two regions in the Ago3 N domain (aa 1–64 and 137–160), which influence slicing. Schürmann *et al.* identified these two regions as well [186]. Instead of a manual approach, this study used a DNA shuffling technique and could narrow down the first region to only five amino acids, the so-called 'FFEMD motif'. Within this motif, the methionine residue seems to affect slicing most [186]. The FFEMD motif is part of the first region that was substituted in the present work. Its importance was also addressed when the slicer function of human Ago4 was analyzed. Indeed, substitution of only five amino acids corresponding to the FFEMD motif in combination

with substitution of a longer second region was sufficient to activate the endonucleolytic activity of a cleavage-compatible Ago4 PIWI domain.

An influence of the N domain on slicer function was likewise observed in subsequent work [61]. Faehnle *et al.* showed that the Ago2 N domain activates slicing in PIWI-adjusted Ago1, whereas the Ago1 N domain negatively affects the endonucleolytic activity of Ago2 [61]. This study investigated also an Ago3 chimera containing the Ago2 N domain. However, in this case Ago3 cleavage activity was much below Ago2 wild type levels [61].

The molecular function of these N-terminal alterations are presently not clear. Structural modeling with the available Ago structures revealed no definable influence on the catalytic center. The N-terminal sequences identified in the present work are localized in loop regions that seem to be very flexible, shown by low structural resolution of these areas. Taking this into account, there may be a dynamic influence that ultimately affects the catalytic center and its positioning towards the guide and target RNAs.

Earlier studies showed that the N domain of human Ago2 affects unwinding of the RNA duplex in the 'pre-RISC' complex, an Ago protein that is loaded with the RNA duplex resulting from Dicer cleavage [55]. Kwak *et al.* used conservation-driven alanine substitutions to identify several residues that affect removal of the passenger strand. Since these residues are not localized to a certain region, the authors suggested that movements and conformational changes of the whole N domain contribute to duplex unwinding [55].

In the present work, the association of Ago chimeras with miRNA and miRNA* strands was tested. All Ago mutants associate with miR-19b, but not with miR-19b*, indicating functional unwinding (Fig. 2.7 A and B). This was expected since the used Ago mutants are based on amino acid exchanges with their highly similar paralogues and all human Ago proteins are able to bind and unwind miRNA duplexes [53]. The same results were obtained in the accompanying study that also investigated Ago3 cleavage function [186]. Additionally, Schürmann *et al.* assayed Ago mutants for unwinding of a perfectly complementary short hairpin RNA. They observed that the passenger strand was continuously associated with cleavage-deficient Agos, confirming that Ago slicing function is important for endonucleolytic cleavage of passenger strands and target RNAs [186].

Apart from its possible effects on catalytic center alignment and duplex unwinding, the Ago3 N domain was suggested to obstruct the RNA binding channel [186]. Generally, eukaryotic Ago proteins adopt a more open conformation with a wider RNA binding cleft than prokaryotic Argonautes [60, 75]. Perfectly complementary base pairing is necessary to initiate conformational changes, i.e. to release the miRNA 3'-end from the PAZ domain and to position the catalytic center correctly [75, 80]. An obstruction of the RNA binding channel may interfere with extensive base pairing and these rearrangements, ultimately impeding on cleavage function. N-terminal changes affected also Ago1 and Ago4 slicer function (this work). Indeed, a comparison of human Ago2 with the subsequently solved structure of human Ago1 revealed that two co-called 'eukaryotic insertion elements' correspond to regions that were substituted in the present work. Noteworthy, these elements localize closer to each other in Ago1 and may therefore block the binding channel [62].

However, it is presently not known to which extent the 3'-part of the RNA duplex is base-paired in human Ago proteins and how it contacts the N domain. Remarkably, it was also hypothesized that the RNA-binding cleft of human Ago2 might be naturally blocked by the N domain and that this is necessary for a 'wedging' function during duplex unwinding [55]. The role of the Ago N domain for slicer function will most likely be unraveled by structural studies of human Ago2 with a perfectly paired target, which also includes pairing with the 3'-part of the guide RNA.

Ago3 requires only N-terminal changes to gain cleavage activity. One might speculate that these changes could also be induced extrinsically, for example by the interaction with binding partners or by post-translational modifications. However, such alterations have not been identified so far.

3.1.2 Structural elements in the PIWI domain define cleavage function

This work identified two PIWI domain elements, which affect the cleavage activity of human Ago proteins. A region termed 'cluster 2' was identified in Ago1 and Ago4, whereas an additional insertion is specifically present in Ago4.

3.1.2.1 Cluster 2

After correction of the incomplete catalytic tetrade of Ago1, the protein (Ago1 DEDH) was still not catalytically active (this work, [61]). For the same mutant, marginal slicing was observed in another study [62], whereas intermediate activity was shown in a third one [186]. Paradoxically, cleavage activity of wild type Ago1 or Ago1 DEDH has been reported before [52, 124].

The present work shows that Ago1 DEDH is not catalytically active. This lack of cleavage activity indicated that additional PIWI domain elements may affect cleavage function. Here, cluster 2 (aa 670–680) was identified. This is fully compatible with the findings of Faehnle *et al.* who identified L674 and with those of Nakanishi *et al.* who identified P670 and P675 to influence slicer function [61, 62]. Notably, cluster 2 contributes also to slicer function of human Ago4 (this work).

Homology modeling and secondary structure analysis of human Ago1 on the basis of the Ago2 structures that were available by then indicated that a short 3_{10}-helical element is present in cluster 2 of Ago2 and connects a loop to an α-helix (Fig. 2.5 A). In Ago1, the 3_{10}-helix is missing and the region is characterized by a longer loop and a shorter α-helix. These differences in secondary structure led to the hypothesis that cluster 2 ultimately affects the position of a catalytic residue located in close proximity (Ago1 D667).

The crystal structures of human Ago1 revealed that this region, esp. the loop part, is indeed different from Ago2 and protrudes further into the RNA binding channel [62]. Both Faehnle *et al.* and Nakanishi *et al.* modeled an RNA duplex into the Ago1 structure [61, 62]. The first group hypothesized the loop to interact with the minor groove of the bound duplex and suggested that the loop, the glutamate finger, and the target RNA undergo complex rearrangements to form the cleavage-competent catalytic center [61]. In contrast, the model of the second group indicated that the loop interferes with correct placement of the substrate opposite of the catalytic center [62].

Recent structural studies of human Ago2 added another line of evidence. Schirle *et al.* observed a magnesium ion in a catalytically inactive position of the catalytic center and suggested that perfect complementarity, esp. opposite of the cleavage site, is needed to reposition and activate the magnesium ion [74]. The change of coordination partners during repositioning may also explain how certain structural elements participate in formation of the active catalytic center [74].

3.1.2.2 The Ago4-specific insertion

Human Ago4 was catalytically activated, when, among other changes, an Ago4-specific insertion in the PIWI domain was removed. Homology modeling showed that these residues form a helix-loop-helix element within the glutamate finger (Fig. 2.5 B). This does probably render the glutamate finger cleavage-incompatible, either by a constitutive mis-positioning or by altering the flexibility that might be required for rearrangements that form the activated catalytic center.

Schürmann *et al.* used their DNA shuffling approach not only for the creation of Ago2–3 chimeras, but also to create chimeras that contain sequences from all four human Ago proteins. None of the chimeras containing Ago4 sequences in their N or PIWI domains was catalytically active [186]. This is surprising, since this approach provides a vast number of chimeras. Notably, Schürmann *et al.* were aware of the

Ago4-specific insertion and deleted these residues. The sequence alterations were combined with changes in the N-terminus, but not with changes in cluster 2. For that reason, a slicing version of Ago4 was not identified in this study [186].

In the present work, the analysis of Ago4 confirms the structural elements that were found to affect Ago1 and Ago3 slicer activity. The protein, although evolutionary farthest related, complies clearly with the same principles as the other human Ago proteins.

3.1.3 Human slicers provide new insights into Ago function

Taken together, the analysis of human Ago1–4 identified important structural features that account for the endonucleolytic function of Ago proteins. On the one hand, an influence of the N domain on slicer function was revealed. On the other hand, specific structural elements in the PIWI domain were identified. These analyses provided information about Ago1, Ago3, and Ago4 that were not based on structural studies. Remarkably, the solution of the Ago1 structure confirmed the structural divergence of cluster 2 [61, 62].

3.2 Ago-APP: a novel purification strategy for Ago proteins

3.2.1 Evolutionary conservation of tryptophan-mediated interactions

Ago-APP is based on a tryptophan-containing peptide derived from the human GW182 protein TNRC6B. This peptide and its interaction with Ago were characterized in detail in a recent study [112]. Notably, the TNRC6B peptide is part of a region that has been linked to Ago binding before [129]. Mutation of a single Trp residue located in this region (W623A) is sufficient to abolish the interaction of TNRC6B with Ago, indicating that this GW region is essential for Ago-binding [112, 129]. However, the Ago binding potential of other GW regions (i.e. the conserved motif II and the 'Ago hook' that is not present in all isoforms) has been demonstrated as well [112, 154, 189, 190], altogether suggesting cooperative effects.

3.2.1.1 The specificity of Ago-APP

The presence of four Ago proteins and three GW182 proteins in humans suggests redundant functions of both protein families. Indeed, members of the GW182 protein family associate with all Ago proteins [128, 129, 190] and Ago paralogues bind all GW182 proteins [190]. Furthermore, the individual human GW182 paralogues associate with a similar set of miRNA targets [107].

Binding of GW182 to Ago proteins is mediated by tryptophans that insert into two specific pockets. This binding interface was first identified in structural studies of human Ago2 [58] and is also present in human Ago1 [62].

To understand GW182 binding to certain Argonaute proteins, residues that participate in formation of the tryptophan binding pockets and GW182 binding were identified from the structure of human Ago2. Therefore, molecular distances and predicted residues of protein-protein interactions were determined [191][1]. Fig. 3.2 compares residues that most likely contribute to tryptophan binding in different Argonaute proteins. Importantly, the identified residues are conserved in human and murine Ago1–4 (Fig. 3.2 A). In contrast, the residues are not conserved in human PIWI proteins (Fig. 3.2 B). These analyses consolidate the binding specificities observed in Fig. 2.11 and are in line with previous reports [192].

A comparison of Drosophila Ago1 and Ago2 shows that the bioinformatically identified residues are well-conserved in the miRNA-specific Ago1, but not in the siRNA-specific Ago2 (Fig. 3.2 C). Indeed, Drosophila Ago2 is not purified by GST-T6B (Fig. 2.11) and does not bind GW182 proteins [134, 192, 193].

Importantly, the characterization of a GW peptide derived from another isoform of TNRC6B came to similar conclusions concerning its specificity. The 'Ago hook' was shown to bind to human Ago1 and Ago2, but not to PIWI proteins in *in vitro* binding assays [154]. Furthermore, interaction with Drosophila Ago1, but not with Ago2 was reported [154].

In addition, Ago-APP was successfully used with Arabidopsis extracts. However, the T6B peptide precipitates smaller amounts of Ago proteins from Drosophila and Arabidopsis lysates than from human and murine extracts (Fig. 2.11). This could be due to expression differences or the enrichment of only one or two paralogues. Alternatively, if the affinity of different Ago proteins might also be defined by the conservation of the tryptophan-binding pockets. Notably, less pocket-contributing residues are conserved between human Ago2 and Drosophila Ago1 and conservation is even lower in Arabidopsis Argonautes (data not shown). Hence, these bioinformatically identified residues might be used to roughly predict specificity and efficiency of Ago-APP in different experimental systems.

[1] contributed by Prof. Dr. Rainer Merkl and Lukas Kater, both University of Regensburg

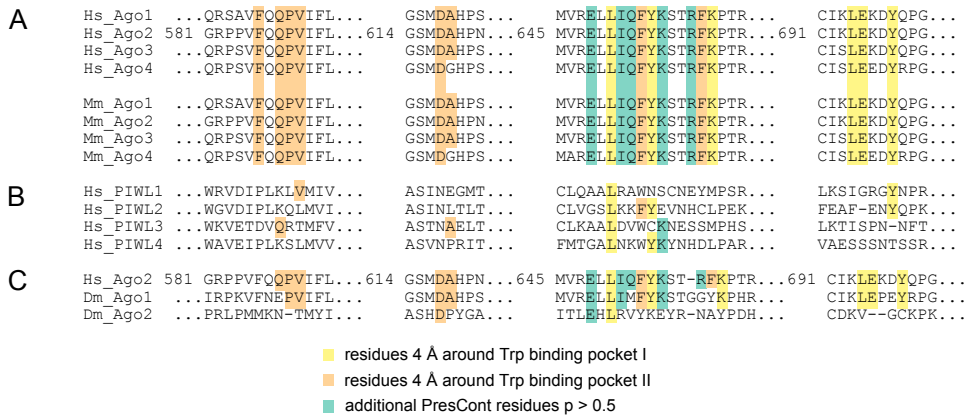

Figure 3.2: Bioinformatic analysis of Ago2 residues that form tryptophan binding pockets The structure of human Ago2 (PDB ID 4EI1, [58]) was used to identify residues that are in close proximity of the tryptophan binding pockets. Additional residues with high interaction probability (specified by conservation, solvent accessibility, hydrophobicity, and local environment of the residues) were identified by PresCont [191]. Conservation of the identified residues was compared by sequence alignments of human and mouse Ago proteins (A), human PIWI proteins (B), and Drosophila Ago proteins (C)

3.2.1.2 Tryptophan-mediated protein interactions: a common theme

As already introduced, many interactions of GW182 proteins depend on tryptophans (cf. subsection 1.2.2). Similar tryptophan-mediated interactions have been observed in different systems and for other binding partners. One example is Tas3, which is part of the RITS complex in *S. pombe* and mediates transcriptional gene silencing of centromeric regions [154, 194].

Moreover, multiple examples of tryptophan-dependent protein association have been recognized in plants. Since Arabidopsis Ago4 and Ago9 were identified in Ago-APPs, the following part gives an overview of plant Agos, small RNA-guided gene silencing, and Trp-mediated interactions in plants.

Ago proteins and small RNA-guided gene silencing in plants. Ten Ago proteins are encoded in the Arabidopsis genome [48, 195]. The proteins associate with small RNAs of different length and are implicated in diverse processes such as conventional miRNA silencing of endogenous genes (Ago1), virus defense (Ago2), or production of trans-acting siRNAs (tasiRNAs, Ago2 and Ago7) [48]. Furthermore, RNA-directed DNA methylation (RdDM) events are very common in plants and a group of Agos—namely Ago4, Ago6, and Ago9—is dedicated to mediate transcriptional repression by cytosine methylation [196–198]. The RdDM Agos interact with the plant-specific polymerase V, which is involved in siRNA production, e.g. from repeats, transposons, or transgenes [199–201]. They are specifically loaded with 24 nt long siRNAs produced by DCL3 (Dicer-like 3) [198].

Plant miRNAs usually target RNAs with near-perfect complementarity and therefore target cleavage plays an important role [202]. In contrast to most other Ago-expressing species, there is no GW182 homologue in plants [134]. Still, Ago4 and Ago9 were enriched by Ago-APP.

Enrichment of RdDM Agos by Ago-APP. Purification of RdDM Agos by the GW peptide can be attributed to their interaction with the C-terminal domain (CTD) of the polymerase V subunit NRPE1. This protein is characterized by GW motifs similar to those of GW182 proteins [155]. When the GW-containing

region of NRPE1 is substituted by an unrelated sequence, *de novo* DNA methylation is abolished, demonstrating that it fulfills an essential function during RdDM. Notably, the GW-containing, plant-specific CTD precipitates human Ago2 in GST pull down assays [155]. Even a chimeric CTD containing the GW-rich region of human TNRC6A is able to purify Arabidopsis Ago4 in these assays [155]. Moreover, this chimeric protein can partially reconstitute DNA methylation in NRPE1-deficient plants [155].

Homology modeling indicated that both tryptophan binding pockets are conserved in plants [203], simultaneously raising the question of why only Agos of the Ago4/6/9 subfamily can be precipitated by Ago-APP.

GW motifs as conserved Ago binding platforms Several additional plant GW proteins were identified, all of which interact with at least one Arabidopsis Ago protein and function at different steps of DNA methylation pathways [204–208]. Interestingly, viral suppressor proteins exploit GW-based interactions to interfere with antiviral silencing [209, 210].

Taken together, Ago-APP can be used to specifically enrich Agos of the RdDM pathway and to characterize associated components.

3.2.2 Ago-APP co-depletes Ago proteins and miRNAs

The T6B peptide used for Ago-APP resembles the function of a pan-Ago antibody and purifies miRNA-loaded Agos. This feature was used to estimate the Ago:miRNA ratios in the cell (Fig. 2.12). In a stepwise depletion experiment it was shown that at least in HeLa extracts and at least for let-7a, miRNAs are depleted from the lysate to the same extent as Ago proteins. These findings suggest that Ago proteins and miRNAs exist as complexes and that their levels are interdependent.

In contrast, Janas *et al.* used depletion of Ago1–4 by a pan-Ago antibody and showed that associated miRNAs are not depleted to the same extent. Complemented by protein and miRNA quantification data, the authors of this study concluded that a pool of non-Ago-bound miRNAs exists in the cell [124]. Two other reports point into a similar direction, showing that free miRNAs exist and that different miRNAs associate with Ago proteins to different extents [125, 126]. However, with the powerful tool of Ago-APP being available, these findings are hard to explain.

The stepwise depletion of Ago proteins from HeLa extract shows that Ago and miRNAs are co-depleted, suggesting that both components exist as complexes. Furthermore, the near-complete depletion of Ago proteins from the lysate indicates that Ago-APP discriminates not between different Ago pools, but targets all Ago proteins of a cell. This is in line with mass-spectrometric characterization of Dicer-dependent (miRNA-loaded) and Dicer-independent (unloaded) Ago complexes, both of which were found to associate with TNRC6B [211].

3.2.3 Efficient target binding requires full length GW182 proteins

Interestingly, co-immunopurifications of endogenous Ago2 and TNRC6B in the presence of GST-T6B showed that the peptide is able to compete with endogenous TNRC6B (Fig. 2.14). Moreover, Ago-APP does not enrich for miRNA target RNAs to the same extent as a classical Ago2-IP does (Fig. 2.13). These observations suggest that the short Ago-binding peptide is not sufficient to stabilize target RNA binding to Ago. Most likely, additional GW182 domains are necessary to stabilize the interaction. This has not

been realized so far and only few observations hint at a mechanistic interplay of additional GW182 domains and target binding. For example, PAM2-mediated PABP binding is hypothesized to facilitate RISC binding to target RNAs [144]. However, although GW182 proteins feature an RRM, a direct interaction of GW182 proteins with target RNAs has not been reported so far. The RRM is most likely used for protein interactions [212]

Experimentally, strategies like conventional UV crosslinking or UV crosslinking of 4-thiouridine could be used to obtain stable Ago complexes. This would allow to combine Ago-APP with target identification approaches such as PAR-CLIP (Photoactivatable-Ribonucleoside-Enhanced Crosslinking and Immunoprecipitation).

3.2.4 Establishment of an Ago1–4 quantification method

In this work, Ago-APP and subsequent SRM analyses with stable isotope-labeled peptides were used to reliably determine Ago1–4 protein levels. Generally, the measured protein levels mirror the data obtained from previous analyses, although these analyses were performed with lower accuracy [53, 102, 112]. However, not much attention has been payed to Ago4 protein levels so far, mostly because Ago4 is expressed below detection limits in many tissues. Nevertheless, analysis of *Ago4* transcript levels by quantitative real time PCR had already indicated that *Ago4* expression is increased in testes [110]. More precisely, this study indicated that *Ago4* transcript levels equal those of *Ago2* or are even twice as high [110]. In the present work it was shown that Ago4 protein contributes ca. 5 % of the total Ago pool. This is substantially less than expected from *Ago4* transcript quantification. Most likely, the huge difference between Ago4 transcript and protein levels can be accounted for by suboptimal codon usage in Ago4 [111]. It seems that the resulting, small Ago4 pool is responsible for the phenotype observed in Ago4 knockout mice [100]. Several questions arise from this finding: Why are transcription and translation of Ago4 so inefficiently coupled? Does the suboptimal codon usage resemble a mechanism to additionally downregulate Ago4 protein expression in all other tissues than testes? And finally, how does Ago4 functionally differ from the other human Ago paralogues?

Apart from these conceptual questions, the combination of Ago-APP and SRM measurements established in this work represents the first and reliable absolute quantification that can be used both for human and murine samples. Numerous application possibilities are conceivable, ranging from Ago1–4 quantification under different conditions to modification quantification of a single Ago paralogue. With that, the established method might assist in clarifying potential specific functions of individual Ago proteins and is a valuable tool for the site-specific analysis of post-translational modifications.

3.2.5 Ago-APP: A novel tool for the characterization of endogenous Ago complexes

The novel Ago purification strategy established in the present work represents a valuable tool for the characterization of Ago proteins and associated (small) RNAs. Main advantages in contrast to conventional immunopurifications lie in its high yields, its pan-Ago properties, and its cross-species applicability. Indeed, the data presented here suggest that Ago-APP can be used to enrich Ago proteins from all species that rely on GW182-dependent gene silencing.

The universal applicability of Ago-APP opens numerous possibilities: First, endogenous Ago proteins themselves can be characterized. This is also shown in this work where Ago-APP, among other purification strategies, was applied to detect endogenous phosphorylation sites of human Ago2 (cf. section 2.3). Second, Ago-APP can be used to characterize Ago-associated miRNAs. This can be of interest for

miRNA validation in species where antibodies are not available or for general miRNA profiling of all Ago-associated miRNAs in a specific lysate. Third, Ago-APP can be optimized and adapted for target RNA profiling. This has been prepared by providing a FLAG-GST-tagged peptide which can be easily used with established PAR-CLIP protocols. Importantly, target RNA profiles after Ago-APP will represent the spectrum of all miRNA-regulated transcripts and it is not yet known if this differs from Ago2-regulated target RNAs. Finally, peptide-derived tools can be used to monitor miRNA-mediated silencing of certain target RNAs. Therefore, the T6B peptide is available in an eukaryotic expression vector with an N-terminal FLAG/HA-tag and a C-terminal GFP-tag that was introduced to protect the unstructured, short peptide from degradation. Indeed, a luciferase reporter carrying the HMGA2 3'-UTR is de-repressed upon co-transfection with this peptide version (data not shown[2]).

Furthermore, Ago-APP can be used as a tool to enrich for RdDM Argonautes and to dissect the RdDM pathway in plants. However, Ago yields are relatively low when using plant lysates and one might consider the establishment of an analogical technique that utilizes the GW motifs present in the CTD of Arabidopsis polymerase V subunit NRPE1. This is further consolidated by the observation that chimeric CTDs carrying the human TNRC6A GW motifs are able to interact with plant Ago4, but interaction is relatively weak compared to human Ago proteins [155].

Apart from these application possibilities of Ago-APP, several limitations of the method should be considered. First, Ago-APP relies on hydrophobic tryptophan interactions and depends therefore on lysis buffers with low amounts of detergent. Second, metabolically highly active lysates (e.g. liver lysate) are prone to degrade the peptide, making it necessary to add high amounts of protease inhibitors. Third, GST-T6B can be easily used with glutathione beads, but these are sensitive to the actual redox state. This can be a problem when using lysates or lysate additives with a high oxidation potential, e.g. the tyrosine phosphatase inhibitor Na_3VO_4. Importantly, the use of FLAG-GST-T6B with an α-FLAG-coupled affinity matrix circumvents this problem.

[2] contributed by Daniel Schraivogel, University of Regensburg

3.3 Endogenous phosphorylation sites of human Ago proteins

For phosphorylation analysis, different purification approaches, including Ago-APP, were used to yield large amounts of endogenous Ago2 and Ago1–4, respectively. The data obtained from mass-spectrometric analysis represent a detailed resource of endogenous phosphorylation sites present in endogenous Ago2 under standard cell culture conditions.

3.3.1 Endogenous phosphorylation sites of human Ago2

To summarize, the application of different purification methods cross-confirms several modification sites, but yields also sites that might be specifically enriched by one method. This is especially interesting since TNRC6-Co-IPs and Ago-APPs were applied. Both methods are based on the interaction of Ago and GW182 proteins and might therefore preclude and/or require certain modifications.

Moreover, previously characterized sites such as pS387 [177, 179] were reliably detected and confirm the experimental approaches used here. Still, a significant part of the detected phosphorylations has not been reported before. Therefore, these sites represent interesting candidates for further analysis. For comparison, publicly available data collected at PhosphoSitePlus® (`www.phosphosite.org`) were used. It is obvious that not all previously known sites were reproduced. This is probably due to the use of different experimental systems and conditions, but one should also note that many sites listed at PhosphoSitePlus® were exclusively obtained from large-scale proteomic screens, implying relatively low reliability compared to modifications that were analyzed site-specifically.

Interestingly, phosphorylation clusters and multiply phosphorylated peptides were detected for human Ago2. Biological and technical aspects of this finding are discussed in the following section.

3.3.1.1 Phosphorylation clusters and multiply phosphorylated peptides of human Ago2

Conservation. The most prominent phosphorylation cluster detected in the present analyses encompasses five potential phosphorylation sites between aa 824 and 834 (cluster 'Phos3'). Importantly, four phosphorylatable residues are conserved in Ago1–4 (Fig. 2.20 B) and unique phosphorylated peptides of this region have been detected in Ago1, Ago3, and Ago4 (Fig. 2.19 B). These residues are conserved across species (Fig. 2.20 B). Indeed, multiply phosphorylated residues corresponding to this cluster have been detected in the *C. elegans* Ago protein ALG-1 (data not shown[3]). Considering the generally low conservation of phosphorylation sites [213], this is remarkable and strongly indicates functional importance.

Biological function. A systematic analysis of phosphosite distribution in eukaryotes showed that phosphorylated serine and threonine residues tend to occur in clusters [214]. Several clustered phosphorylations with different biological functions have been described [215].

For example, phosphorylated repeats in the C-terminal domain of RNA polymerase II provide multiple highly specific binding platforms. Their phosphorylation pattern changes during transcription, adapting the repertoire of associated transcription factors to the transcription phase [216]. Clustered phosphorylations were also observed in the *Saccharomyces cerevisiae* protein Sic1, a cyclin-dependent kinase inhibitor.

[3] collaboration with Martin Simard, Laval University, Quebec City (Canada);
data contributed by Astrid Bruckmann, University of Regensburg

Here, the number of phosphorylated residues is more important than their position. When six out of nine potential sites are phosphorylated, an ubiquitin ligase binds to Sic1 and targets it for degradation, ensuring onset of the cell cycle [217, 218].

At the molecular basis, clustered phosphorylations result in local charge accumulation and often influence protein interactions. This involves binding to other proteins, especially if these rely on ionic interactions or if phosphates are recognized in (or excluded from) binding pockets [215]. Moreover, multiple phosphorylations can disrupt membrane association or DNA binding [219, 220]. However, the analysis of miRNA binding and cleavage function of phospho-mimicking and non-phosphorylatable Ago2 Phos3 cluster mutants showed that small RNA and target RNA binding are not affected by the negative charge introduced here (Figs. 2.21 and 2.22).

Mechanistically, phosphorylation clusters represent biological switches whose mode of action, rheostat or binary switch, is determined by cooperative effects between individual phosphorylatable sites [215]. In addition, clustered phosphorylations were suggested to ensure evolutionary robustness [214].

Asking for kinases. The detection of multiply phosphorylated peptides intensifies the questions of implicated kinases. Are all residues phosphorylated by one kinase with low specificity? Or is there crosstalk between phosphorylation sites, i.e. does modification of a certain position alter kinase specificity of a neighboring position?

Few kinases, so-called 'priming-dependent' kinases, depend indeed on phosphorylated sites. Many substrates of GSK3 (glycogen synthase kinase 3) require a priming phosphorylation at a serine four amino acids downstream of the actual modification site [221]. The same is true for CK1 (caseine kinase 1), which depends on serine phosphorylations three positions upstream of the modification [222]. These phosphorylation-dependent kinases were observed to cooperate at one substrate [223].

In context of the phosphorylation sites detected here, such a mechanism would turn S828 into a key residue, with S824 being potentially phosphorylated by GSK3 and S831 and S834 being modified by CK1. Phosphosite analysis of a S828A non-phosphorylatable mutant will provide information about implication of these priming-dependent kinases.

Technical challenges. The mass-spectrometric analysis of phosphopeptides is generally difficult, which is for example due to their poor ionization efficiency and their specific fragmentation behavior. Since some of these difficulties depend on negative charges, the analysis of multiply phosphorylated peptides is even more problematic [224]. Furthermore, the assignment of phosphorylations to a certain amino acid can be ambiguous when several phosphorylatable residues are present and when fragment ion spectra do not provide sufficient sequence information [225]. Additionally to that, rearrangements of phosphorylations in the gas phase have been observed, implementing another positional uncertainty factor [226].

Apart from mass-spectrometric issues, cluster phosphorylations can be difficult to handle during site-specific analysis. First, the design of appropriate phosphomutants would require information on site-specificity or minimum number of phosphorylated residues. Since these information are usually not available, a large number of combinatorial mutants has to be used to narrow down possible phenotypic effects. Second, phosphosite-specific antibodies generally represent a valuable tool. However, these antibodies are highly specific and will in many cases not recognize a phosphorylated residue when the neighboring residue is phosphorylated as well.

3.3.2 Phosphorylation sites of human Ago1, Ago3, and Ago4

The present work focused mainly on endogenous phosphorylation sites of human Ago2. However, since TNRC6-Co-IPs and Ago-APPs purify the other human Ago proteins as well, an exemplary analysis of paralogue-specific modification sites was included (Fig. 2.19). Phosphorylation of human Ago1, Ago3, and Ago4 has not been characterized by site-specific methods before and available data are exclusively based on high-throughput screens. This is most likely the reason for the large variations between the sites detected here and previously known sites listed at PhosphoSitePlus®.

Two observations are apparent from the paralogue-specific phosphorylations identified here: First, unique phosphorylated peptides of the cluster ranging from aa 824–834 can be detected in all human Ago paralogues and show conservation of this region in terms of post-translational modifications. Second, paralogue-specific phosphorylations are present in the N-terminal regions of Ago1 and Ago3. This is of particular interest since N-terminal regions of both Ago1 and Ago3 were shown to negatively affect endonucleolytic function (cf. 3.1.1). One could speculate that post-translational modifications in these regions contribute to fulfill structural requirements necessary for slicing.

3.3.3 Characterization of selected Ago2 phosphomutants

One subset of potentially phosphorylated residues was chosen for further characterization by means of non-phosphorylatable and phospho-mimicking mutants. In the present work, the assessment of miRNA binding and cleavage activity is shown. These functional assays revealed two main findings.

First, a phospho-mimicking Ago2 mutant of cluster 220–225 (Phos4) binds shorter miRNAs than wild type Ago2 or a non-phosphorylatable mutant (Fig. 2.21 B, lanes 1–3). Site-specific analysis showed that the phenotype depends rather on the number of negative charges than on the exact modification site. Surprisingly, this is an Ago2-specific effect. It does closely resemble the observation that wild type Ago2 associates preferentially with shorter miRNA species [95, 121]. It is not known if the observed effect is due to loading of shorter miRNAs or shortening of the miRNA after incorporation into the Ago2 mutant. Additionally, it is not known to which extent 3'-shortening of a miRNA would affect the identity of bound targets.

Second, a phospho-mimicking cluster mutant of aa 555–561 (Phos2) has reduced endonucleolytic function (Fig. 2.22, lane 13). Interestingly, the recently published structure of human Ago2 with bound target RNA shows that S561 engages in specific interactions with the target RNA [74], making this and neighboring residues candidates for modification-regulated target binding.

However, it has often been observed that mutant side chains mimick phosphorylations only partially. As an example, phosphorylation of Ago2 Y393 decreases Dicer binding, whereas a phospho-mimicking mutant does not [181]. Therefore, mutant approaches should be complemented by different methods.

3.3.4 Phosphorylation of Ago proteins—an outlook

Here, several potential phosphorylation sites of human Ago2 were identified mass-spectrometrically. Importantly, the representation of phosphosites in Fig. 2.18 is based on search engine thresholds and does not include manual validation of fragment ion spectra.

In a first step of functional characterization, a subset of mutants was characterized in terms of miRNA binding and cleavage activity. These functional assays should be complemented by assays which provide information about association with binding partners (e.g. Dicer, GW182 proteins, other RISC components), cellular localization, and stability of the phosphomutants.

Apart from the clustered phosphorylations shown here, many different sites have been detected and are currently characterized, among them are also paralogue-specific phosphorylations.

To understand Ago function, it is essential to analyze regulatory networks that affect its post-translational modification. For all detected sites, involved kinases and phosphatases and their implication into signaling pathways remain completely open questions. Since many kinases depend on vaguely-defined consensus sequences, sequence-based predictions are often ambiguous. Future approaches for the identification of modifying enzymes will for example include kinase inhibitor screens combined with the mass-spectrometric detection of Ago phosphorylation patterns. Moreover, *in vitro* phosphorylation experiments could be used for kinase identification and the evolutionary conservation of Phos3 in *C. elegans* may provide further information.

Quantification of phosphorylated residues is another step towards understanding the functional importance of these modifications. A well suitable method for protein quantification has been established as part of this thesis. It is based on protein enrichment by Ago-APP and subsequent mass-spectrometric protein quantification by means of stable isotope-labeled peptides. In the present work, this approach has been used to quantify Ago paralogues. It is straightforward to adapt it to the quantification of phosphorylated peptides under different conditions. Since Ago-APP is based on conserved interactions, this would facilitate phosphorylation quantification in many species and enable phosphorylation analyses beyond cell culture systems.

4. Material and Methods

4.1 Material

4.1.1 Consumables and chemicals

All frequently used chemicals were purchased from Sigma-Aldrich (St. Louis, USA), Merck (Whitehouse Station, USA), Roth (Karlsruhe, Germany), AppliChem GmbH (Darmstadt, Germany) and Thermo Fisher Scientific (Waltham, USA) at the highest degree of purity.

Radiochemicals were obtained from Hartmann Analytic GmbH (Braunschweig, Germany), whereas stable isotope-labeled peptides were purchased from JPT Peptide Technologies GmbH (Berlin, Germany). Oligonucleotides were synthesized by Metabion GmbH (Planegg, Germany). Cell culture reagents were purchased from Sigma-Aldrich (St. Louis, USA). Enzymes, nucleotides, and molecular weight markers were obtained from Thermo Fisher Scientific (Waltham, USA), unless stated otherwise.

The composition of individual buffers is specified with the respective method they were used for (sections 4.2–4.4).

4.1.2 Bacterial strains and cell lines

Bacterial strains and cell lines are listed in Tables 4.1 and 4.2.

Table 4.1: Bacterial strains

strain	genotype
XL1-blue	F^- *recA1 endA1 gyrA96 thi-1 hsdR17 supE44 relA1 lac* F'[*proAB lacI*^{q}ZΔ*M15* Tn*10* (Tet^R)]
Bl21 (DE3)	F^- *dcm ompT lon hsdS*$_B$(r_B^- m_B^-) *gal* λ(DE3)
Rosetta	F^- *dcm ompT lon hsdS*$_B$(r_B^- m_B^-) *gal* λ(DE3) pRARE (Cam^R)
Bl21 (DE3) Gold pRARE	F^- *dcm ompT* Hte *lon hsdS*$_B$(r_B^- m_B^-) *gal EndAI* λ(DE3) pRARE (Cam^R)

Table 4.2: Cell lines

cell line	specification
HEK 293T	human embryonic kidney cells
HeLa	human cervical cancer cells
LNT-229	human glioma cells
MCF-7	human breast cancer cells
MEF Ago2 -/-	mouse embryonic fibroblasts
N2A	mouse neuroblastoma cells

4.1.3 Vectors, oligonucleotides, and cloned constructs

4.1.3.1 Vectors

Used vectors are listed in Tab. 4.3.

Table 4.3: Vectors

vector name	resistance	tag	application
VP5 (modified pIRES neo)	Amp, Neo	N-terminal FLAG + HA	eukaryotic expression vector; used for all Ago mutants
pUC18	Amp	none	cloning
pGEX-6P-1	Amp	N-terminal GST	prokaryotic expression vector; used for T6B peptide expression
pEC-K-3C-GST	Kana	N-terminal 6× His + GST	prokaryotic expression vector; used for T6B peptide expression

4.1.3.2 Constructs

FLAG/HA-tagged GFP and FLAG/HA-tagged human Ago1–4 were described before [72]. A codon-optimized Ago4 construct was used to generate Ago4 chimeras [111]. However, Ago4 PIWI domain sequences were amplified from the wild type Ago4 sequence. The mutants Ago3–2 PIWI, Ago2–3 PIWI, MutA, MutB, MutC, MutD, Ago2–1 PIWI, and a pUC18 construct encoding a perfectly complementary target RNA for miR-19b were provided by Simone Harlander (Biochemistry I, University of Regensburg). The target RNA sequence for miR-19b was described before [72]. Ago1 DEDH was provided by Dr. Sabine Rüdel (Biochemistry I, University of Regensburg). FLAG/HA-tagged HIWI, HIWI2, and HILI were provided by Prof. Dr. Gunter Meister. The pSUPER plasmid encoding miR-451 shRNA was described before [95]. 6×His-GST-tagged TNRC6B(599-683) (termed 'GST-T6B') and 6×His-GST-tagged TNRC6B(599-683) W623A W634A W653A W666A W680A (termed 'GST-T6B mutant') are based on the vector pEC-K-3C-GST and were described before [112].

Tab. 4.5 includes an overview on all constructs used in the present work. It lists the oligonucleotides that were used to generate them and indicates the respective cloning strategies.

All Ago constructs were cloned into the eukaryotic expression vector VP5 via *Not*I/*Eco*RI.

TNRC6B constructs for the recombinant expression of FLAG-GST-tagged peptides were subcloned into pGEX-6P-1. Therefore, TNRC6B 599-683 (wild type and mutant) was amplified from the pEC-K-3C-GST constructs [112] and inserted into pGEX-6P-1 via *Bam*HI/*Not*I. Two overlapping DNA fragments were

Table 4.4: Oligonucleotides for Northern Blotting, quantitative real time PCR, sequencing, and *in vitro* transcription scale up PCRs

oligonucleotide	orientation	ID	sequence (5´→ 3´)
Probes for Northern Blotting			
miR-19b	fwd		TCAGTTTTGCATGGATTTGCACA
miR-19b* 1/2	fwd		ATGCAAACCTGCAAAACT
miR-451	fwd		AACTCAGTAATGGTAACG
let-7a	fwd		AACTATACAACCTACTACCTCA
U6 snRNA	fwd		GAATTTGCGTGTCATCCTTGCGCAGGGGCCATGCTAA
Oligonucleotides for quantitative real time PCR			
GAPDH	fwd		ATGGGTGTGAACCATGAGAA
GAPDH	rev		GTGCTAAGCAGTTGGTGGTG
HMGA2	fwd		CGATTTCTACCTCAGCAGCA
HMGA2	rev		GGAAAGACCATGGCAATACA
Sequencing primers			
T7	fwd		TAATACGACTCACTATAGGG
VP5 seq rev	rev	JH s4	CCCAACAGCTGGCCCTCGCAGA
M13	fwd		TGTAAAACGACGGCCAGT
Ago1 int 1	fwd	SH s16	GCCAGTGATTGAGTTCATGTGTG
Ago1 int 2	fwd	SH s17	AGGTGCTCAAGAACTTCACAGA
Ago2 int 1	fwd	SH s14	GGCACAGCCAGTAATCGAGT
Ago2 int 2	fwd	SH s15	CGGAAGTCCATCTGAAGTCCT
GST N-Term	rev	JH s5	CATGTTGTGCTTGTCAGCTATATAACG
Oligonucleotides for amplification of *in vitro* transcription templates			
T7	rev	SH1	TAATACGACTCACTATAGAACAATTGCTTTTACAG
SP6	fwd	SH2	ATTTAGGTGACACTATAGGCATAAAGAATTGAAGA

amplified from the obtained constructs ('FLAG I' and 'FLAG II' in Tab. 4.5). In this step, the FLAG sequence and a short linker region containing a *Bgl*II restriction site were inserted 5' of the GST tag. The overlapping parts were annealed, filled up by Phusion DNA Polymerase, and inserted into the vector backbone via *Eco*RV/*Not*I.

4.1.3.3 Oligonucleotides

Oligonucleotides were diluted in water to a working concentration of 10 µM (primers) or 20 µM (probes) and stored at −20 °C. Tab. 4.5 lists oligonucleotides used for cloning and Tab. 4.4 lists all other nucleotides.

Table 4.5: Oligonucleotides for cloning. Construct names and cloning strategies are indicated. 'QuikChange' refers to site-directed mutagenesis, 'chimera' represents the use of chimeric primers with two different templates, and '3-way' refers to amplification of two inserts that were ligated in a 3-way blunt end ligation.

construct name	orientation	ID	primer sequence (5´→ 3´)	strategy
Ago3 slicer mutants				
Ago1	fwd	SH41	TAAT GCGGCCGC ATGGAAGCGGGACCCTCGGGA	regular
	rev	SH42	CGTA GAATTC TCAAGCGAAGTACATGGTGCGC	
Ago2	fwd	SH30	TAAT GCGGCCGC ATGTACTCGGGAGCCGGCCC	regular
	rev	SH31	CGTA GAATTC TCAAGCAAAGTACATGGTGCGCA	
Ago3	fwd	SH26	TAAT GCGGCCGC ATGGAAATCGGCTCCGCAGGAC	regular
	rev	SH27	CGTA GAATTC TTAAGCGAAGTACATTGTGCGTAAGG	
Ago3/2 PIWI	fwd/rev	SH36	ACCTTCTGTGTTCCAGCAACCAGT CATCTTTCTGGGAGCAGACGTCA	chimera
Ago2/3 PIWI	fwd/rev	SH45	AGGCCGCCGGTGTTCCAGCAG CCAGTGATCTTTTTGGGAGCCGAT	chimera
MutA	rev/fwd	SH37	CCTCGCATGTCCCATACTCCATG GACAGGGGTCGCAATAGCTTTATTC	chimera
MutB	rev/fwd	SH38	GTGGAAGTCTGATTGTCTGTTAGCTT TTTAATACATCTTTGTCCTGCCACAATG	chimera
MutC	rev/fwd	SH39	CTTCACACATGAACTGAATTACAGGTTG TGCCTTGTAAAACGCTGTTGCTG	chimera
MutD	rev/fwd	SH40	CAGGTGTGTATTTCATGGAGGGCAG GTGCCTCATGACCACGTCCAGG	chimera
Mut1	fwd	JH65	AGACCTGGCTATGGCACCATGG	3-way
	rev	JH64	AGGTGGAGGCTTGAAGGCATATCC	
Mut2	fwd	JH9	CCTGTCCATGCCGTTGATGTGGT	3-way
	rev	JH8	TTCCAGTGGCTCAGGCAAGGTC	
Mut3	fwd	JH61	CTGCCCAGCGTCCCTTTTGAGACGATCCAG GCCGTTGATGTGGTGCTACGAC	3-way
	rev	JH62	CCGTCCTGTCAGTACTTCATGCAG	
Mut4	fwd	JH61	CTGCCCAGCGTCCCTTTTGAGACGATCCAGGCCGTTGATGTGGTGCTACGAC	3-way
	rev	JH63	CCGCCCTGAAAGTGCATCGTGTAACGCCTGCAAGCTCACGCAAGAGACAAATTTGATTGACACCTTGAAAGGTC	
Mut5	rev/fwd	JH74	CCCTGTTCACTCTCCTAGGACACTT CTCTGGCTTGATATCCAATTCATAATGATAG	chimera
Mut6	rev/fwd	JH75	CACAGGAAGTGGATTGGCGGTGTA TAGATTCTTCCTGCCGTCAAACACG	chimera
Ago1 slicer mutants				
Ago1 DEDH	fwd	SR	CCTGCCTACTATGCCCACCTGGTGGC	QuikChange
	rev	SR	GCCACCAGGTGGGCATAGTAGGCAGG	
Ago2/1 PIWI	fwd/rev	SH44	AGGCCGCCGGTGTTCCAGCAG CCAGTGATATTCCTGGGAGCAGAT	chimera
Ago2/1 PIWI DEDH cl1	fwd	JH79	ATTCAAGACTTGGCCGCC ATGGTGCGTGAGCTCCTCATCC	3-way
	rev	JH78	GATCTCTTGCCGATGTTG CTGTACCCGCACAGTAGCACAG	
Ago(2/)1 PIWI DEDH cl2	fwd	JH72	GTGTCTGAAGGCCAG TTCCAGCAGGTACTCCACCAT GAGCTACTGGCCATTC	QuikChange
	rev	JH73	GAATGGCCAGTAGCTCATGGTGGAGTACCTGCTGGAACTGGCCTTCAGACAC	

Continued on next page

Table 4.5 – *Continued from previous page*

construct name	orientation	ID	primer sequence (5´→ 3´)	strategy
Ago1 N	rev/fwd	JH81	GGGGTGTACCTCATGGATGCCA GGTGCCTCATGACCACGTCCAGG	chimera
Ago1 $N_{1\text{-}64}$	rev/fwd	JH80	CCGGTTGACTCTACGGGGACACTT CTCTGGCTTGATATCCAATTCATAATGATAG	chimera
Ago4 slicer mutants				
Ago4	fwd	JH129	GATC GCGGCCGC ATGGAGGCGCTGGGACCCG	regular
Ago4	rev	JH130	ATC GAATTC TCAGGCAAAATACATCGTGTGCTGG	
Ago4-opt	fwd	JH151	GATC GCGGCCGC ATGGAAGCCCTGGGCCCTGG	regular
(Ago4 DEDR)	fwd	JH117	CGGATCATCTATTACCGTGACGGGGTATCTGAGGGACAAATG	QuikChange
	rev	JH118	CATTTGTCCCTCAGATACCCCGTCACGGTAATAGATGATCCG	
Ago4 DEDH	fwd	JH119	GCCCCTGCATATTATGCCCATCTTGTAGCATTTAGGGCAAG	QuikChange
	rev	JH120	CTTGCCCTAAATGCTACAAGATGGGCATAATATGCAGGGGC	
Ago2-4 DEDH	fwd/rev	JH131	GCCGCCGGTGTTCCAGCAG CCTGTCATCTTCCTGGGAGCGG	chimera
Ago2-4 DEDH cl2	rev	JH135	CTGCTGGAATTGTCCCTCAGATACCCCGTCACG	3-way
	fwd	JH136	GTACTCCACCATGAACTAATAGCAATTCGAAAGGCATGTATTAG	
Ago2-4 DEDH Δ	rev	JH138	GATCTCCTGCCGGGAAGTCTGCACC	3-way
	fwd	JH137	ATCCAGGACCTGACTAACATGGTTCGAGAG	
NT1	rev/fwd	JH154	GGTGTACCGCATGCTGGGCAG GTGCCTCATGACCACGTCCAGGG	chimera
NT2	rev/fwd	JH152	GTAGTGGTACACGTCGATCTTGGGGAT GTCCATTTCGAAGAAATTGGCCTGTAATTTG	chimera
NT3, NT8	rev/fwd	JH156	CGCCTGCAAGCTCACGCA GGACACCCACTGCACGGACACC	chimera
NT4	rev/fwd	JH157	CAAAGTCGGGTCTAGGTGGAGGCTT GAACAGGCTGGCGGGAGGGC	chimera
NT5	rev/fwd	JH158	GGCCTGTAATTTGATTGTTCTCCCGGA GGTGCCCAGGCCAGGCCG	chimera
NT6	rev/fwd	JH159	GATCTTGGGGATGTCCATTTCGAAGAA GTTGGCCAGCAGCCGGATGG	chimera
NT7	rev/fwd	JH155	AGGGACGCTGGGCAGCCG TCCAGCGAGAGCTTCCAGC	chimera
non-phosphorylatable and phospho-mimicking Ago mutants				
Ago2 Phos1 Ala	fwd	JH169	GCC ATGATCAGAGCGACTGCTAGGTC	3-way
	rev	JH168	TGCGGC CTGATTGTCCGTTAATTTTTTAATACATCTTTGTC	
Ago2 Phos2 Ala	fwd	JH165	GCCCTGGCT AACCTCTGCCTGAAGATCAACGTC	3-way
	rev	JH164	CTGTGGTGCGGC CCTCTGCACGTTCTTCATCTGC	
Ago2 Phos3 4 Ala	fwd	JH162	CATACCGCTGGGCAGGCC AACGGGCGAGACCACCAAGC	3-way
	rev	JH161	CGCTCCTTCAGCTGC GTCATGTTCCTTATCCACCAGGTGGTAC	
Ago2 Phos3 5 Ala	fwd	JH174	GCTGAAGGAGCGCAT GCA GCTGGGCAGGCCAAC	QuikChange
	rev	JH175	GTTGGCCTGCCCAGC TGC ATGCGCTCCTTCAGC	
Ago2 Phos4 AAF	fwd	JH177	GCGTTCTTC AAGGCACAGCCAGTAATCGAGTTTG	3-way
	rev	JH176	GGCTGCTGC CACATCAATATTCAGCATCATTTTCCAGAG	

Continued on next page

Table 4.5 – *Continued from previous page*

construct name	orientation	ID	primer sequence (5´→ 3´)	strategy
Ago2 Phos1 Glu	fwd	JH181	GAG ATGATCAGAGCGACTGCTAGGTC	3-way
	rev	JH180	CTCTTC CTGATTGTCCGTTAATTTTTTAATACATCTTTGTC	
Ago2 Phos2 Glu	fwd	JH183	GAGCTGGAG AACCTCTGCCTGAAGATCAACGTC	3-way
	rev	JH182	CTGTGGCTCTTC CCTCTGCACGTTCTTCATCTGC	
Ago2 Phos3 Glu	fwd	JH185	CATGAAGAGGGGCAGGAG AACGGGCGAGACCACCAAGC	3-way
	rev	JH184	CTCTCCTTCAGCCTC GTCATGTTCCTTATCCACCAGGTGGTAC	
Ago2 Phos4 Glu	fwd	JH179	GCGTTCGAG AAGGCACAGCCAGTAATCGAGTTTG	3-way
	rev	JH178	CTCTGCTTC CACATCAATATTCAGCATCATTTTCCAGAG	
Ago2 S220E	fwd	JH210	GGAAAATGATGCTGAATATTGATGTG GAG GCAACAGCGTTTTACAAGGCAC	QuikChange
	rev	JH211	GTGCCTTGTAAAACGCTGTTGC CTC CACATCAATATTCAGCATCATTTTCC	
Ago2 T222E	fwd	JH212	CTGAATATTGATGTGTCAGCA GAA GCGTTTTACAAGGCACAGC	QuikChange
	rev	JH213	GCTGTGCCTTGTAAAACGC TTC TGCTGACACATCAATATTCAG	
Ago2 Y225E	fwd	JH214	GTGTCAGCAACAGCGTTT GAG AAGGCACAGCCAGTAATCG	QuikChange
	rev	JH215	CGATTACTGGCTGTGCCTT CTC AAACGCTGTTGCTGACAC	
Ago2 S220E T222E	fwd	JH222	GAATATTGATGTGGAGGCA GAA GCGTTTTACAAGGCACAGC	QuikChange
	rev	JH223	GCTGTGCCTTGTAAAACGC TTC TGCCTCCACATCAATATTC	
Ago2 S220E Y225E	fwd	JH224	GTGGAGGCAACAGCGTTT GAG AAGGCACAGCCAGTAATC	QuikChange
	rev	JH225	GATTACTGGCTGTGCCTT CTC AAACGCTGTTGCCTCCAC	
Ago2 T222E Y225E	fwd	JH226	GTCAGCAGAAGCGTTT GAG AAGGCACAGCCAGTAATCGAG	QuikChange
	rev	JH227	CTCGATTACTGGCTGTGCCTT CTC AAACGCTTCTGCTGAC	
Ago1 Phos4 Glu	fwd	JH229	GCCTTCGAG AAGGCACAGCCAGTGATTGAGTTC	3-way
	rev	JH228	CTCGGCTTC GACATCAATGTTGAGCATCATCTTCCAC	
Ago2 Phos4 Asp	fwd	JH231	GCGTTCGAC AAGGCACAGCCAGTAATCGAGTTTG	3-way
	rev	JH230	GTCTGCATC CACATCAATATTCAGCATCATTTTCCAGAG	
TNRC6B constructs				
TNRC6B 599-683	fwd	JH124	CGTA GGATCC GATTGTCAGGCTGTCTTGCAGAC	regular
	rev	JH111	TACG GCGGCCGC TCA GAGCTCCCCCCATCCAGAC	
TNRC6B 599-683 mutant	rev	JH221	CGTA GCGGCCGC TCA GAGCTCCCCGGCTCCAGACTTC	regular, with JH124
FLAG I	fwd	JH121	CGTA GATATCTCGGTAGTGGGATACGACG	regular
	rev	JH147	GGGACATAGATCTGCTCTTGTCATC GTCGTCCTTGTAGTCCAT GAATACTGTTTCCTGTGTGAAATTGTTATCCG	
FLAG II	fwd	JH140	GATGACAAGAGCAGATCT ATGTCCCCTATACTAGGTTATTGGAAAATTAAG	regular, with JH111

4.1.4 Antibodies

Table 4.6: Primary and secondary antibodies. Hs, *Homo sapiens*; Mm, *Mus musculus*. WB, Western Blotting; IP, immunoprecipitation.

antibody	origin	application	dilution	supplier
antibodies against endogenous proteins				
α–Hs_Ago1, clone 1C9	rat	WB	1:5	
α–Hs_Ago2, clone 11A9 [187]	rat	WB, IP	1:5	
α–Mm_Ago2, clone 6F4	rat	WB	1:5	Dr. E. Kremmer,
α–Hs_TNRC6B, clone 6G3	rat	WB	1:5	Helmholtz Zentrum
α–Hs_TNRC6A–C, clone 7A9	rat	IP	1:5	München
α–Hs_TNRC6A–C, clone 11C12	rat	IP	1:5	
α–Rmc	rat	IP	1:5	
antibodies against tags				
α–HA, clone 16B12	mouse	WB	1:1000	Covance Research Products
α–FLAG M2	rabbit	WB	1:1000	Sigma-Aldrich
secondary antibodies				
α rat IRDye® 800CW	goat	WB	1:10,000	LI-COR Biosciences
α mouse IRDye® 800CW	goat	WB	1:15,000	LI-COR Biosciences
α rabbit IRDye® 800CW	goat	WB	1:5,000	LI-COR Biosciences

4.1.5 Exactly quantifiable heavy peptides for SRM measurements

Peptides were obtained as SpikeTides™ TQL peptides contain an exactly quantifiable tag that is cleaved off during tryptic digest and $^{15}N/^{13}C$-labeled C-terminal lysine (+8 kDa) or arginine (+10 kDa). Amino acid sequences of the proteotypic peptides used in selected reaction monitoring experiments are listed in Tab. 4.7.

Table 4.7: Stable isotope-labeled peptides used for relative quantification of Ago paralogues by selected reaction monitoring

paralogue (human/mouse)	paralogue-specific peptide I	paralogue-specific peptide II
Ago1	VLPAPILQYGGR	NIYTVTALPIGNER
Ago2	DYQPGITFIVVQK	VLQPPSILYGGR
Ago3	SANYETDPFVQEFQFK	SFFSAPEGYDHPLGGGR
Ago4	QVAWPELIAIR	EFGIVVHNEMTELTGR

4.1.6 Technical equipment

device	supplier
Mass-spectrometric equipment	
maXis plus UHR-QTOF	Bruker (Billerica, USA)
CaptiveSpray nanoBooster Source	Bruker (Billerica, USA)
QTRAP® 4500	AB SCIEX (Framingham, USA)
NanoSprayIII Ion source	AB SCIEX (Framingham, USA)
Chromatography system for both mass spectrometers:	
UltiMate 3000 RSLCnano System with Acclaim® PepMap100 C18 Nano-Trap column (300 µm i.d. × 5 mm) and Acclaim® PepMap C18 column (75 µm i.d. ×150 mm)	Thermo Fisher Scientific (Waltham, USA)
Other equipment	
FastPrep®24 (with Lysing Matrix D)	MP Biomedicals (Santa Ana, USA)
Odyssey Infrared Imaging System	LI-COR Biosciences (Lincoln, USA)
Personal Molecular Imager™ (Phosphoimager)	Bio-Rad Laboratories, Inc. (Hercules, USA)

4.2 Generation of DNA constructs

4.2.1 Polymerase Chain Reaction (PCR), restriction digests, and ligation

The composition of a standard PCR reaction and standard cycling conditions are listed below. Site-directed mutagenesis, PCR conditions for the generation of chimeric products, and 3-way blunt end cloning procedures are listed in the subsections 4.2.2–4.2.4.

PCR Mix, 50 µl	
5–50 ng	DNA template
1×	HF Buffer
0.2 mM	dNTPs
0.5 µM	reverse primer
0.5 µM	forward primer
2 U	Phusion DNA Polymerase

Cycling Conditions		
Initial denaturation	98 °C	30 s
Denaturation	98 °C	10 s
Annealing	55–72 °C	30 s
Elongation	72 °C	1 min/kbp
Terminal elongation	72 °C	10 min
		25–30 cycles

PCR products were separated on 0.7–2 % agarose gels, cut, and gel-extracted using the NucleoSpin® Gel and PCR Clean-up kit (MACHEREY-NAGEL GmbH). For preparative restrictions, the whole PCR reaction (alternatively 2 µg of plasmid DNA) was incubated with the appropriate FastDigest restriction enzymes (Thermo Fisher Scientific) at 37 °C. To prevent religation of vectors, 2 µl FastAP Thermosensitive Alkaline Phosphatase (Thermo Fisher Scientific) were added to the restriction mix after 4–6 h and incubated at 37 °C for 30 min. The restricted DNA was either directly purified by the NucleoSpin® Extract II kit or separated on 0.7–2 % agarose gels first.

For ligations, 50 ng of the cut and dephosphorylated vector were incubated with the 4 × molar excess of the restricted insert, 0.1 U/µl T4 DNA Ligase (Thermo Fisher Scientific), appropriate buffer and eventually PEG 4000. Ligations were incubated at 22 °C for 1 h before proceeding to transformation.

4.2.2 Site-directed mutagenesis ('QuikChange')

Single amino acid changes were inserted by site-directed mutagenesis. Therefore, the whole plasmid was amplified with mutagenic primers and template DNA was removed by *Dpn*I digestion. The composition of the PCR reaction and cycling conditions for QuikChanges are listed below.

PCR Mix, 50 µl	
50 ng	template DNA
1×	HF Buffer
0.2 mM	dNTPs
0.2 µM	reverse primer
0.2 µM	forward primer
1 U	Phusion DNA Polymerase

Cycling Conditions		
Initial denaturation	98 °C	30 s
Denaturation	98 °C	10 s
Annealing	55 °C	30 s
Elongation	72 °C	1 min/kbp
Terminal elongation	72 °C	10 min
		18 cycles

4.2.3 Generation of Chimeras

For chimeric constructs, a terminal cloning primer and an internal chimeric primer were used. The shorter part of the construct was amplified first using the first template. Therefore, a standard PCR as described in 4.2.1 was performed. The resulting product resembles an elongated primer. It was used together with the other terminal cloning primer to amplify the second part of the construct from the second template. The composition of the second amplification reaction and cycling conditions are listed below.

PCR Mix, 50 µl	
250 ng	template DNA
1×	HF Buffer
0.2 mM	dNTPs
300 ng	PCR I
0.25 µM	primer
1 U	Phusion DNA Polymerase

Cycling Conditions		
Initial denaturation	98 °C	30 s
Denaturation	98 °C	10 s
Annealing	55 °C	45 s
Elongation	72 °C	1 min/kbp
Terminal elongation	72 °C	10 min
		25–30 cycles

4.2.4 Mutagenesis by 3-way blunt end ligation

The substitution of longer sequence stretches was achieved by generation of two PCR fragments that each carried part of the intended alterations at the 'central end' and a restriction site at the 'external end'. After restriction, the fragments were phosphorylated with T4 Polynucleotide Kinase (Thermo Fisher Scientific) and ligated into a cut and dephosphorylated vector in a three way blunt end ligation. Here, PEG 4000 was added to increase ligation efficiency.

4.2.5 Transformation of *E. coli*

For transformations, chemically competent *E. coli* (XL1-blue for propagation pf plasmid DNA; Bl21 (DE3) and Rosetta for prokaryotic protein expression) were thawed on ice. Approximately 0.5 µg of DNA were used for re-transformations, whereas 10 µl ligation mixture were used for cloned constructs. For site-directed mutagenesis, up to the whole volume of the *Dpn*I-digested and purified PCR product was used. The cells were incubated on ice for at least 10 min and subjected to a 30 s heatshock at 42 °C thereafter. After 5 min incubation on ice, 1 ml of LB medium was added, and the cells were incubated at 37 °C for at least 20 min while shaking. For re-transformations, 30 µl were plated on LB plates containing the appropriate antibiotic. For cloning, the whole volume was plated. LB plates were incubated overnight at 37 °C.

4.2.6 Extraction of plasmid DNA from *E. coli*

For overnight cultures, 5 ml of LB containing the appropriate antibiotic were inoculated with a single colony. To screen large numbers of clones by analytical digests, a fast DNA extraction method was applied [227]. Briefly, 2 ml of the overnight culture were pelleted and resuspended

in 40 µl EasyPrep Buffer. The samples were incubated at 99 °C for 1 min, followed by an incubation on ice for 1 min, and clearance by centrifugation at 15,000 g for 15 min. 5–10 µl of the supernatants were used for analytical digests with 0.1 µl of the appropriate FastDigest restriction enzyme(s) (Thermo Fisher Scientific).

For all other applications than analytical digests, plasmid DNA was extracted by means of the NucleoBond® Plasmid and Xtra Midi kits (MACHEREY-NAGEL GmbH) according to the manufacturer's protocols.

LB medium	10 g/l NaCl, 5 g/l yeast extract, 10 g/l tryptone (pH 7.2–7.5)
EasyPrep Buffer	10 mM Tris/HCl (pH 8), 1 mM EDTA, 15 % saccharose, 2 mg/ml lysozyme, 0.2 mg/ml RNase A, 0.1 mg/ml BSA

4.2.7 Sequencing

Plasmid DNA was sequenced by GATC Biotech AG (Köln, Germany), SEQLAB Sequence Laboratories Göttingen GmbH (Göttingen, Germany), or Macrogen (Amsterdam, The Netherlands). Sequencing primers are listed in Tab. 4.4.

4.3 Protein-based methods

4.3.1 Expression and purification of recombinant protein

Wild type and mutant T6B expression constructs were transformed into chemically competent *E. coli* Bl21 (DE3) GOLD pRARE (constructs present in pEC-K-3C , i.e. GST-T6B wild type and mutant) or Bl21 (constructs present in pGEX-6P-1, i.e. FLAG-GST-T6B wild type and mutant).

Typically, recombinant GST-tagged proteins was purified from 2–3 l of bacterial culture. Cells were grown at 37 °C to an optical density (OD) of 0.4, incubated at 18 °C until an OD of 0.6 was reached, and protein expression was induced with 1 mM isopropyl β-D-1-thiogalactopyranoside (IPTG). The cultures were harvested after incubation overnight at 18 °C.

For initial experiments, protein was batch-purified. Therefore, the bacteria pellet of 1 l culture was resuspended in 25 ml Resuspension Buffer. After cell lysis by sonification, the lysate was incubated rotating at 4 °C for 30 min and clarified by centrifugation at 10,000 g. Per 1 l culture volume, 1 ml of Glutathione Sepharose 4 Fast Flow (50 % slurry, GE Healthcare) was washed with cold PBS two times. The lysate were added to the washed matrix and incubated rotating at 4 °C for 2 h to let GST fusion proteins bind to the glutathione matrix. Thereafter, the matrix was washed with cold PBS three times and loaded onto a gravity flow column (Bio-Rad Laboratories). Elution was carried out in five steps by addition of each 0.5 ml elution buffer. The flowthrough was collected in microcentrifuge tubes. A shortened Bradford test was used to optically assess the protein content of the eluted fractions. Therefore, 1–5 µl of an elution fraction were diluted in 1 ml 1 × Bradford Reagent (Bio-Rad Laboratories). Protein-containing fractions were unified and dialyzed against 1 l PBS two times for each 1–2 h. Dialyzed protein was aliquoted and stored at −80 °C.

Resuspension Buffer	PBS supplemented with 1× Complete Protease Inhibitor Cocktail (Roche Diagnostics GmbH (Mannheim, Germany), 0.1 mg/ml lysozyme, 10 U/ml benzonase, 0.1 mM DTT, 0.5 % Triton X-100, 10 mM $MgCl_2$
Glutathione Elution Buffer	20 mM glutathione, 50 mM Tris/HCl pH 8, 120 mM NaCl

For large scale purifications[1], the bacterial cell pellet was resuspended in GST-A. After sonication, the lysate was clarified by centrifugation at 40,000 g for 40 min and loaded onto a 15 ml Glutathione Sepharose column (GE Healthcare). The column was washed with 10 colume volumes (cv) of GST-A before the GST-tagged protein was eluted in 4 cv of GST-B. The fractions containing the GST fusion protein were concentrated and further purified by a desalting chromatography column (HiPrep 26/10 Desalting, GE Healthcare) equilibrated in PBS supplemented with 5% gylcerol. Desalted fractions were adjusted to ca. 2 mg/ml and stored at $-80\,^{\circ}C$.

GST-A	PBS supplemented with 1 mM AEBSF, 1 mM DTT, 1 mg/ml lysozyme
GST-B	PBS supplemented with 20 mM Tris pH 8.0, 10 mM glutathione

4.3.2 Cell culture

Human and murine cells were cultured under standard conditions (37 °C, 5 % CO_2) using Dulbecco's modified Eagle's medium (DMEM, Sigma-Aldrich) supplemented with 10% FBS (Sigma-Aldrich) and Penicillin/Streptomycin (Sigma-Aldrich). An overview of the cell lines used in the present work is given in Tab. 4.2.

4.3.2.1 Transfection by calcium phosphate

HEK 293T cells were transfected using calcium phosphate, ideally at a confluency of 30 %. Per 15 cm plate, 5–15 µg DNA and 123 µl of 2 M $CaCl_2$ were filled up to 1 ml with water in a reaction tube. In a second reaction tube, 1 ml of 2×HEPES-buffered saline was prepared. The DNA-containing solution was addded to the HEPES-buffered saline while shaking. The mixture was incubated at room temperature for 10 min and thereafter carefully added to the cells. The cells were harvested after 24–48 h.

2×HEPES-buffered saline	274 mM NaCl, 1.5 mM Na_2HPO_4, 54.6 mM HEPES (pH 7.1)

4.3.2.2 Transfection by Lipofectamine LTX and PLUS Reagent

MEF Ago2$^{-/-}$ cells were transfected by Lipofectamine® LTX and PLUS™ Reagent (Thermo Fisher Scientific) according to the manufacturer's protocol. Briefly, the cells were seeded to 6-well plates in antibiotics-free medium one day before transfection. Transfection was ideally performed at about 80 % confluency. Therefore, 2.5 µg of DNA (for co-transfections 2×5µg DNA) were diluted in 100 µl Opti-MEM® I Reduced Serum Media (Thermo Fisher Scientific) and 2.5 µl of PLUS™ Reagent were added. After 5 min incubation, 17.5 µl Lipofectamine® LTX were added

[1] conducted by Leonhard Jakob, Biochemistry I, University of Regensburg

and the mixture was incubated at room temperature for 20 min. The cell culture medium was changed before the Lipofectamine mixture was applied to the cells. The cells were harvested 2 d after transfection.

4.3.3 Lysate preparation

4.3.3.1 Lysate preparation from cell culture samples

Cells were usually grown on 10 cm or 15 cm cell culture dishes. For cell harvest, the medium was removed thoroughly and 1–1.5 ml of cold PBS were added. A rubber policemen was used to scrape the cells off the plate. The cells were transferred to 2 ml reaction tubes and pelleted for 10 min at 200 g. The supernatant was removed and the pellet was either lysed directly or frozen in liquid nitrogen and stored at −80 °C. For cell lysis, the pellet was resuspended in 0.5–1.3 ml lysis buffer and incubated on ice for 20 min. Generally, NET buffer was applied for immunopurifications and Ago-APPs, whereas RIPA buffer was used for FLAG-IPs and subsequent RISC cleavage assays. V Buffer does not contain ingredients that interfere with the tyrosine phosphatase inhibitor Na_3VO_4 and was therefore used for Ago-APPs that were intended for mass-spectrometric analysis of phosphorylation sites. After lysis, the cell debris was removed by centrifugation (20 min at 15,000 g).

NET buffer	50 mM Tris/HCl pH 7.5, 150 mM NaCl, 5 mM EDTA, 0.5 % NP-40, 10 % Glycerol, 1 mM NaF, 0.5 mM DTT, 1 mM AEBSF
RIPA buffer	50 mM Tris/HCl, pH 7.5, 150 mM NaCl, 0.1 % SDS, 1 % sodium deoxycholate, 1 % NP-40, 1 mM NaF, 0.5 mM DTT, 1 mM AEBSF
V Buffer	10 mM HEPES pH 7.5, 150 mM NaCl, 10 % glycerol, 0.5 % NP-40, 1 mM NaF, 5 mM Na_3VO_4, 1 mM AEBSF

4.3.3.2 Lysate preparation from tissues

Mouse tissue lysates were prepared in 800 µl NET buffer. The tissue was mechanically disrupted using FastPrep®-24 with lysing matrix D (45 s at 6.5 m/s,). Thereafter, the ceramic beads were spinned down for 1 min at 13,000 g. The supernatant was transferred to a new reaction tube and the ceramic beads were washed with NET buffer once. The supernatants of the disruption and washing steps were united and spinned down at 15,000 g for 30 min.

Arabidopsis cell extract was obtained from suspension cultured PSB-D cells as described before [228]. Drosophila embryonic extracts were obtained as described before [229].

4.3.4 Immunoprecipitation (IP)

For IPs of endogenous proteins, monoclonal antibodies were coupled to Protein G Sepharose (GE Healthcare). Depending on the amount of input material, 30–100 µl beads were washed with cold PBS twice and coupled with 0.5–1.5 ml hybridoma supernatant for at least 3 h, preferably overnight. The coupled beads were washed with PBS twice to remove excess antibody.

For IPs of FLAG/HA-tagged proteins that were overexpressed in HEK 293T cells, anti-FLAG M2 agarose (Sigma-Aldrich) was used. Prior to use, the matrix was washed with cold PBS twice.

Eventually, the total protein concentration of the lysate was determined by a short Bradford test. Input samples of the lysates were taken, mixed with Laemmli sample buffer, and stored at −20 °C. For immunoprecipitation, the lysate was incubated with the antibody-coupled beads for at least 3 h while rotating at 4 °C. After incubation, supernatant samples were taken and mixed with Laemmli sample buffer. The affinity matrix was sedimented by centrifugation for 1 min at 1,000 g and the supernatant was removed. The beads were washed with the lysis buffer four times. During the first washing step, the samples were transferred to new reaction tubes to minimize contamination by unspecific protein binding to the tube material. After a final washing step with PBS, the supernatant was removed quantitatively and the beads were eluted by addition of 2 × Laemmli sample buffer.

5×SDS sample buffer	300 mM Tris/HCl pH 6.8, 10 % SDS, 62.5 % glycerol, 0.05 % bromophenol blue, 10 % β-mercaptoethanol

4.3.5 Ago-APP (Ago Affinity Purification by Peptides)

Ago-APP is based on a GST pulldown approach. In the first step, recombinant 6×His-GST-TNRC6B(599-683) (termed 'GST-T6B') or 6×His-GST-TNRC6B(599-683) W623A W634A W653A W666A W680A (termed 'GST-T6B mutant') was coupled to Glutathione Sepharose (GE Healthcare). Therefore, the beads were washed with cold PBS twice. At least 100 µg of the peptide were added to 50 µl beads (50 % slurry) in 0.5–1 ml PBS. The coupling reaction was incubated for a minimum of 1 h while rotating at 4 °C. After coupling, the beads were washed with cold PBS three times to remove excess peptide. Next, the lysate, optimally prepared in NET buffer, was added to the peptide-coupled beads. The samples were incubated for 3 h while rotating at 4 °C. Thereafter, the affinity matrix was transferred to a new reaction tube and washed with NET buffer four times. After a final washing step with PBS or PreScission Cleavage Buffer, the supernatant was removed quantitatively and the beads were eluted using one of the following strategies:

- elution by SDS sample buffer: most stringent
  2 × SDS sample buffer was added to the beads and incubated at 95 °C.

- elution by Glutathione Elution Buffer: selective
  At least the packed bead volume of Glutathione Elution Buffer was added and incubated with the beads at room temperature for 30 min.

- elution by PreScission Cleavage: selective
  PreScission Cleavage Buffer and 0.1 µg/µl PreScission Protease were added to the beads and incubated overnight at 4 °C.

Glutathione Elution Buffer	20 mM GSH, 50 mM Tris/HCl pH 8, 120 mM NaCl
PreScission Cleavage Buffer	50 mM Tris/HCl pH 7.5, 150 mM NaCl, 1 mM EDTA, 1 mM DTT

4.3.6 SDS-PAGE, Western Blot, and Coomassie staining

Depending on the molecular weight of the protein of interest, 6 % or 10 % SDS polyacrylamide gels were used. For input and supernatant samples, 25–100 µg of total protein was loaded. For eluates of affinity-purified samples, loading volumes depended on the type of subsequent analysis. The maximum possible volume (approximately 100 µl after widening the wells) was loaded for subsequent mass-spectrometric identification of phosphorylation sites. SDS polyacrylamide gels were run at 140 V until the dye front had passed the stacking gel. Thereafter, voltage was increased to 220 V and the gel was run until the dye front had completely passed it.

stacking gel	125 mM Tris/HCl pH 6.8, 0.1 % SDS, 0.15 % TEMED, 5 % Acrylamide/Bis solution (37.5:1), 0.05 % APS
Separating gel	380 mM Tris/HCl PH 8.8, 0.1 % SDS, 0.1 % TEMED, 6–10 % Acrylamide/Bis solution (37.5:1), 0.05 % APS
SDS Running Buffer	25 mM Tris, 192 mM glycine, 1 % SDS

For Western Blotting, three equally-sized Whatman papers and a Hybond ECL membrane (GE Healthcare) were soaked in Towbin Blotting Buffer and placed on the positive electrode. The SDS gel was equilibrated in Blotting Buffer and transferred to the layers. Three additional Whatman papers of the same size were soaked in Towbin Blotting Buffer, placed on top of the gel, and air was removed. Western Blots were performed at 10 V with a blotting time of 1–3 h (approximately 1 min per kDa). The blotted membrane was blocked in 5 % milk in TBS-T for at least 30 min. Antibodies were diluted in 5 % milk in TBS-T. The blot was incubated with the primary antibody for at least one hour, if possible overnight. Thereafter, the blot was washed with TBST-T three times for 10 min and incubated with the secondary antibody for one hour. After three additional washing steps with TBS-T, the blot was scanned at the Odyssey Infrared Imaging System (Biorad).

Towbin Blotting Buffer	25 mM Tris, 192 mM glycine, 20 % methanol (pH 8.6)
TBS-T	10 mM Tris, 150 mM NaCl, 0.05 % Tween (pH 8)

For Coomassie staining, the SDS gel was placed in Coomassie Staining Solution for at least 1 h. It was destained until protein bands were clearly visible. Samples for MS analysis were handled with extreme care, i.e. use of clean gel running equipment and high purity SDS Running Buffer, Coomassie Staining, and Coomassie Destaining Solutions.

Coomassie Stain	10 % acetic acid, 30 % ethanol, 0.25 % Coomassie R250
Coomassie Destain	10 % acetic acid, 30 % ethanol

4.3.7 Mass-spectrometric analyses

All mass-spectrometric analyses were performed by the group of Prof. Dr. Rainer Deutzmann (Biochemistry I, University of Regensburg).

4.3.7.1 MS sample preparation

Gel bands were cut and transferred into 2 ml Eppendorf tubes containing freshly prepared 50 mM NH_4HCO_3. The gel slices were washed for 15–30 min while shaking vigorously. NH_4HCO_3/AN 3:1 was used in the next washing step and the solution was exchanged until the gel slices had lost their blue color. After washing with NH_4HCO_3/AN 1:1, the gel slices were washed with 100–200 µl acetonitrile. The liquid was removed and the samples were lyophilized for 0.5–1 h.

Free cysteines were reduced by treating the samples with 200 µl Reduction Reagent for 35 min at 56 °C. The samples were carbaimdomethylated with 200 µl freshly prepared Carbamidomethylation Reagent for 35 min in the dark at room temperature. Thereafter, the initial washing steps with 50 mM NH_4HCO_3 and acetonitrile were repeated, the liquid was removed, and the samples were again lyophilized.

For tryptic in-gel digest, 10–15 µl trypsin working solution were added to the gel slices and incubated at 37 °C until the gel was soaked with liquid (ca. 2 µg trypsin per 100 µl gel volume). 50 mM NH_4HCO_3 was added until the gel slices were covered well. The samples were incubated overnight at 37 °C.

For elution steps, low-bind tips (Axygen Scientific Inc.) were used. The supernatant of the tryptic digest was transferred to a new 0.5 ml reaction tube and 5 % formic acid was added to the remaining gel slices until they were covered well. The second elution was incubated at 37 °C for at least 30 min while shaking at 300 rpm. The supernatant was added to the first eluate and a third elution step was performed with NH_4HCO_3/AN 1:1. The unified elutions were lyophilized and the lyophilisate was resuspended in 20 µl of 5 % formic acid.

50 mM NH_4HCO_3	50 mM NH_4HCO_3
NH_4HCO_3/AN 3:1	75 % NH_4HCO_3 (50 mM), 25 % acetonitrile
NH_4HCO_3/AN 1:1	50 % NH_4HCO_3 (50 mM), 50 % acetonitrile
Reduction Reagent	1 mg/ml DTT, 50 mM NH_4HCO_3
Carbamidomethylation Reagent	5 mg/ml iodoacetamide, 50 mM NH_4HCO_3
trypsin stock solution	0.133 µg/µl Trypsin Gold Mass Spectrometry Grade (Promega) solved in 1 M HCl
trypsin working solution	40 µg/ml trypsin, 50 mM NH_4HCO_3

4.3.7.2 Mass spectrometers

The QTRAP 4500 (termed 'QTRAP') is a hybrid triple quadrupole/linear ion trap mass spectrometer, whereas the maXis plus UHR-QTOF (termed 'MAXIS') is an ultra-high resolution quadrupole time-of-flight mass spectrometer. Both mass spectrometers work with electrospray ionization and are coupled to liquid chromatography systems (cf. subsection 4.1.6). After concentration on a trapping column, peptides were separated by reversed-phase chromatography using a linear gradient of 4 % to 40 % acetonitrile in 0.1 % formic acid at a flow rate of 300 nl/min, performed in 45 min (QTRAP) or 60 min (MAXIS).

4.3.7.3 Mass-spectrometric measurements

For protein identification, samples were analyzed on the MAXIS mass spectrometer. Up to the 20 most abundant precursor ions were selected for fragmentation by collisional dissociation.

Phosphorylation sites of human Ago proteins were detected on both the QTRAP 4500 and the MAXIS mass spectrometers by data-dependent analysis.

For quantification of Ago1-4, Ago-APP was applied in combination with an SRM-based method. Therefore, unique synthetic peptides applicable to human and murine samples were used as internal standard (peptides are listed in Tab. 4.7). An exactly quantified amount of the individual stable isotope-labeled peptides was spiked into tryptic digests and incubated overnight at 37°C. Ago1-4 quantification was performed on the QTRAP 4500 mass spectrometer.

4.3.7.4 MS data analysis

Data obtained on the MAXIS mass spectrometer were launched to MASCOT using the ProteinScape software (Bruker Daltonics). Mascot (v2.3.02) was used to search the NCBI nr protein data base or the SWISS-PROT nr database. Optionally, the search was restricted to certain taxa. Mascot scores and expectation values were used to assess the reliability of identified proteins and phosphorylation sites.

4.4 RNA-based methods

4.4.1 RNA isolation

For quantitative real time PCRs, RNA was extracted from inputs and affinity-purified samples with TRIzol® (Thermo Fisher Scientific) according to the manufacturer's guidelines. Thereby, TRIzol was directly added to the beads of affinity-purified samples.

For cleavage assays and miRNA binding analyses, RNA was isolated after protein digestion by Proteinase K. Therefore, 250 µl Proteinase K buffer (containing 40 µg Proteinase K) were directly added to the beads and incubated at 65 °C for 15 min. Next, 300 µl of Roti®Aqua-Phenol/Chloroform/Isoamyl alcohol (25:24:1, Roth) were added. The samples were vortexed and centrifuged at 15,000 g for 10 min. The aqueous phase was transferred to a new reaction tube and 2.5 volumes of ethanol and 1 µl Glycogen RNA grade (Thermo Fisher Scientific) were added. The RNA was precipitated overnight at −20 °C (alternatively for 30 min at −80 °C) and thereafter pelleted by centrifugation at 15,000 g for 30 min. The resulting pellet was washed with 70 % ethanol, air-dried, and resuspended in water or RNA sample buffer.

Proteinase K Buffer	0.4 µg/µl Proteinase K (Thermo Fisher Scientific), 300 mM NaCl, 25 mM EDTA, 2 % SDS, 200 mM Tris pH 7.5
2× RNA sample buffer	bromophenol blue and xylene cyanol in formamide

4.4.2 Quantitative real time PCR (qRT-PCR)

For quantitative real time PCR, RNA from TRIzol extractions was resuspended in water. DNA contaminants were digested with DNAse I for 30 min at 37 °C. DNase I was inactivated by addition of EDTA and 10 min incubation at 65 °C. cDNA was synthesized by means of the iScript™ cDNA Synthesis Kit (Bio-Rad Laboratories), which was used according to the manufacturer's protocol. Thereby, the total volume of RNA isolated from affinity purifications (IPs or APPs) was used. 1 µg RNA was used for cDNA synthesis from input samples containing total RNA. After cDNA synthesis, 20 µl of cDNA were diluted with 30 µl of water. Per sample, 2 µl cDNA, each 0.6 µl forward and reverse primers, and 7.5 µl SsoFast™ EvaGreen Supermix (Bio-Rad Laboratories) were mixed in a total volume of 15 µl. DNA amplification was monitored on a C1000™ thermal cycler with CFX96™ real time detection system (Bio-Rad Laboratories).

For determination of ratios (fold changes), all possible $\Delta\Delta C_t$ ratios of sample triplicates and the control triplicates were calculated. Errors are based on standard deviations, which were determined from all received ratios (adapted from [230]).

4.4.3 RNA separation by urea PAGE and Northern Blotting

Dependent on the length of the investigated RNA, 8–18 % urea polyacrylamide gels (Urea Gel Systems, National Diagnostics) were prepared according to the manufacturer's protocols. The gels were prerun in 1×TBE at 400 V, wells were washed thoroughly, and RNA samples (mixed with 2× RNA sample buffer) were loaded. For Northern Blotting, a loading volume of 20 µl per well was not exceeded. 8 % urea polyacrylamide gels were run at 400 V for ca. 1 h, 12 % polyacrylamide gels for ca. 1.5 h, and 18 % polyacrylamide gels for ca. 5 h.

10×TBE	890 mM Tris, 890 mM boric acid, 20 mM EDTA
2× RNA sample buffer	bromophenol blue and xylene cyanol in formamide

Optionally, the urea gel was stained with ethidiumbromide for 10 min to assess RNA quality. For blotting, three Whatman papers and an Amersham Hybond-N membrane (GE Healthcare) of the same size were soaked in water and assembled on the positive electrode. The gel was rinsed with water, transferred to the paper-membrane layer and covered with three more Whatman papers soaked in water. Blotting was conducted at 20 V for 30 min. Afterwards, the miRNA 5' ends were crosslinked to the membrane [231]. Therefore, an EDC crosslinking solution was prepared from 184 mg EDC (1-ethyl-3-(3-dimethyl-aminopropyl)-carbodiimid), 61.25 µl 1-methylimidazol (12.5 M), 75 µl HCl (1M) and H_20 in a total volume of 6 ml. One Whatman paper was placed on plastic film and soaked with the freshly prepared EDC crosslinking solution. The membrane was placed on the Whatman paper with the RNA side facing up and wrapped in plastic film together with the EDC-soaked paper. Crosslinking took place at 50 °C for 1 h. Thereafter, the membrane was gently washed with water and dried.

Probes were labeled by T4 Polynucleotide Kinase (Thermo Fisher Scientific), which transfers the terminal phosphate from ^{32}P-γ-ATP to the 5' end of the DNA oligonucleotide. The reaction was

incubated at 37 °C for at least 30 min and stopped by addition of 30 µl 30 mM EDTA. The probes were purified by Sephadex G25 columns (GE Healthcare).

The membrane was prehybridized at 50 °C in hybridization solution. After about one hour, the labeled probe was added and incubated with the membrane overnight at 50 °C. Afterwards, the membrane was washed with Wash Buffer I two times for each 10 min and with Wash Buffer II one time. It was wrapped in plastic film, exposed to a screen and this was scanned at a phosphoimaging system (BioRad).

ethidiumbromide staining solution	1 µg/ml ethidiumbromide in 1×TBE
20×SSC	3 M NaCl, 0.3 M trisodium citrate (pH 7)
50×Denhardt's solution	1 % Bovine serum albumin fraction V, 1 % Polyvinylpyrrolidon K30, 1 % Ficoll 400
Hybridization solution	1×SSC, 20 mM Na_2HPO_4 pH 7.2, 7 % SDS, 1× Denhardt's solution
Wash buffer I	5×SSC, 1 % SDS
Wash Buffer II	1×SSC, 1 % SDS

4.4.4 RISC cleavage assays

4.4.4.1 *In vitro* transcription

The composition of an *in vitro* transcription reaction is listed below.

In vitro transcription, 200 µl	
20 mM	NTPs
10 mM	DTT
1 %	Triton X-100
2 mM	Sperimidin
25 mM	$MgCl_2$
30 mM	Tris/HCl pH 8
10 µg	template
0.2 µl	pyrophosphatase
20 µg	T7 RNA polymerase

A T7 RNA Polymerase purified by Dres. Nora Treiber and Thomas Treiber (both Biochemistry I, University of Regensburg) was used for *in vitro* transcriptions. The reactions were incubated at 37 °C for 3–4 h. Thereafter, 40 U DNase I (Thermo Fisher Scientific) were added and incubated for 15 min at 37 °C to remove template DNA.

4.4.4.2 Cap-labeling of the target RNA

A perfectly complementary target RNA for miR-19b has been described before [72]. The DNA template was cloned into a pUC18 vector and amplified by T7 and SP6 primers in a 250 µl PCR reaction (Tab. 4.4. After gel separation, the appropriate band was excised and DNA was extracted. For *in vitro* transcription, 400 ng of the DNA template were used. The *in vitro* transcribed RNA was separated on an 8 % urea gel. The transcription product was visualized by UV shadowing, excised, and eluted from the gel by addition of RNA Elution Buffer. It was incubated at 65 °C for

1 h while shaking. After gel elution, the liquid was transferred to a new reaction tube. The RNA was precipitated with 2.5 volumes of ethanol and resuspended in water. The RNA concentration was determined and working aliquots were stored at −80 °C.

For cap-labeling, the *in vitro* transcribed RNA was incubated in a 20 µl cap labeling reaction for 4 h at 30 °C. The cap-labeled target RNA was again separated on an 8 % urea gel, visualized by UV shadowing, excised, and eluted from the gel. After ethanol precipiation, the substrate was disolved in ca. 20 µl water and stored at −20 °C.

RNA Elution Buffer	
10 × GT buffer	400 mM Tris pH 8, 60 mM $MgCl_2$, 150 mM DTT, 20 mM spermidine
cap labeling reaction	1 × GT buffer, 50 µg/µl target RNA, 25 µM S-Adenosyl methionine, 0.5 U/µl RiboLock RNase Inhibitor (Thermo Fisher Scientific), 10 % guanylyltransferase, 1 µCi/µl ^{32}P-α-GTP

4.4.4.3 RISC cleavage assay

RISC cleavage assays were performed with 50 % (v/v) immunoprecipitated protein in 1× Translation Mix in a 20 µl reaction. The cleavage reactions were started by addition of 1–2 Bq/cm^2 cap-labeled target RNA per sample. After incubation for 90 min at 30 °C, the reaction was stopped by addition of 250 µl Proteinase K Buffer. The RNA was extracted using aqua-phenol/chloroform/isoamyl alcohol (25:24:1, Roth) and precipitated overnight with 20 µg of glycogen RNA grade (Thermo Fisher Scientific). The RNA was pelleted by centrifugation, solved in 10 µl of formamide loading dye, and stored at −20 °C.

A partial RNase T1 digest of the radiolabeled target RNA was used as a ladder. Therefore, 83.6 µl of the carrier RNA solution and 4 µl of the RNase T1 dilution were mixed. This 'T1 Mix' was stored at −20 °C. The ladder was prepared by adding the same amount of radiolabeled target that was used for a single cleavage reaction to 10 µl of the T1 Mix. The digest was incubated at 50 °C for exactly 10 min and immediately transferred to −20 °C. It was thawed only shortly before use. Typically, 2 µl of the T1 digest were loaded into one lane.

3 × Translation Mix	200 mM KCl, 20 mM $MgCl_2$, 25 mM DTT, 5 mM ATP, 1 mM GTP, 0.5 U/µl RiboLock RNase Inhibitor
Proteinase K Buffer	0.4 µg/µl Proteinase K (Thermo Fisher Scientific), 300 mM NaCl, 25 mM EDTA, 2 % SDS, 200 mM Tris pH 7.5
carrier RNA solution	25 µM sodium citrate pH 5.0, 7.5 M urea, 1 mM EDTA, 0.1 µg/µl yeast tRNA (Ambion), 0.05 % bromophenol blue, 0.05 % xylene cyanol
RNase T1 dilution	25 µM sodium citrate pH 5.0, 7.5 M urea, 1 mM EDTA, 5 U/µl RNase T1 (Fermentas), 0.05 % bromophenol blue, 0.05 % xylene cyanol

4.4.4.4 Autoradiographic sequencing gels

Samples of *in vitro* RISC cleavage assays were resolved on 8 % sequencing gels (UreaGel System, National Diagnostics). Therefore, a SequiGen Sequencing Cell (21 × 40 cm, 0.4 mm spacers, 16-well plastic comb, supplied by Bio-Rad Laboratories) was used. To facilitate gel pouring and

disassembly, the glass plate connected to the buffer tank was treated with Sigmacote® (Sigma-Aldrich) before each use. To increase roughness of the opposing surface, the other glass plate was regularly covered with 1 M NaOH and incubated with the solution overnight.

Each well was washed directly before loading. MiniFlex Flat tips (Sorenson BioScience) were used to reach the bottom of the well. Usually, 5 µl of cleavage samples and 2 µl of the T1 partial digest were loaded. The gel was run at 50 W (approximately 1,700 V) until the bromophenol blue front had reached the height of the lower plastic tank, ca. 8 cm from the bottom of the gel. The glass plates were disassembled and eventual wrinkles were carefully moved to the edges. After transferring the gel onto a Whatman filter paper, it was covered with plastic film, vacuum-dried at 80 °C for 1 h, and exposed to a screen for up to 3 d.

4.5 Bioinformatic analyses

4.5.1 Sequence retrieval and alignments

The protein sequences that were used for alignments are listed below. The sequences were retrieved from `www.uniprot.org` and their accession codes within the database are indicated (as of December 7th, 2014).

Homo sapiens	AGO1, Q9UL18; AGO2, Q9UKV8; AGO3, Q9H9G7; AGO4, Q9HCK5 PIWIL1/HIWI, Q96J94; PIWIL2/HILI, Q8TC59; PIWIL3, Q7Z3Z3; PIWIL4/HIWI2, Q7Z3Z4
Mus musculus	AGO1, Q8CJG1; AGO2, Q8CJG0; AGO3, Q8CJF9; AGO4, Q8CJF8
Rattus norvegicus	AGO2, Q9QZ81
Caenorhabditis elegans	ALG-1, G5EES3; ALG-2, O16720
Drosophila melanogaster	AGO1, Q32KD4; AGO2, Q9VUQ5

Alignments were carried out by MAFFT version 7 (L-INS-i, scoring matrix BLOSUM62, gap opening penalty 1.53, offset value 0.0) [232].

4.5.2 Homology models

A homology model of Ago1 as built by means of the I-TASSER server (version 2.1) [233], which selected the human Ago2 structures (PDB 4EI1/4OLA and 4F3T) and *Kluyveromyces polysporus* Argonaute (PDB 4F1N) as templates. The secondary structure content of the Ago1 homology model and the Ago2 structures was determined by means of DSSP [185].

The homology models of human Ago3 and Ago4 were constructed by Prof. Dr. Rainer Merkl and Lukas Kater (both Biochemistry II, University of Regensburg) by means of Yasara Structure (V 13.4.21) [234]. Therefore, initial 3D-models were built on the basis of the human Ago2 and Ago1 structures (PDB IDs 4EI1/4OLA, 4F3T, 4KRE and 4KXT) [235, 236]. The models were refined by means of loop modeling and side chain optimization. Subsequently, the best scoring fragments were combined to deduce the final homology models.

PyMol (`www.pymol.org`) was used to analyze the 3D data sets of Ago structures and homology models.

A. Appendix

Tables A.1–A.6 list phosphorylated peptides of all mass-spectrometric measurements summarized in Fig. 2.18 and Tab. A.7 lists all phosphorylated peptides represented in Fig. 2.19. In case of technical replicates, several elutions, or several analyzed Ago bands, duplicates were removed and only the phosphopeptide with the highest score and lowest expectation value is listed. Phosphorylated residues are underlined. Non-unique peptides in Tables A.1–A.6 are indicated by an asterisk. Measurements were conducted on two different mass spectrometers [QTRAP 4500 (ABSciex) and maXis plus UHR-QTOF (Bruker)] as indicated for each data set. This accounts for different scores and expectation values. These data should only be compared when measurements were conducted on the same mass spectrometer.

Phosphosites that were retrieved from PhosphoSitePlus® (`www.phosphosite.org`) ar displayed in Tab. A.8.

Table A.1: Phosphopeptides: Ago2-IP I, QTRAP

peptide	score	expectation value	position in Ago2
YHLVDKEHDSAEGSHTSGQSNGR	71.45	0.00000072	S[824]
RPASHQTFPLQQESGQTVECTVAQY	47.63	0.00021	T[303], T[307], Y[311]
YHLVDKEHDSAEGSHTSGQSNGR	32.42	0.0053	S[828]
QILTYQLCHTYVR*	28.6	0.0086	T[783]
VGDTVLGMATQCVQM	28.25	0.0094	T[544]
EHDSAEGSHTSGQSNGR	25.04	0.018	S[824], S[828], S[834]
VGDTVLGMATQCVQMKNVQRTTPQTLS	23.36	0.058	S[561]
DVTGRVLQPPSILYGGR	23.24	0.042	T[409], S[417], Y[420]
SHQTFPLQQESGQTVECTVAQYFK	22.08	0.079	S[290], T[293], S[300], T[303]
LQPPSILYGGRNK	18.55	0.096	S[417]
KLTDNQTST*	18.22	0.069	T[363]
KLTDNQTSTM*	17.93	0.066	T[361], T[362], T[363]
SFFTASEGCSNP	17.2	0.071	S[180], T[183], S[185], S[189]
NTYAGLQ	16.46	0.042	Y[512]
HLKNTYAGLQ	15.96	0.077	T[511]
MMLNIDVSATA*	15.47	0.077	T[222]

Table A.2: Phosphopeptides: Ago2-IP II, QTRAP

peptide	score	expectation value	position in Ago2
SA<u>S</u>FNTDPYVR	60.19	0.00000096	S[387]
DEMTDV<u>T</u>GRVLQPPSILYGGR	54.28	0.000011	T[409]
YHLVDKEHDSAEGSH<u>TS</u>GQ<u>S</u>NGRDHQALAK	36.75	0.00021	T[830], S[831], S[834]
SIEEQQKPLTD<u>S</u>QR	32.99	0.0005	S[253]
VGDTVLGMA<u>T</u>QCVQMK	29.12	0.0012	T[544]
YHLVDKEHD<u>S</u>AEGSHTSGQ<u>S</u>NGRDHQALAK	28.29	0.0019	S[824], S[834]
YHLVDKEHD<u>S</u>AEGSHT<u>S</u>GQ<u>S</u>NGRDHQALAK	27.11	0.0019	S[824], S[831], S[834]
YHLVDKEHDSAEG<u>S</u>HTSGQSNGRDHQALAK	26.82	0.0027	S[828]
PDFG<u>T</u>SGRTIKLQANFFEMDIPK	25.31	0.0066	T[33]
YHLVDKEHDSAEGSHT<u>S</u>GQ<u>S</u>NGR	24.47	0.0036	S[831], S[834]
YHLVDKEHDSAEG<u>S</u>H<u>TS</u>GQSNGRDHQALAK	24.45	0.0036	S[828], T[830], S[831]
SFF<u>T</u>ASEGCSNPLGGGR	22.3	0.0059	T[183]
PDFGTSGR<u>T</u>IKLQANFFEMDIPK	21.94	0.015	T[37]
YHLVDKEHDSAEGSHTSGQ<u>S</u>NGRDHQALAK	21.4	0.01	S[834]
YHLVDKEHDSAEGSH<u>TS</u>GQSNGR	21.38	0.0073	T[830], S[831]
YHLVDKEHDSAEGSH<u>T</u>SGQSNGRDHQALAK	19.71	0.014	T[830]
<u>Y</u>CA<u>T</u>VRVQQHRQEIIQDLAAMVR	17.44	0.026	Y[625], T[628]
SFFTA<u>S</u>EGCSNPLGGGR	17.43	0.018	S[185]
VGD<u>T</u>VLGMATQCVQMK	15.94	0.025	T[538]
VKF<u>T</u>KEIK*	15.45	0.029	T[259]

Table A.3: Phosphopeptides: TNRC6A–C Co-IP I (α-TNRC6A–C 11C12), MAXIS

peptide	score	expectation value	position in Ago2
<u>S</u>FFTASEGCSNPLGGGR	84.54	0.00000025	S[180]
RPASHQTFPLQQESGQTVECTVAQYFK	65.44	0.000042	T[307]
H<u>T</u>YLPLEVCNIVAGQR*	65.37	0.000025	T[337]
WV<u>S</u>CVSLQALHDALSGR	63.46	0.000045	S[136]
VGD<u>T</u>VLGMATQCVQMK	61.54	0.000065	T[538]
FS<u>S</u>DELQILTYQLCHTYVR	58.51	0.00017	S[776]
T<u>T</u>PQTLSNLCLK	56.4	0.00017	T[556]
<u>Y</u>PHLPCLQVGQEQK*	55.29	0.00027	Y[322]
SA<u>S</u>FNTDPYVR	48.48	0.00094	S[387]
<u>T</u>TPQTLSNLCLK	45.88	0.002	T[555]
RPASHQ<u>T</u>FPLQQESGQTVECTVAQYFK	42.27	0.009	T[303]
CIKKL<u>T</u>DNQTSTMIR	40.28	0.008	T[357]
RPASHQTFPLQQESGQTVECTVAQ<u>Y</u>FK	32.23	0.091	Y[311]

Table A.4: Phosphopeptides: TNRC6A–C Co-IP II (α-TNRC6A–C 7A9), MAXIS

peptide	score	expectation value	position in Ago2
<u>S</u>FFTASEGCSNPLGGGR	63.32	0.00000047	S[180]
H<u>T</u>YLPLEVCNIVAGQR*	62.99	0.0000005	T[337]

Continued on next page

Table A.4 – *Continued from previous page*

peptide	score	expectation value	position in Ago2
WVSCVSLQALHDALSGR	58.46	0.0000014	S[136]
SFFTASEGCSNPLGGGR	56.13	0.0000024	T[183]
SASFNTDPYVR	55.88	0.0000026	S[387]
TTPQTLSNLCLK	53.37	0.0000046	T[556]
TTPQTLSNLCLK	45.65	0.000027	T[555]
IDIYHYELDIKPEKCPR	44.94	0.000032	Y[55]
VGDTVLGMATQCVQMK	41.86	0.000065	T[538]
WVSCVSLQALHDALSGR	36.09	0.00025	S[139]
YPHLPCLQVGQEQK*	32.39	0.00078	Y[322]
FSSDELQILTYQLCHTYVR	30.87	0.00082	S[776]
VSIKWVSCVSLQALHDALSGR	25.08	0.0031	S[131]
RVGDTVLGMATQCVQMK	23.98	0.004	T[544]
RNKAIATPVQGVWDMR	22.35	0.0058	T[429]
YHLVDKEHDSAEGSHTSGQSNGRDHQALAK	19.95	0.014	S[828]
FFTASEGCSNPLGGGR	19.43	0.011	S[185]
RPASHQTFPLQQESGQTVECTVAQYFK	18.28	0.026	T[307]
HTYLPLEVCNIVAGQR*	16.99	0.02	Y[338]
YHLVDKEHDSAEGSHTSGQSNGRDHQALAK	15.62	0.037	S[824]

Table A.5: Phosphopeptides: Ago-APP I, QTRAP

peptide	score	expectation value	position in Ago2
RVGDTVLGMATQCVQM	27.28	0.015	T[544]
NVQRTTPQTLSNLCLKI	27.21	0.027	T[555], T[556], T[559], S[561]
LTDNQTSTM*	24.38	0.014	T[361], S[362], T[363]
TTPQTLSNLCLKINVKLGGVNNILLP	23.51	0.058	T[559]
PNRYCATVRVQQHR	23.06	0.03	Y[625], T[628]
YHLVDKEHDSAEGSHTSGQSNGR	22.85	0.04	S[824]
HDALSGRLPSVPFETIQALDVVMR	20.87	0.09	S[153], T[158]
YTPVGRSFFTASEGCSNPLGGGR	20.68	0.075	S[185]
DGKKPSIAAVVGSMDAHPNR	20.66	0.073	S[610]
QEEISKLMRSASFNTD	20.63	0.083	S[380], S[387], T[390]
TSTMIRATAR	17.68	0.061	S[362], T[363], T[368]
SFFTASEGCSNP	17.2	0.082	S[180], T[183], S[185], S[189]
NVQRTTPQTLSNL	17.2	0.088	T[556], T[559]
QTSTMIRATARSAPDR	17.06	0.08	T[363]
VECTVAQYFK*	16.97	0.061	T[307]
TPVYAEVKRVGDT*	16.94	0.083	T[526], T[538]
EHDSAEGSHTSG	15.98	0.052	S[831]
LTDNQTST*	15.26	0.064	T[357]
AIATPVQGV	15.22	0.057	T[429]

Table A.6: Phosphopeptides: Ago-APP II, QTRAP

peptide	score	expectation value	position in Ago2
YHLVDKEHDSAEGSHTSGQSNGR	75.01	0.00000024	S[824]
ELLIQFYKSTRFKPT*	31.02	0.0069	T[657]
PSILYGGRNKAIATPVQGVWDMR	30.14	0.011	T[429]
VQRTTPQTLSNLCLK	20.46	0.055	T[555], S[561]
EHDSAEGSHTSGQSNGR	20.39	0.064	S[824], T[830], S[834]
KLTDNQTSTM*	20.25	0.041	T[361], S[362], T[363]
TTPQTLSNLCLKINV	18.26	0.092	T[555], T[556], T[559], S[561]
MYSGAGPA	18.22	0.024	Y[2], S[3]
QEEISKLMRSASFN	17.36	0.073	S[387]
RVGDTVLGMATQCV	17.27	0.086	T[538]
KLTDNQTSTMI*	16.60	0.085	S[362]
GSHTSGQSNGR	15.12	0.088	S[828], T[830], S[834]

Table A.7: Phosphopeptides of Ago1–4

peptide	score	expectation value	position in Ago1–4
Unique phosphopeptides of Ago1			
MEAGPSGAAAGAYLPPLQQVFQAPR	57.61	0.0000018	S[6]
YHLVDKEHDSGEGSHISGQSNGRDPQ	35.83	0.0004	S[826]
YHLVDKEHDSGEGSHISGQSNGR	33.93	0.0004	S[822], S[826]
MEAGPSGAAAGAYLPPLQQVFQAPR	28.05	0.0017	Y[13]
YHLVDKEHDSGEGSHISGQSNGRDPQALAK	26.1	0.0025	S[822]
YHLVDKEHDSGEGSHISGQSNGRDPQALAK	23.74	0.0042	S[829]
YHLVDKEHDSGEGSHISGQSNGRDPQALAK	19.99	0.011	S[832]
YHLVDKEHDSGEGSHISGQSNGR	17.02	0.02	S[826], S[829]
YHLVDKEHDSGEGSHISGQSN	16.57	0.026	S[829], S[832]
Unique phosphopeptides of Ago2			
SFFTASEGCSNPLGGGR	63.32	0.00000047	S[180]
WVSCVSLQALHDALSGR	58.46	0.0000014	S[136]
SFFTASEGCSNPLGGGR	56.13	0.0000024	T[183]
SASFNTDPYVR	55.88	0.0000026	S[387]
TTPQTLSNLCLK	53.37	0.0000046	T[556]
TTPQTLSNLCLK	45.65	0.000027	T[555]
IDIYHYELDIKPEKCPR	44.94	0.000032	Y[55]
VGDTVLGMATQCVQMK	41.86	0.000065	T[538]
WVSCVSLQALHDALSGR	36.09	0.00025	S[139]
FSSDELQILTYQLCHTYVR	30.87	0.00082	S[776]
VSIKWVSCVSLQALHDALSGR	25.08	0.0031	S[131]
RVGDTVLGMATQCVQMK	23.98	0.004	T[544]
RNKAIATPVQGVWDMR	22.35	0.0058	T[429]
YHLVDKEHDSAEGSHTSGQSNGRDHQALAK	19.95	0.014	S[828]
FFTASEGCSNPLGGGR	19.43	0.011	S[185]
RPASHQTFPLQQESGQTVECTVAQYFK	18.28	0.026	T[307]
YHLVDKEHDSAEGSHTSGQSNGRDHQALAK	15.62	0.037	S[824]
Unique phosphopeptides of Ago3			
YHLVDKEHDSAEGSHVSGQSNGRDPQ	35.91	0,0004	S[829]
YHLVDKEHDSAEGSHVSGQSNGRDPQALAK	34.48	0,00036	S[825]
MEIGSAGPAGAQPLLMVPR	30.07	0,0011	S[5]
QVLYYELLAIREACISLEKDYQPGIT	27.77	0,0017	T[704]
VSWHLLHEVLTGR	24.52	0,0035	S[132]
YHLVDKEHDSAEGSHVSGQSNGRDPQALAK	23.74	0,0042	S[832]
YHLVDKEHDSAEGSHVSGQSNGR	23.69	0,0043	S[825], S[829]
YHLVDKEHDSAEGSHVSGQSNGRDPQALAK	19.99	0,011	S[835]
RPASHQTFPLQLENGQTVERTVAQYF	19.74	0,011	T[304]
LYTANPLPVATTGVDLDVTLPGEGGK	19.71	0,018	T[103]

Continued on next page

Table A.7 – *Continued from previous page*

peptide	score	expectation value	position in Ago1–4
YHLVDKEHDSAEGSHVSGQSN	16.57	0,026	S[832], S[835]
YHLVDKEHDSAEGSHVSGQSNGR	15.84	0,026	Y[816], S[825]
MWAIACFATQRQ	15.42	0,029	T[459]
Unique phosphopeptides of Ago4			
YHLVDKDHDSAEGSHVSGQSNGRDPQ	23.83	0.0089	S[830]
YHLVDKDHDSAEGSHVSGQSNGRDPQALAK	21.76	0.011	S[826]
CNVTRRPASHQTFPLQLENGQAMECTVAQYFK	18.63	0.027	S[280], T[283]
Non-unique phosphopeptides of Ago1–4			
HTYLPLEVCNIVAGQR	62.99	0.0000005	T[335] (Ago1) T[337] (Ago2) T[338] (Ago3) T[327] (Ago4)
TQCVQVKNVVKTSPQTLSNLCLK	46.95	0.000029	T[553] S[554] (Ago1) T[547], S[548] (Ago4)
TSPQTLSNLCLK	33.52	0.00044	S[554] (Ago1) S[557] (Ago3) S[548] (Ago4)
VGDTLLGMATQCVQVK	32.75	0.00053	T[536] (Ago1) T[539] (Ago3) T[530] (Ago4)
YPHLPCLQVGQEQK	32.39	0.00078	Y[320] (Ago1) Y[322] (Ago2) Y[323] (Ago3) Y[312] (Ago4)
TSPQTLSNLCLK	27.11	0.0019	S[554] (Ago1) S[557] (Ago3) S[548] (Ago4)
VGDTLLGMATQCVQVK	23.8	0.0042	T[536] (Ago1) T[539] (Ago3) T[530] (Ago4)
HTYLPLEVCNIVAGQR	16.99	0.02	Y[336] (Ago1) Y[338] (Ago2) Y[339] (Ago3) Y[328] (Ago4)
RVGDTLLGMATQCVQVK	16.75	0.021	T[542] (Ago1) T[545] (Ago3) T[536] (Ago4)

Table A.8: Phosphopeptides of Ago1–4 as listed at PhosphoSitePlus®

sequence context	position in Ago1–4	detection method site-specific	mass-spectrometric
Ago1			
GQEQKHTYLPLEVCN	Y[336]	0	3
IVILPGKTPVYAEVK	T[524]	0	1
GSMDAHPSRYCATVR	S[621]	0	1
HPSRYCATVRVQRPR	T[626]	0	1
LVDKEHDSGEGSHIS	S[822]	0	1
EHDSGEGSHISGQSN	S[826]	0	2
Ago2			
ALSGRLPSVPFETIQ	S[153]	0	2
QQKPLTDSQRVKFTK	S[253]	1	1
LQQESGQTVECTVAQ	T[303]	1	1
SGQTVECTVAQYFKD	T[307]	1	1
GQEQKHTYLPLEVCN	Y[338]	0	3
QRCIKKLTDNQTSTM	T[357]	0	1
EISKLMRSASFNTDP	S[385]	0	3
SKLMRSASFNTDPYV	S[387]	3	26
MRSASFNTDPYVREF	T[390]	0	1
ASFNTDPYVREFGIM	Y[393]	4	1
VVILPGKTPVYAEVK	T[526]	0	1
LPGKTPVYAEVKRVG	Y[529]	1	1
HPTEFDFYLCSHAGI	Y[749]	0	1
EFDFYLCSHAGIQGT	S[752]	0	1
sHAGIQGTSRPSHYH	T[759]	0	1
HAGIQGTSRPSHYHV	S[760]	0	1
VRCTRSVSIPAPAYY	S[798]	1	1
LVDKEHDSAEGSHTS	S[824]	0	1
EHDSAEGSHTSGQSN	S[828]	0	1
SAEGSHTSGQSNGRD	S[831]	0	1
Ago3			
MEIGSAGPAGAQ	S[5]	0	1
FFSAPEGYDHPLGGG	Y[189]	0	66
AQYFREKYTLQLKYP	Y[317]	0	1
KYTLQLKYPHLPCLQ	Y[323]	0	1
GQEQKHTYLPLEVCN	Y[339]	0	3
MRGKQFHTGVEIKMW	T[445]	0	1
IVILPGKTPVYAEVK	T[527]	0	1
GQFRQVLYYELLAIR	Y[682]	0	2
QFRQVLYYELLAIRE	Y[683]	0	6
DYQPGITYIVVQKRH	Y[705]	0	1
LVDKEHDSAEGSHVS	S[825]	0	3
EHDSAEGSHVSGQSN	S[829]	0	2

Continued on next page

Table A.8 – *Continued from previous page*

sequence context	position in Ago1–4	detection method	
		Ago-specific	proteomic screening
SAEGSHVSGQSNGRD	S[832]	0	2
GSHVSGQSNGRDPQA	S[835]	0	1
Ago4			
LGPGPPASLFQPPRR	S[11]	0	2
PKIDVYHYDVDIKPE	Y[47]	0	1
DRVDMEVTLPGEGKD	T[108]	0	1
GQEQKHTYLPLEVCN	Y[328]	0	3
VVILPGKTPVYAEVk	T[518]	0	1
TYVRCTRSVSIPAPA	S[798]	0	1

Bibliography

[1] Ender, C. and Meister, G.: Argonaute proteins at a glance. *Journal of Cell Science*, 123(Pt 11):1819–23, 2010.

[2] Yigit, E., Batista, P. J., Bei, Y., Pang, K. M., Chen, C.-C. G., Tolia, N. H., Joshua-Tor, L., Mitani, S., Simard, M. J., and Mello, C. C.: Analysis of the C. elegans Argonaute family reveals that distinct Argonautes act sequentially during RNAi. *Cell*, 127(4):747–57, 2006.

[3] Tolia, N. H. and Joshua-Tor, L.: Slicer and the argonautes. *Nature Chemical Biology*, 3(1):36–43, 2007.

[4] Meister, G.: Argonaute proteins: functional insights and emerging roles. *Nature Reviews Genetics*, 14(7):447–59, 2013.

[5] Hutvagner, G. and Simard, M. J.: Argonaute proteins: key players in RNA silencing. *Nature Reviews Molecular Cell Biology*, 9(1):22–32, 2008.

[6] Fabian, M. R. and Sonenberg, N.: The mechanics of miRNA-mediated gene silencing: a look under the hood of miRISC. *Nature Structural & Molecular Biology*, 19(6):586–93, 2012.

[7] Weinmann, L., Höck, J., Ivacevic, T., Ohrt, T., Mütze, J., Schwille, P., Kremmer, E., Benes, V., Urlaub, H., and Meister, G.: Importin 8 is a gene silencing factor that targets argonaute proteins to distinct mRNAs. *Cell*, 136(3):496–507, 2009.

[8] Gagnon, K. T., Li, L., Chu, Y., Janowski, B. a., and Corey, D. R.: RNAi Factors Are Present and Active in Human Cell Nuclei. *Cell Reports*, 6(1):211–21, 2014.

[9] Schraivogel, D. and Meister, G.: Import routes and nuclear functions of Argonaute and other small RNA-silencing proteins. *Trends in Biochemical Sciences*, 39(9):420–431, 2014.

[10] Castel, S. E. and Martienssen, R. a.: RNA interference in the nucleus: roles for small RNAs in transcription, epigenetics and beyond. *Nature Reviews Genetics*, 14(2):100–12, 2013.

[11] Aravin, A. a., Sachidanandam, R., Girard, A., Fejes-Toth, K., and Hannon, G. J.: Developmentally regulated piRNA clusters implicate MILI in transposon control. *Science*, 316(5825):744–7, 2007.

[12] Kuramochi-Miyagawa, S., Watanabe, T., Gotoh, K., Totoki, Y., Toyoda, A., Ikawa, M., Asada, N., Kojima, K., Yamaguchi, Y., Ijiri, T. W., Hata, K., Li, E., Matsuda, Y., Kimura, T., Okabe, M., Sakaki, Y., Sasaki, H., and Nakano, T.: DNA methylation of retrotransposon genes is regulated by

Piwi family members MILI and MIWI2 in murine fetal testes. *Genes & Development*, 22(7):908–17, 2008.

[13] Siomi, M. C., Sato, K., Pezic, D., and Aravin, A. a.: PIWI-interacting small RNAs: the vanguard of genome defence. *Nature Reviews Molecular Cell Biology*, 12(4):246–58, 2011.

[14] Ketting, R. F.: The many faces of RNAi. *Developmental Cell*, 20(2):148–61, 2011.

[15] Sijen, T., Steiner, F. a., Thijssen, K. L., and Plasterk, R. H. a.: Secondary siRNAs result from unprimed RNA synthesis and form a distinct class. *Science*, 315(5809):244–7, 2007.

[16] Pak, J. and Fire, A.: Distinct populations of primary and secondary effectors during RNAi in C. elegans. *Science*, 315(5809):241–4, 2007.

[17] Swarts, D. C., Makarova, K., Wang, Y., Nakanishi, K., Ketting, R. F., Koonin, E. V., Patel, D. J., and van der Oost, J.: The evolutionary journey of Argonaute proteins. *Nature Structural & Molecular Biology*, 21(9):743–753, 2014.

[18] Swarts, D. C., Jore, M. M., Westra, E. R., Zhu, Y., Janssen, J. H., Snijders, A. P., Wang, Y., Patel, D. J., Berenguer, J., Brouns, S. J. J., and van der Oost, J.: DNA-guided DNA interference by a prokaryotic Argonaute. *Nature*, 2014.

[19] Olovnikov, I., Chan, K., Sachidanandam, R., Newman, D. K., and Aravin, A. a.: Bacterial argonaute samples the transcriptome to identify foreign DNA. *Molecular Cell*, 51(5):594–605, 2013.

[20] Cai, X., Hagedorn, C. H., and Cullen, B. R.: Human microRNAs are processed from capped, polyadenylated transcripts that can also function as mRNAs. *RNA*, 10(12):1957–66, 2004.

[21] Lee, Y., Kim, M., Han, J., Yeom, K.-H., Lee, S., Baek, S. H., and Kim, V. N.: MicroRNA genes are transcribed by RNA polymerase II. *The EMBO Journal*, 23(20):4051–60, 2004.

[22] Lee, Y., Jeon, K., Lee, J.-t., Kim, S., and Kim, V. N.: MicroRNA maturation: stepwise processing and subcellular localization. *The EMBO Journal*, 21(17):4663–70, 2002.

[23] Lee, Y., Ahn, C., Han, J., Choi, H., Kim, J., Yim, J., Lee, J., Provost, P., Rå dmark, O., Kim, S., and Kim, V. N.: The nuclear RNase III Drosha initiates microRNA processing. *Nature*, 425(6956):415–9, 2003.

[24] Denli, A. M., Tops, B. B. J., Plasterk, R. H. a., Ketting, R. F., and Hannon, G. J.: Processing of primary microRNAs by the Microprocessor complex. *Nature*, 432(7014):231–5, 2004.

[25] Han, J., Lee, Y., Yeom, K.-H., Kim, Y.-K., Jin, H., and Kim, V. N.: The Drosha-DGCR8 complex in primary microRNA processing. *Genes & Development*, 18(24):3016–27, 2004.

[26] Gregory, R. I., Yan, K.-P., Amuthan, G., Chendrimada, T., Doratotaj, B., Cooch, N., and Shiekhattar, R.: The Microprocessor complex mediates the genesis of microRNAs. *Nature*, 432(7014):235–40, 2004.

[27] Lund, E., Güttinger, S., Calado, A., Dahlberg, J. E., and Kutay, U.: Nuclear export of microRNA precursors. *Science*, 303(5654):95–8, 2004.

[28] Bohnsack, M. T.: Exportin 5 is a RanGTP-dependent dsRNA-binding protein that mediates nuclear export of pre-miRNAs. *RNA*, 10(2):185–191, 2004.

[29] Yi, R., Qin, Y., Macara, I. G., and Cullen, B. R.: Exportin-5 mediates the nuclear export of pre-microRNAs and short hairpin RNAs. *Genes & Development*, 17(24):3011–6, 2003.

[30] Hutvágner, G., McLachlan, J., Pasquinelli, a. E., Bálint, E., Tuschl, T., and Zamore, P. D.: A cellular function for the RNA-interference enzyme Dicer in the maturation of the let-7 small temporal RNA. *Science*, 293(5531):834–8, 2001.

[31] Ketting, R. F., Fischer, S. E., Bernstein, E., Sijen, T., Hannon, G. J., and Plasterk, R. H.: Dicer functions in RNA interference and in synthesis of small RNA involved in developmental timing in C. elegans. *Genes & Development*, 15(20):2654–9, 2001.

[32] Chendrimada, T. P., Gregory, R. I., Kumaraswamy, E., Norman, J., Cooch, N., Nishikura, K., and Shiekhattar, R.: TRBP recruits the Dicer complex to Ago2 for microRNA processing and gene silencing. *Nature*, 436(7051):740–4, 2005.

[33] Haase, A. D., Jaskiewicz, L., Zhang, H., Lainé, S., Sack, R., Gatignol, A., and Filipowicz, W.: TRBP, a regulator of cellular PKR and HIV-1 virus expression, interacts with Dicer and functions in RNA silencing. *EMBO Reports*, 6(10):961–7, 2005.

[34] Lee, Y., Hur, I., Park, S.-Y., Kim, Y.-K., Suh, M. R., and Kim, V. N.: The role of PACT in the RNA silencing pathway. *The EMBO Journal*, 25(3):522–32, 2006.

[35] Bernstein, E., Caudy, A. A., Hammond, S. M., and Hannon, G. J.: Role for a bidentate ribonuclease in the initiation step of RNA interference. *Nature*, 409(6818):363–6, 2001.

[36] Zamore, P. D., Tuschl, T., Sharp, P. A., and Bartel, D. P.: RNAi: double-stranded RNA directs the ATP-dependent cleavage of mRNA at 21 to 23 nucleotide intervals. *Cell*, 101(1):25–33, 2000.

[37] Okamura, K. and Lai, E. C.: Endogenous small interfering RNAs in animals. *Nature Reviews Molecular Cell Biology*, 9(9):673–8, 2008.

[38] Watanabe, T., Takeda, A., Tsukiyama, T., Mise, K., Okuno, T., Sasaki, H., Minami, N., and Imai, H.: Identification and characterization of two novel classes of small RNAs in the mouse germline: retrotransposon-derived siRNAs in oocytes and germline small RNAs in testes. *Genes & Development*, 20(13):1732–43, 2006.

[39] Watanabe, T., Totoki, Y., Toyoda, A., Kaneda, M., Kuramochi-Miyagawa, S., Obata, Y., Chiba, H., Kohara, Y., Kono, T., Nakano, T., Surani, M. A., Sakaki, Y., and Sasaki, H.: Endogenous siRNAs from naturally formed dsRNAs regulate transcripts in mouse oocytes. *Nature*, 453(7194):539–43, 2008.

[40] Tam, O. H., Aravin, A. a., Stein, P., Girard, A., Murchison, E. P., Cheloufi, S., Hodges, E., Anger, M., Sachidanandam, R., Schultz, R. M., and Hannon, G. J.: Pseudogene-derived small interfering RNAs regulate gene expression in mouse oocytes. *Nature*, 453(7194):534–8, 2008.

[41] Babiarz, J. E., Ruby, J. G., Wang, Y., Bartel, D. P., and Blelloch, R.: Mouse ES cells express endogenous shRNAs, siRNAs, and other Microprocessor-independent, Dicer-dependent small RNAs. *Genes & Development*, 22(20):2773–85, 2008.

[42] Vagin, V. V., Sigova, A., Li, C., Seitz, H., Gvozdev, V., and Zamore, P. D.: A distinct small RNA pathway silences selfish genetic elements in the germline. *Science*, 313(5785):320–4, 2006.

[43] Le Thomas, A., Tóth, K. F., and Aravin, A. a.: To be or not to be a piRNA: genomic origin and processing of piRNAs. *Genome Biology*, 15(1):204, 2014.

[44] Haase, A. D., Fenoglio, S., Muerdter, F., Guzzardo, P. M., Czech, B., Pappin, D. J., Chen, C., Gordon, A., and Hannon, G. J.: Probing the initiation and effector phases of the somatic piRNA pathway in Drosophila. *Genes & Development*, 24(22):2499–504, 2010.

[45] Ipsaro, J. J., Haase, A. D., Knott, S. R., Joshua-Tor, L., and Hannon, G. J.: The structural biochemistry of Zucchini implicates it as a nuclease in piRNA biogenesis. *Nature*, 1–7, 2012.

[46] Brennecke, J., Aravin, A. a., Stark, A., Dus, M., Kellis, M., Sachidanandam, R., and Hannon, G. J.: Discrete small RNA-generating loci as master regulators of transposon activity in Drosophila. *Cell*, 128(6):1089–103, 2007.

[47] Gunawardane, L. S., Saito, K., Nishida, K. M., Miyoshi, K., Kawamura, Y., Nagami, T., Siomi, H., and Siomi, M. C.: A slicer-mediated mechanism for repeat-associated siRNA 5' end formation in Drosophila. *Science*, 315(5818):1587–90, 2007.

[48] Dueck, A. and Meister, G.: Assembly and function of small RNA - argonaute protein complexes. *Biological Chemistry*, 395(6):611–29, 2014.

[49] Matranga, C., Tomari, Y., Shin, C., Bartel, D. P., and Zamore, P. D.: Passenger-strand cleavage facilitates assembly of siRNA into Ago2-containing RNAi enzyme complexes. *Cell*, 123(4):607–20, 2005.

[50] Rand, T. a., Petersen, S., Du, F., and Wang, X.: Argonaute2 cleaves the anti-guide strand of siRNA during RISC activation. *Cell*, 123(4):621–9, 2005.

[51] Leuschner, P. J. F., Ameres, S. L., Kueng, S., and Martinez, J.: Cleavage of the siRNA passenger strand during RISC assembly in human cells. *EMBO Reports*, 7(3):314–20, 2006.

[52] Wang, B., Li, S., Qi, H. H., Chowdhury, D., Shi, Y., and Novina, C. D.: Distinct passenger strand and mRNA cleavage activities of human Argonaute proteins. *Nature Structural & Molecular Biology*, 16(12):1259–66, 2009.

[53] Petri, S., Dueck, A., Lehmann, G., Putz, N., Rüdel, S., Kremmer, E., and Meister, G.: Increased siRNA duplex stability correlates with reduced off-target and elevated on-target effects. *RNA*, 17(4):737–49, 2011.

[54] Gu, S., Jin, L., Zhang, F., Huang, Y., Grimm, D., Rossi, J. J., and Kay, M. a.: Thermodynamic stability of small hairpin RNAs highly influences the loading process of different mammalian Argonautes. *PNAS*, 108(22):9208–13, 2011.

[55] Kwak, P. B. and Tomari, Y.: The N domain of Argonaute drives duplex unwinding during RISC assembly. *Nature Structural & Molecular Biology*, 19(2):145–51, 2012.

[56] Yuan, Y.-R., Pei, Y., Ma, J.-B., Kuryavyi, V., Zhadina, M., Meister, G., Chen, H.-Y., Dauter, Z., Tuschl, T., and Patel, D. J.: Crystal structure of A. aeolicus argonaute, a site-specific DNA-guided endoribonuclease, provides insights into RISC-mediated mRNA cleavage. *Molecular Cell*, 19(3):405–19, 2005.

[57] Wang, Y., Sheng, G., Juranek, S., Tuschl, T., and Patel, D. J.: Structure of the guide-strand-containing argonaute silencing complex. *Nature*, 456(7219):209–213, 2008.

[58] Schirle, N. T. and MacRae, I. J.: The crystal structure of human Argonaute2. *Science*, 336(6084):1037–40, 2012.

[59] Elkayam, E., Kuhn, C.-d., Tocilj, A., Haase, A. D., Greene, E. M., Hannon, G. J., and Joshua-Tor, L.: The structure of human argonaute-2 in complex with miR-20a. *Cell*, 150(1):100–10, 2012.

[60] Nakanishi, K., Weinberg, D. E., Bartel, D. P., and Patel, D. J.: Structure of yeast Argonaute with guide RNA. *Nature*, 1–9, 2012.

[61] Faehnle, C., Elkayam, E., Haase, A., Hannon, G., and Joshua-Tor, L.: The Making of a Slicer: Activation of Human Argonaute-1. *Cell Reports*, 1–9, 2013.

[62] Nakanishi, K., Ascano, M., Gogakos, T., Ishibe-Murakami, S., Serganov, A., Briskin, D., Morozov, P., Tuschl, T., and Patel, D.: Eukaryote-Specific Insertion Elements Control Human ARGONAUTE Slicer Activity. *Cell Reports*, 3(6):1893–1900, 2013.

[63] Parker, J. S., Roe, S. M., and Barford, D.: Structural insights into mRNA recognition from a PIWI domain-siRNA guide complex. *Nature*, 434(7033):663–6, 2005.

[64] Ma, J.-B., Yuan, Y.-R., Meister, G., Pei, Y., Tuschl, T., and Patel, D. J.: Structural basis for 5'-end-specific recognition of guide RNA by the A. fulgidus Piwi protein. *Nature*, 434(7033):666–70, 2005.

[65] Wang, Y., Juranek, S., Li, H., Sheng, G., Tuschl, T., and Patel, D. J.: Structure of an argonaute silencing complex with a seed-containing guide DNA and target RNA duplex. *Nature*, 456(7224):921–6, 2008.

[66] Frank, F., Sonenberg, N., and Nagar, B.: Structural basis for 5'-nucleotide base-specific recognition of guide RNA by human AGO2. *Nature*, 465(7299):818–22, 2010.

[67] Boland, A., Tritschler, F., Heimstädt, S., Izaurralde, E., and Weichenrieder, O.: Crystal structure and ligand binding of the MID domain of a eukaryotic Argonaute protein. *EMBO Reports*, 11(7):522–7, 2010.

[68] Yan, K. S., Yan, S., Farooq, A., Han, A., Zeng, L., and Zhou, M.-M.: Structure and conserved RNA binding of the PAZ domain. *Nature*, 426(6965):468–74, 2003.

[69] Lingel, A., Simon, B., Izaurralde, E., and Sattler, M.: Nucleic acid 3'-end recognition by the Argonaute2 PAZ domain. *Nature Structural & Molecular Biology*, 11(6):576–7, 2004.

[70] Ma, J.-B., Ye, K., and Patel, D. J.: Structural basis for overhang-specific small interfering RNA recognition by the PAZ domain. *Nature*, 429(6989):318–22, 2004.

[71] Song, J.-J., Smith, S. K., Hannon, G. J., and Joshua-Tor, L.: Crystal structure of Argonaute and its implications for RISC slicer activity. *Science*, 305(5689):1434–7, 2004.

[72] Meister, G., Landthaler, M., Patkaniowska, A., Dorsett, Y., Teng, G., and Tuschl, T.: Human Argonaute2 mediates RNA cleavage targeted by miRNAs and siRNAs. *Molecular Cell*, 15(2):185–97, 2004.

[73] Liu, J., Carmell, M. a., Rivas, F. V., Marsden, C. G., Thomson, J. M., Song, J.-J., Hammond, S. M., Joshua-Tor, L., and Hannon, G. J.: Argonaute2 is the catalytic engine of mammalian RNAi. *Science*, 305(5689):1437–41, 2004.

[74] Schirle, N. T., Sheu-Gruttadauria, J., and MacRae, I. J.: Structural basis for microRNA targeting. *Science*, 346(6209):608–13, 2014.

[75] Wang, Y., Juranek, S., Li, H., Sheng, G., Wardle, G. S., Tuschl, T., and Patel, D. J.: Nucleation, propagation and cleavage of target RNAs in Ago silencing complexes. *Nature*, 461(7265):754–61, 2009.

[76] Bartel, D. P.: MicroRNAs: target recognition and regulatory functions. *Cell*, 136(2):215–33, 2009.

[77] Tomari, Y. and Zamore, P. D.: Perspective: machines for RNAi. *Genes & Development*, 19(5):517–29, 2005.

[78] Zander, A., Holzmeister, P., Klose, D., Tinnefeld, P., and Grohmann, D.: Single-molecule FRET supports the two-state model of Argonaute action. *RNA Biology*, 11(1):1–12, 2013.

[79] Deerberg, A., Willkomm, S., and Restle, T.: Minimal mechanistic model of siRNA-dependent target RNA slicing by recombinant human Argonaute 2 protein. *PNAS*, 110(44):17,850–5, 2013.

[80] Sheng, G., Zhao, H., Wang, J., Rao, Y., Tian, W., Swarts, D. C., van der Oost, J., Patel, D. J., and Wang, Y.: Structure-based cleavage mechanism of Thermus thermophilus Argonaute DNA guide strand-mediated DNA target cleavage. *PNAS*, 111(2):652–7, 2014.

[81] Yekta, S., Shih, I.-H., and Bartel, D. P.: MicroRNA-directed cleavage of HOXB8 mRNA. *Science*, 304(5670):594–6, 2004.

[82] Davis, E., Caiment, F., Tordoir, X., Cavaillé, J., Ferguson-Smith, A., Cockett, N., Georges, M., and Charlier, C.: RNAi-mediated allelic trans-interaction at the imprinted Rtl1/Peg11 locus. *Current Biology*, 15(8):743–9, 2005.

[83] Shin, C., Nam, J.-W., Farh, K. K.-H., Chiang, H. R., Shkumatava, A., and Bartel, D. P.: Expanding the microRNA targeting code: functional sites with centered pairing. *Molecular Cell*, 38(6):789–802, 2010.

[84] Karginov, F. V., Cheloufi, S., Chong, M. M. W., Stark, A., Smith, A. D., and Hannon, G. J.: Diverse endonucleolytic cleavage sites in the mammalian transcriptome depend upon microRNAs, Drosha, and additional nucleases. *Molecular Cell*, 38(6):781–8, 2010.

[85] Bracken, C. P., Szubert, J. M., Mercer, T. R., Dinger, M. E., Thomson, D. W., Mattick, J. S., Michael, M. Z., and Goodall, G. J.: Global analysis of the mammalian RNA degradome reveals widespread miRNA-dependent and miRNA-independent endonucleolytic cleavage. *Nucleic Acids Research*, 39(13):5658–68, 2011.

[86] Lee, Y. S., Nakahara, K., Pham, J. W., Kim, K., He, Z., Sontheimer, E. J., and Carthew, R. W.: Distinct roles for Drosophila Dicer-1 and Dicer-2 in the siRNA/miRNA silencing pathways. *Cell*, 117(1):69–81, 2004.

[87] Okamura, K., Ishizuka, A., Siomi, H., and Siomi, M. C.: Distinct roles for Argonaute proteins in small RNA-directed RNA cleavage pathways. *Genes & Development*, 18(14):1655–66, 2004.

[88] Tabara, H., Sarkissian, M., Kelly, W. G., Fleenor, J., Grishok, A., Timmons, L., Fire, A., and Mello, C. C.: The rde-1 gene, RNA interference, and transposon silencing in C. elegans. *Cell*, 99(2):123–32, 1999.

[89] Tabara, H., Yigit, E., Siomi, H., and Mello, C. C.: The dsRNA binding protein RDE-4 interacts with RDE-1, DCR-1, and a DExH-box helicase to direct RNAi in C. elegans. *Cell*, 109(7):861–71, 2002.

[90] Wu, L., Fan, J., and Belasco, J. G.: Importance of translation and nonnucleolytic Ago proteins for on-target RNA interference. *Current Biology*, 18(17):1327–32, 2008.

[91] Cheloufi, S., Dos Santos, C. O., Chong, M. M. W., and Hannon, G. J.: A dicer-independent miRNA biogenesis pathway that requires Ago catalysis. *Nature*, 465(7298):584–9, 2010.

[92] Cifuentes, D., Xue, H., Taylor, D. W., Patnode, H., Mishima, Y., Cheloufi, S., Ma, E., Mane, S., Hannon, G. J., Lawson, N. D., Wolfe, S. a., and Giraldez, A. J.: A novel miRNA processing pathway independent of Dicer requires Argonaute2 catalytic activity. *Science*, 328(5986):1694–8, 2010.

[93] Yang, J.-S., Maurin, T., Robine, N., Rasmussen, K. D., Jeffrey, K. L., Chandwani, R., Papapetrou, E. P., Sadelain, M., O'Carroll, D., and Lai, E. C.: Conserved vertebrate mir-451 provides a platform for Dicer-independent, Ago2-mediated microRNA biogenesis. *PNAS*, 107(34):15,163–8, 2010.

[94] Yang, J.-S., Maurin, T., and Lai, E. C.: Functional parameters of Dicer-independent microRNA biogenesis. *RNA*, 18(5):945–57, 2012.

[95] Dueck, A., Ziegler, C., Eichner, A., Berezikov, E., and Meister, G.: microRNAs associated with the different human Argonaute proteins. *Nucleic Acids Research*, 40(19):9850–62, 2012.

[96] Yoda, M., Cifuentes, D., Izumi, N., Sakaguchi, Y., Suzuki, T., Giraldez, A. J., and Tomari, Y.: Poly(A)-specific ribonuclease mediates 3'-end trimming of Argonaute2-cleaved precursor microRNAs. *Cell Reports*, 5(3):715–26, 2013.

[97] O'Carroll, D., Mecklenbrauker, I., Das, P. P., Santana, A., Koenig, U., Enright, A. J., Miska, E. a., and Tarakhovsky, A.: A Slicer-independent role for Argonaute 2 in hematopoiesis and the microRNA pathway. *Genes & Development*, 21(16):1999–2004, 2007.

[98] Morita, S., Horii, T., Kimura, M., Goto, Y., Ochiya, T., and Hatada, I.: One Argonaute family member, Eif2c2 (Ago2), is essential for development and appears not to be involved in DNA methylation. *Genomics*, 89(6):687–96, 2007.

[99] Van Stry, M., Oguin, T. H., Cheloufi, S., Vogel, P., Watanabe, M., Pillai, M. R., Dash, P., Thomas, P. G., Hannon, G. J., and Bix, M.: Enhanced susceptibility of Ago1/3 double-null mice to influenza A virus infection. *Journal of Virology*, 86(8):4151–7, 2012.

[100] Modzelewski, A. J., Holmes, R. J., Hilz, S., Grimson, A., and Cohen, P. E.: AGO4 regulates entry into meiosis and influences silencing of sex chromosomes in the male mouse germline. *Developmental Cell*, 23(2):251–64, 2012.

[101] Su, H., Trombly, M. I., Chen, J., and Wang, X.: Essential and overlapping functions for mammalian Argonautes in microRNA silencing. *Genes & Development*, 23(3):304–17, 2009.

[102] Wang, D., Zhang, Z., O'Loughlin, E., Lee, T., Houel, S., O'Carroll, D., Tarakhovsky, A., Ahn, N. G., and Yi, R.: Quantitative functions of Argonaute proteins in mammalian development. *Genes & Development*, 26(7):693–704, 2012.

[103] Förstemann, K., Horwich, M. D., Wee, L., Tomari, Y., and Zamore, P. D.: Drosophila microRNAs are sorted into functionally distinct argonaute complexes after production by dicer-1. *Cell*, 130(2):287–97, 2007.

[104] Tomari, Y., Du, T., and Zamore, P. D.: Sorting of Drosophila small silencing RNAs. *Cell*, 130(2):299–308, 2007.

[105] Mi, S., Cai, T., Hu, Y., Chen, Y., Hodges, E., Ni, F., Wu, L., Li, S., Zhou, H., Long, C., Chen, S., Hannon, G. J., and Qi, Y.: Sorting of small RNAs into Arabidopsis argonaute complexes is directed by the 5' terminal nucleotide. *Cell*, 133(1):116–27, 2008.

[106] Hafner, M., Landthaler, M., Burger, L., Khorshid, M., Hausser, J., Berninger, P., Rothballer, A., Ascano, M., Jungkamp, A.-C., Munschauer, M., Ulrich, A., Wardle, G. S., Dewell, S., Zavolan, M., and Tuschl, T.: Transcriptome-wide identification of RNA-binding protein and microRNA target sites by PAR-CLIP. *Cell*, 141(1):129–41, 2010.

[107] Landthaler, M., Gaidatzis, D., Rothballer, A., Chen, P. Y., Soll, S. J., Dinic, L., Ojo, T., Hafner, M., Zavolan, M., and Tuschl, T.: Molecular characterization of human Argonaute-containing ribonucleoprotein complexes and their bound target mRNAs. *RNA*, 14(12):2580–96, 2008.

[108] Cikaluk, D. E., Tahbaz, N., Hendricks, L. C., DiMattia, G. E., Hansen, D., Pilgrim, D., and Hobman, T. C.: GERp95, a membrane-associated protein that belongs to a family of proteins involved in stem cell differentiation. *Molecular Biology of the Cell*, 10(10):3357–72, 1999.

[109] Sasaki, T., Shiohama, A., Minoshima, S., and Shimizu, N.: Identification of eight members of the Argonaute family in the human genome. *Genomics*, 82(3):323–30, 2003.

[110] González-González, E., López-Casas, P. P., and del Mazo, J.: The expression patterns of genes involved in the RNAi pathways are tissue-dependent and differ in the germ and somatic cells of mouse testis. *Biochimica et Biophysica Acta*, 1779(5):306–11, 2008.

[111] Valdmanis, P. N., Gu, S., Schuermann, N., Sethupathy, P., Grimm, D., and Kay, M. a.: Expression determinants of mammalian argonaute proteins in mediating gene silencing. *Nucleic Acids Research*, 1–10, 2011.

[112] Pfaff, J., Hennig, J., Herzog, F., Aebersold, R., Sattler, M., Niessing, D., and Meister, G.: Structural features of Argonaute-GW182 protein interactions. *PNAS*, 110(40):E3770–9, 2013.

[113] Hauptmann, J. and Meister, G.: Argonaute Regulation: Two Roads to the Same Destination. *Developmental Cell*, 25(6):553–554, 2013.

[114] Smibert, P., Yang, J.-S., Azzam, G., Liu, J.-L., and Lai, E. C.: Homeostatic control of Argonaute stability by microRNA availability. *Nature Structural & Molecular Biology*, 20(7):789–95, 2013.

[115] Martinez, N. J. and Gregory, R. I.: Argonaute2 expression is post-transcriptionally coupled to microRNA abundance. *RNA*, 19(5):605–12, 2013.

[116] Winter, J. and Diederichs, S.: Argonaute proteins regulate microRNA stability: Increased microRNA abundance by Argonaute proteins is due to microRNA stabilization. *RNA Biology*, 8(6):1149–57, 2011.

[117] Zamudio, J. R., Kelly, T. J., and Sharp, P. A.: Argonaute-bound small RNAs from promoter-proximal RNA polymerase II. *Cell*, 156(5):920–34, 2014.

[118] Grishok, A., Pasquinelli, A. E., Conte, D., Li, N., Parrish, S., Ha, I., Baillie, D. L., Fire, A., Ruvkun, G., and Mello, C. C.: Genes and mechanisms related to RNA interference regulate expression of the small temporal RNAs that control C. elegans developmental timing. *Cell*, 106(1):23–34, 2001.

[119] Vaucheret, H., Vazquez, F., Crété, P., and Bartel, D. P.: The action of ARGONAUTE1 in the miRNA pathway and its regulation by the miRNA pathway are crucial for plant development. *Genes & Development*, 18(10):1187–97, 2004.

[120] Diederichs, S. and Haber, D. a.: Dual role for argonautes in microRNA processing and posttranscriptional regulation of microRNA expression. *Cell*, 131(6):1097–108, 2007.

[121] Juvvuna, P. K., Khandelia, P., Lee, L. M., and Makeyev, E. V.: Argonaute identity defines the length of mature mammalian microRNAs. *Nucleic Acids Research*, 40(14):6808–20, 2012.

[122] Lund, E., Sheets, M. D., Imboden, S. B., and Dahlberg, J. E.: Limiting Ago protein restricts RNAi and microRNA biogenesis during early development in Xenopus laevis. *Genes & Development*, 25(11):1121–31, 2011.

[123] Khan, A. a., Betel, D., Miller, M. L., Sander, C., Leslie, C. S., and Marks, D. S.: Transfection of small RNAs globally perturbs gene regulation by endogenous microRNAs. *Nature Biotechnology*, 27(6):549–55, 2009.

[124] Janas, M. M., Wang, B., Harris, A. S., Aguiar, M., Shaffer, J. M., Subrahmanyam, Y. V. B. K., Behlke, M. a., Wucherpfennig, K. W., Gygi, S. P., Gagnon, E., and Novina, C. D.: Alternative RISC assembly: binding and repression of microRNA-mRNA duplexes by human Ago proteins. *RNA*, 18(11):2041–55, 2012.

[125] Stalder, L., Heusermann, W., Sokol, L., Trojer, D., Wirz, J., Hean, J., Fritzsche, A., Aeschimann, F., Pfanzagl, V., Basselet, P., Weiler, J., Hintersteiner, M., Morrissey, D. V., and Meisner-Kober, N. C.: The rough endoplasmatic reticulum is a central nucleation site of siRNA-mediated RNA silencing. *The EMBO Journal*, 32(8):1115–1127, 2013.

[126] Flores, O., Kennedy, E. M., Skalsky, R. L., and Cullen, B. R.: Differential RISC association of endogenous human microRNAs predicts their inhibitory potential. *Nucleic Acids Research*, 1–11, 2014.

[127] Bronevetsky, Y., Villarino, A. V., Eisley, C. J., Barbeau, R., Barczak, A. J., Heinz, G. a., Kremmer, E., Heissmeyer, V., McManus, M. T., Erle, D. J., Rao, A., and Ansel, K. M.: T cell activation induces proteasomal degradation of Argonaute and rapid remodeling of the microRNA repertoire. *The Journal of Experimental Medicine*, 210(2):417–32, 2013.

[128] Meister, G., Landthaler, M., Peters, L., Chen, P. Y., Urlaub, H., Lührmann, R., and Tuschl, T.: Identification of novel argonaute-associated proteins. *Current Biology*, 15(23):2149–55, 2005.

[129] Baillat, D. and Shiekhattar, R.: Functional dissection of the human TNRC6 (GW182-related) family of proteins. *Molecular and Cellular Biology*, 29(15):4144–55, 2009.

[130] Rehwinkel, J., Behm-Ansmant, I., Gatfield, D., and Izaurralde, E.: A crucial role for GW182 and the DCP1:DCP2 decapping complex in miRNA-mediated gene silencing. *RNA*, 11(11):1640–7, 2005.

[131] Liu, J., Rivas, F. V., Wohlschlegel, J., Yates, J. R., Parker, R., and Hannon, G. J.: A role for the P-body component GW182 in microRNA function. *Nature Cell Biology*, 7(12):1261–6, 2005.

[132] Jakymiw, A., Lian, S., Eystathioy, T., Li, S., Satoh, M., Hamel, J. C., Fritzler, M. J., and Chan, E. K. L.: Disruption of GW bodies impairs mammalian RNA interference. *Nature Cell Biology*, 7(12):1267–74, 2005.

[133] Ding, L., Spencer, A., Morita, K., and Han, M.: The developmental timing regulator AIN-1 interacts with miRISCs and may target the argonaute protein ALG-1 to cytoplasmic P bodies in C. elegans. *Molecular Cell*, 19(4):437–47, 2005.

[134] Behm-Ansmant, I., Rehwinkel, J., Doerks, T., Stark, A., Bork, P., and Izaurralde, E.: mRNA degradation by miRNAs and GW182 requires both CCR4:NOT deadenylase and DCP1:DCP2 decapping complexes. *Genes & Development*, 20(14):1885–98, 2006.

[135] Giraldez, A. J., Mishima, Y., Rihel, J., Grocock, R. J., Van Dongen, S., Inoue, K., Enright, A. J., and Schier, A. F.: Zebrafish MiR-430 promotes deadenylation and clearance of maternal mRNAs. *Science*, 312(5770):75–9, 2006.

[136] Wu, L., Fan, J., and Belasco, J. G.: MicroRNAs direct rapid deadenylation of mRNA. *PNAS*, 103(11):4034–9, 2006.

[137] Braun, J. E., Huntzinger, E., Fauser, M., and Izaurralde, E.: GW182 proteins directly recruit cytoplasmic deadenylase complexes to miRNA targets. *Molecular Cell*, 44(1):120–33, 2011.

[138] Chekulaeva, M., Mathys, H., Zipprich, J. T., Attig, J., Colic, M., Parker, R., and Filipowicz, W.: miRNA repression involves GW182-mediated recruitment of CCR4-NOT through conserved W-containing motifs. *Nature Structural & Molecular Biology*, 18(11):1218–1226, 2011.

[139] Fabian, M. R., Cieplak, M. K., Frank, F., Morita, M., Green, J., Srikumar, T., Nagar, B., Yamamoto, T., Raught, B., Duchaine, T. F., and Sonenberg, N.: miRNA-mediated deadenylation is orchestrated by GW182 through two conserved motifs that interact with CCR4-NOT. *Nature Structural & Molecular Biology*, 18(11):1211–7, 2011.

[140] Zekri, L., KuzuoÄŸlu-Öztürk, D., and Izaurralde, E.: GW182 proteins cause PABP dissociation from silenced miRNA targets in the absence of deadenylation. *The EMBO Journal*, 32(7):1052–1065, 2013.

[141] Humphreys, D. T., Westman, B. J., Martin, D. I. K., and Preiss, T.: MicroRNAs control translation initiation by inhibiting eukaryotic initiation factor 4E/cap and poly(A) tail function. *PNAS*, 102(47):16,961–6, 2005.

[142] Fabian, M. R., Mathonnet, G., Sundermeier, T., Mathys, H., Zipprich, J. T., Svitkin, Y. V., Rivas, F., Jinek, M., Wohlschlegel, J., Doudna, J. A., Chen, C.-Y. A., Shyu, A.-B., Yates, J. R., Hannon, G. J., Filipowicz, W., Duchaine, T. F., and Sonenberg, N.: Mammalian miRNA RISC recruits CAF1 and PABP to affect PABP-dependent deadenylation. *Molecular Cell*, 35(6):868–80, 2009.

[143] Zekri, L., Huntzinger, E., Heimstädt, S., and Izaurralde, E.: The silencing domain of GW182 interacts with PABPC1 to promote translational repression and degradation of microRNA targets and is required for target release. *Molecular and Cellular Biology*, 29(23):6220–31, 2009.

[144] Moretti, F., Kaiser, C., Zdanowicz-Specht, A., and Hentze, M. W.: PABP and the poly(A) tail augment microRNA repression by facilitated miRISC binding. *Nature Structural & Molecular Biology*, 19(6):603–8, 2012.

[145] Meijer, H. a., Kong, Y. W., Lu, W. T., Wilczynska, a., Spriggs, R. V., Robinson, S. W., Godfrey, J. D., Willis, a. E., and Bushell, M.: Translational Repression and eIF4A2 Activity Are Critical for MicroRNA-Mediated Gene Regulation. *Science*, 340(6128):82–85, 2013.

[146] Fukao, A., Mishima, Y., Takizawa, N., Oka, S., Imataka, H., Pelletier, J., Sonenberg, N., Thoma, C., and Fujiwara, T.: MicroRNAs Trigger Dissociation of eIF4AI and eIF4AII from Target mRNAs in Humans. *Molecular Cell*, 56(1):79–89, 2014.

[147] Fukaya, T., Iwakawa, H.-o., and Tomari, Y.: MicroRNAs Block Assembly of eIF4F Translation Initiation Complex in Drosophila. *Molecular Cell*, 56(1):67–78, 2014.

[148] Mathys, H., Basquin, J., Ozgur, S., Czarnocki-Cieciura, M., Bonneau, F., Aartse, A., Dziembowski, A., Nowotny, M., Conti, E., and Filipowicz, W.: Structural and biochemical insights to the role of the CCR4-NOT complex and DDX6 ATPase in microRNA repression. *Molecular Cell*, 54(5):751–65, 2014.

[149] Chen, Y., Boland, A., KuzuoÄŸlu-Öztürk, D., Bawankar, P., Loh, B., Chang, C.-T., Weichenrieder, O., and Izaurralde, E.: A DDX6-CNOT1 complex and W-binding pockets in CNOT9 reveal direct links between miRNA target recognition and silencing. *Molecular Cell*, 54(5):737–50, 2014.

[150] Béthune, J., Artus-Revel, C. G., and Filipowicz, W.: Kinetic analysis reveals successive steps leading to miRNA-mediated silencing in mammalian cells. *EMBO Reports*, 13(8):716–23, 2012.

[151] Djuranovic, S., Nahvi, A., and Green, R.: miRNA-mediated gene silencing by translational repression followed by mRNA deadenylation and decay. *Science*, 336(6078):237–40, 2012.

[152] Bazzini, A. a., Lee, M. T., and Giraldez, A. J.: Ribosome Profiling Shows That miR-430 Reduces Translation Before Causing mRNA Decay in Zebrafish. *Science*, 233, 2012.

[153] Eichhorn, S. W., Guo, H., McGeary, S. E., Rodriguez-Mias, R. a., Shin, C., Baek, D., Hsu, S.-H., Ghoshal, K., Villén, J., and Bartel, D. P.: mRNA Destabilization Is the Dominant Effect of Mammalian MicroRNAs by the Time Substantial Repression Ensues. *Molecular Cell*, 2014.

[154] Till, S., Lejeune, E., Thermann, R., Bortfeld, M., Hothorn, M., Enderle, D., Heinrich, C., Hentze, M. W., and Ladurner, A. G.: A conserved motif in Argonaute-interacting proteins mediates functional interactions through the Argonaute PIWI domain. *Nature Structural & Molecular Biology*, 14(10):897–903, 2007.

[155] El-Shami, M., Pontier, D., Lahmy, S., Braun, L., Picart, C., Vega, D., Hakimi, M.-A., Jacobsen, S. E., Cooke, R., and Lagrange, T.: Reiterated WG/GW motifs form functionally and evolutionarily conserved ARGONAUTE-binding platforms in RNAi-related components. *Genes & Development*, 21(20):2539–44, 2007.

[156] Takimoto, K., Wakiyama, M., and Yokoyama, S.: Mammalian GW182 contains multiple Argonaute-binding sites and functions in microRNA-mediated translational repression. *RNA*, 15(6):1078–89, 2009.

[157] Lian, S. L., Li, S., Abadal, G. X., Pauley, B. a., Fritzler, M. J., and Chan, E. K. L.: The C-terminal half of human Ago2 binds to multiple GW-rich regions of GW182 and requires GW182 to mediate silencing. *RNA*, 15(5):804–13, 2009.

[158] Christie, M., Boland, A., Huntzinger, E., Weichenrieder, O., and Izaurralde, E.: Structure of the PAN3 pseudokinase reveals the basis for interactions with the PAN2 deadenylase and the GW182 proteins. *Molecular Cell*, 51(3):360–73, 2013.

[159] Tang, X., Zhang, Y., Tucker, L., and Ramratnam, B.: Phosphorylation of the RNase III enzyme Drosha at Serine300 or Serine302 is required for its nuclear localization. *Nucleic Acids Research*, 38(19):6610–9, 2010.

[160] Tang, X., Li, M., Tucker, L., and Ramratnam, B.: Glycogen synthase kinase 3 beta (GSK3β) phosphorylates the RNAase III enzyme Drosha at S300 and S302. *PloS ONE*, 6(6):e20,391, 2011.

[161] Tang, X., Wen, S., Zheng, D., Tucker, L., Cao, L., Pantazatos, D., Moss, S. F., and Ramratnam, B.: Acetylation of drosha on the N-terminus inhibits its degradation by ubiquitination. *PloS ONE*, 8(8):e72,503, 2013.

[162] Paroo, Z., Ye, X., Chen, S., and Liu, Q.: Phosphorylation of the human microRNA-generating complex mediates MAPK/Erk signaling. *Cell*, 139(1):112–22, 2009.

[163] Heo, I. and Kim, V. N.: Regulating the regulators: posttranslational modifications of RNA silencing factors. *Cell*, 139(1):28–31, 2009.

[164] Kirino, Y., Kim, N., de Planell-Saguer, M., Khandros, E., Chiorean, S., Klein, P. S., Rigoutsos, I., Jongens, T. a., and Mourelatos, Z.: Arginine methylation of Piwi proteins catalysed by dPRMT5 is required for Ago3 and Aub stability. *Nature Cell Biology*, 11(5):652–8, 2009.

[165] Reuter, M., Chuma, S., Tanaka, T., Franz, T., Stark, A., and Pillai, R. S.: Loss of the Mili-interacting Tudor domain-containing protein-1 activates transposons and alters the Mili-associated small RNA profile. *Nature Structural & Molecular Biology*, 16(6):639–46, 2009.

[166] Vagin, V. V., Wohlschlegel, J., Qu, J., Jonsson, Z., Huang, X., Chuma, S., Girard, A., Sachidanandam, R., Hannon, G. J., and Aravin, A. a.: Proteomic analysis of murine Piwi proteins reveals a role for arginine methylation in specifying interaction with Tudor family members. *Genes & Development*, 23(15):1749–62, 2009.

[167] Rybak, A., Fuchs, H., Hadian, K., Smirnova, L., Wulczyn, E. a., Michel, G., Nitsch, R., Krappmann, D., and Wulczyn, F. G.: The let-7 target gene mouse lin-41 is a stem cell specific E3 ubiquitin ligase for the miRNA pathway protein Ago2. *Nature Cell Biology*, 11(12):1411–20, 2009.

[168] Sahin, U., Lapaquette, P., Andrieux, A., Faure, G., and Dejean, A.: Sumoylation of human argonaute 2 at lysine-402 regulates its stability. *PloS ONE*, 9(7):e102,957, 2014.

[169] Qi, H. H., Ongusaha, P. P., Myllyharju, J., Cheng, D., Pakkanen, O., Shi, Y., Lee, S. W., Peng, J., and Shi, Y.: Prolyl 4-hydroxylation regulates Argonaute 2 stability. *Nature*, 455(7211):421–4, 2008.

[170] Wu, C., So, J., Davis-Dusenbery, B. N., Qi, H. H., Bloch, D. B., Shi, Y., Lagna, G., and Hata, A.: Hypoxia potentiates microRNA-mediated gene silencing through posttranslational modification of Argonaute2. *Molecular and Cellular Biology*, 31(23):4760–74, 2011.

[171] Chen, J., Lai, F., and Niswander, L.: The ubiquitin ligase mLin41 temporally promotes neural progenitor cell maintenance through FGF signaling. *Genes & Development*, 26(8):803–15, 2012.

[172] Loedige, I., Gaidatzis, D., Sack, R., Meister, G., and Filipowicz, W.: The mammalian TRIM-NHL protein TRIM71/LIN-41 is a repressor of mRNA function. *Nucleic Acids Research*, 41(1):518–532, 2012.

[173] Chang, H.-M., Martinez, N. J., Thornton, J. E., Hagan, J. P., Nguyen, K. D., and Gregory, R. I.: Trim71 cooperates with microRNAs to repress Cdkn1a expression and promote embryonic stem cell proliferation. *Nature Communications*, 3(617):923, 2012.

[174] Johnston, M., Geoffroy, M.-C., Sobala, A., Hay, R., and Hutvagner, G.: HSP90 protein stabilizes unloaded argonaute complexes and microscopic P-bodies in human cells. *Molecular Biology of the Cell*, 21(9):1462–9, 2010.

[175] Gibbings, D., Leblanc, P., Jay, F., Pontier, D., Michel, F., Schwab, Y., Alais, S., Lagrange, T., and Voinnet, O.: Human prion protein binds Argonaute and promotes accumulation of microRNA effector complexes. *Nature Structural & Molecular Biology*, 19(5):517–24, S1, 2012.

[176] Jee, D. and Lai, E. C.: Alteration of miRNA activity via context-specific modifications of Argonaute proteins. *Trends in Cell Biology*, 24(9):546–553, 2014.

[177] Zeng, Y., Sankala, H., Zhang, X., and Graves, P. R.: Phosphorylation of Argonaute 2 at serine-387 facilitates its localization to processing bodies. *The Biochemical Journal*, 413(3):429–36, 2008.

[178] Horman, S., Janas, M., Litterst, C., Wang, B., MacRae, I., Sever, M., Morrissey, D., Graves, P., Luo, B., Umesalma, S., Qi, H., Miraglia, L., Novina, C., and Orth, A.: Akt-Mediated Phosphorylation of Argonaute 2 Downregulates Cleavage and Upregulates Translational Repression of MicroRNA Targets. *Molecular Cell*, 1–12, 2013.

[179] Rüdel, S., Wang, Y., Lenobel, R., Körner, R., Hsiao, H.-H., Urlaub, H., Patel, D., and Meister, G.: Phosphorylation of human Argonaute proteins affects small RNA binding. *Nucleic Acids Research*, 39(6):2330–2343, 2010.

[180] Mazumder, A., Bose, M., Chakraborty, A., Chakrabarti, S., and Bhattacharyya, S. N.: A transient reversal of miRNA-mediated repression controls macrophage activation. *EMBO Reports*, 14(11):1008–16, 2013.

[181] Shen, J., Xia, W., Khotskaya, Y. B., Huo, L., Nakanishi, K., Lim, S.-O., Du, Y., Wang, Y., Chang, W.-C., Chen, C.-H., Hsu, J. L., Wu, Y., Lam, Y. C., James, B. P., Liu, X., Liu, C.-G., Patel, D. J., and Hung, M.-C.: EGFR modulates microRNA maturation in response to hypoxia through phosphorylation of AGO2. *Nature*, 1–5, 2013.

[182] Tahbaz, N., Kolb, F. a., Zhang, H., Jaronczyk, K., Filipowicz, W., and Hobman, T. C.: Characterization of the interactions between mammalian PAZ PIWI domain proteins and Dicer. *EMBO Reports*, 5(2):189–94, 2004.

[183] Yang, M., Haase, A. D., Huang, F.-K., Coulis, G., Rivera, K. D., Dickinson, B. C., Chang, C. J., Pappin, D. J., Neubert, T. a., Hannon, G. J., Boivin, B., and Tonks, N. K.: Dephosphorylation of Tyrosine 393 in Argonaute 2 by Protein Tyrosine Phosphatase 1B Regulates Gene Silencing in Oncogenic RAS-Induced Senescence. *Molecular Cell*, 782–790, 2014.

[184] Mori, M., Triboulet, R., Mohseni, M., Schlegelmilch, K., Shrestha, K., Camargo, F. D., and Gregory, R. I.: Hippo signaling regulates microprocessor and links cell-density-dependent miRNA biogenesis to cancer. *Cell*, 156(5):893–906, 2014.

[185] Kabsch, W. and Sander, C.: Dictionary of protein secondary structure: pattern recognition of hydrogen-bonded and geometrical features. *Biopolymers*, 22(12):2577–637, 1983.

[186] Schürmann, N., Trabuco, L. G., Bender, C., Russell, R. B., and Grimm, D.: Molecular dissection of human Argonaute proteins by DNA shuffling. *Nature Structural & Molecular Biology*, 20(7):818–26, 2013.

[187] Rüdel, S., Flatley, A., Weinmann, L., Kremmer, E., and Meister, G.: A multifunctional human Argonaute2-specific monoclonal antibody. *RNA*, 14(6):1244–53, 2008.

[188] Hur, J. K., Zinchenko, M. K., Djuranovic, S., and Green, R.: Regulation of Argonaute slicer activity by guide RNA 3' end interactions with the N-terminal lobe. *The Journal of Biological Chemistry*, 182:1–20, 2013.

[189] Eulalio, A., Tritschler, F., and Izaurralde, E.: The GW182 protein family in animal cells: new insights into domains required for miRNA-mediated gene silencing. *RNA*, 15(8):1433–42, 2009.

[190] Lazzaretti, D., Tournier, I., and Izaurralde, E.: The C-terminal domains of human TNRC6A, TNRC6B, and TNRC6C silence bound transcripts independently of Argonaute proteins. *RNA*, 15(6):1059–66, 2009.

[191] Zellner, H., Staudigel, M., Trenner, T., Bittkowski, M., Wolowski, V., Icking, C., and Merkl, R.: PresCont: predicting protein-protein interfaces utilizing four residue properties. *Proteins*, 80(1):154–68, 2012.

[192] Miyoshi, K., Okada, T. N., Siomi, H., and Siomi, M. C.: Characterization of the miRNA-RISC loading complex and miRNA-RISC formed in the Drosophila miRNA pathway. *RNA (New York, NY)*, 15(7):1282–91, 2009.

[193] Iwasaki, S., Kawamata, T., and Tomari, Y.: Drosophila argonaute1 and argonaute2 employ distinct mechanisms for translational repression. *Molecular Cell*, 34(1):58–67, 2009.

[194] Partridge, J. F., DeBeauchamp, J. L., Kosinski, A. M., Ulrich, D. L., Hadler, M. J., and Noffsinger, V. J. P.: Functional separation of the requirements for establishment and maintenance of centromeric heterochromatin. *Molecular Cell*, 26(4):593–602, 2007.

[195] Morel, J.-B., Godon, C., Mourrain, P., Béclin, C., Boutet, S., Feuerbach, F., Proux, F., and Vaucheret, H.: Fertile hypomorphic ARGONAUTE (ago1) mutants impaired in post-transcriptional gene silencing and virus resistance. *The Plant Cell*, 14(3):629–39, 2002.

[196] Zilberman, D., Cao, X., and Jacobsen, S. E.: ARGONAUTE4 control of locus-specific siRNA accumulation and DNA and histone methylation. *Science*, 299(5607):716–9, 2003.

[197] Zheng, X., Zhu, J., Kapoor, A., and Zhu, J.-K.: Role of Arabidopsis AGO6 in siRNA accumulation, DNA methylation and transcriptional gene silencing. *The EMBO Journal*, 26(6):1691–701, 2007.

[198] Havecker, E. R., Wallbridge, L. M., Hardcastle, T. J., Bush, M. S., Kelly, K. a., Dunn, R. M., Schwach, F., Doonan, J. H., and Baulcombe, D. C.: The Arabidopsis RNA-directed DNA methylation argonautes functionally diverge based on their expression and interaction with target loci. *The Plant Cell*, 22(2):321–34, 2010.

[199] Matzke, M., Kanno, T., Daxinger, L., Huettel, B., and Matzke, A. J. M.: RNA-mediated chromatin-based silencing in plants. *Current Opinion in Cell Biology*, 21(3):367–76, 2009.

[200] Herr, a. J., Jensen, M. B., Dalmay, T., and Baulcombe, D. C.: RNA polymerase IV directs silencing of endogenous DNA. *Science*, 308(5718):118–20, 2005.

[201] Onodera, Y., Haag, J. R., Ream, T., Costa Nunes, P., Pontes, O., and Pikaard, C. S.: Plant nuclear RNA polymerase IV mediates siRNA and DNA methylation-dependent heterochromatin formation. *Cell*, 120(5):613–22, 2005.

[202] Rogers, K. and Chen, X.: Biogenesis, turnover, and mode of action of plant microRNAs. *The Plant Cell*, 25(7):2383–99, 2013.

[203] Poulsen, C., Vaucheret, H., and Brodersen, P.: Lessons on RNA silencing mechanisms in plants from eukaryotic argonaute structures. *The Plant Cell*, 25(1):22–37, 2013.

[204] Bies-Etheve, N., Pontier, D., Lahmy, S., Picart, C., Vega, D., Cooke, R., and Lagrange, T.: RNA-directed DNA methylation requires an AGO4-interacting member of the SPT5 elongation factor family. *EMBO Reports*, 10(6):649–54, 2009.

[205] He, X.-J., Hsu, Y.-F., Zhu, S., Wierzbicki, A. T., Pontes, O., Pikaard, C. S., Liu, H.-L., Wang, C.-S., Jin, H., and Zhu, J.-K.: An effector of RNA-directed DNA methylation in arabidopsis is an ARGONAUTE 4- and RNA-binding protein. *Cell*, 137(3):498–508, 2009.

[206] Karlowski, W. M., Zielezinski, A., Carrère, J., Pontier, D., Lagrange, T., and Cooke, R.: Genome-wide computational identification of WG/GW Argonaute-binding proteins in Arabidopsis. *Nucleic Acids Research*, 38(13):4231–45, 2010.

[207] Garcia, D., Garcia, S., Pontier, D., Marchais, A., Renou, J. P., Lagrange, T., and Voinnet, O.: Ago hook and RNA helicase motifs underpin dual roles for SDE3 in antiviral defense and silencing of nonconserved intergenic regions. *Molecular Cell*, 48(1):109–20, 2012.

[208] Pontier, D., Picart, C., Roudier, F., Garcia, D., Lahmy, S., Azevedo, J., Alart, E., Laudié, M., Karlowski, W. M., Cooke, R., Colot, V., Voinnet, O., and Lagrange, T.: NERD, a plant-specific GW protein, defines an additional RNAi-dependent chromatin-based pathway in Arabidopsis. *Molecular Cell*, 48(1):121–32, 2012.

[209] Azevedo, J., Garcia, D., Pontier, D., Ohnesorge, S., Yu, A., Garcia, S., Braun, L., Bergdoll, M., Hakimi, M. A., Lagrange, T., and Voinnet, O.: Argonaute quenching and global changes in Dicer homeostasis caused by a pathogen-encoded GW repeat protein. *Genes & Development*, 24(9):904–15, 2010.

[210] Giner, A., Lakatos, L., García-Chapa, M., López-Moya, J. J., and Burgyán, J.: Viral protein inhibits RISC activity by argonaute binding through conserved WG/GW motifs. *PLoS Pathogens*, 6(7):e1000,996, 2010.

[211] Frohn, A., Eberl, H. C., Stöhr, J., Glasmacher, E., Rüdel, S., Heissmeyer, V., Mann, M., and Meister, G.: Dicer-dependent and -independent Argonaute2 protein interaction networks in mammalian cells. *Molecular & Cellular Proteomics*, 11(11):1442–56, 2012.

[212] Eulalio, A., Tritschler, F., Büttner, R., Weichenrieder, O., Izaurralde, E., and Truffault, V.: The RRM domain in GW182 proteins contributes to miRNA-mediated gene silencing. *Nucleic Acids Research*, 37(9):2974–83, 2009.

[213] Palmeri, A., Ausiello, G., Ferre, F., Helmer-Citterich, M., and Gherardini, P. F.: A proteome-wide Domain-centric Perspective on Protein Phosphorylation. *Molecular & Cellular Proteomics*, 2198–2212, 2014.

[214] Schweiger, R. and Linial, M.: Cooperativity within proximal phosphorylation sites is revealed from large-scale proteomics data. *Biology Direct*, 5:6, 2010.

[215] Serber, Z. and Ferrell, J. E.: Tuning bulk electrostatics to regulate protein function. *Cell*, 128(3):441–4, 2007.

[216] Phatnani, H. P. and Greenleaf, A. L.: Phosphorylation and functions of the RNA polymerase II CTD. *Genes & Development*, 20(21):2922–36, 2006.

[217] Nash, P., Tang, X., Orlicky, S., Chen, Q., Gertler, F. B., Mendenhall, M. D., Sicheri, F., Pawson, T., and Tyers, M.: Multisite phosphorylation of a CDK inhibitor sets a threshold for the onset of DNA replication. *Nature*, 414(6863):514–21, 2001.

[218] Deshaies, R. J. and Ferrell, J. E.: Multisite phosphorylation and the countdown to S phase. *Cell*, 107(7):819–22, 2001.

[219] Strickfaden, S. C., Winters, M. J., Ben-Ari, G., Lamson, R. E., Tyers, M., and Pryciak, P. M.: A mechanism for cell-cycle regulation of MAP kinase signaling in a yeast differentiation pathway. *Cell*, 128(3):519–31, 2007.

[220] Pufall, M. a., Lee, G. M., Nelson, M. L., Kang, H.-S., Velyvis, A., Kay, L. E., McIntosh, L. P., and Graves, B. J.: Variable control of Ets-1 DNA binding by multiple phosphates in an unstructured region. *Science*, 309(5731):142–5, 2005.

[221] Cohen, P. and Frame, S.: The renaissance of GSK3. *Nature Reviews Molecular Cell Biology*, 2(10):769–76, 2001.

[222] Flotow, H., Graves, P. R., Wang, A. Q., Fiol, C. J., Roeske, R. W., and Roach, P. J.: Phosphate groups as substrate determinants for casein kinase I action. *The Journal of Biological Chemistry*, 265(24):14,264–9, 1990.

[223] Hergovich, A., Lisztwan, J., Thoma, C. R., Wirbelauer, C., Barry, R. E., and Krek, W.: Priming-dependent phosphorylation and regulation of the tumor suppressor pVHL by glycogen synthase kinase 3. *Molecular and Cellular Biology*, 26(15):5784–96, 2006.

[224] Steen, H., Jebanathirajah, J. a., Rush, J., Morrice, N., and Kirschner, M. W.: Phosphorylation analysis by mass spectrometry: myths, facts, and the consequences for qualitative and quantitative measurements. *Molecular & Cellular Proteomics*, 5(1):172–81, 2006.

[225] Boersema, P. J., Mohammed, S., and Heck, A. J. R.: Phosphopeptide fragmentation and analysis by mass spectrometry. *Journal of Mass Spectrometry*, 44(6):861–78, 2009.

[226] Palumbo, A. M. and Reid, G. E.: Evaluation of Gas-Phase Rearrangement and Competing Fragmentation Reactions on Protein Phosphorylation Site Assignment Using Collision Induced Dissociation-MS/MS and MS(3). *Analytical Chemistry*, 80(24):9735–47, 2008.

[227] Berghammer, H. and Auer, B.: "Easypreps": fast and easy plasmid minipreparation for analysis of recombinant clones in E. coli. *Biotechniques*, 14(4):524, 528, 1993.

[228] Dürr, J., Lolas, I. B., Sø rensen, B. B., Schubert, V., Houben, A., Melzer, M., Deutzmann, R., Grasser, M., and Grasser, K. D.: The transcript elongation factor SPT4/SPT5 is involved in auxin-related gene expression in Arabidopsis. *Nucleic Acids Research*, 42(7):4332–47, 2014.

[229] Gebauer, F. and Hentze, M. W.: Studying translational control in Drosophila cell-free systems. *Methods in Enzymology*, 429:23–33, 2007.

[230] Pfaffl, M. W., Horgan, G. W., and Dempfle, L.: Relative expression software tool (REST) for group-wise comparison and statistical analysis of relative expression results in real-time PCR. *Nucleic Acids Research*, 30(9):e36, 2002.

[231] Pall, G. S. and Hamilton, A. J.: Improved northern blot method for enhanced detection of small RNA. *Nature Protocols*, 3(6):1077–84, 2008.

[232] Katoh, K., Misawa, K., Kuma, K.-i., and Miyata, T.: MAFFT: a novel method for rapid multiple sequence alignment based on fast Fourier transform. *Nucleic Acids Research*, 30(14):3059–66, 2002.

[233] Roy, A., Kucukural, A., and Zhang, Y.: I-TASSER: a unified platform for automated protein structure and function prediction. *Nature Protocols*, 5(4):725–38, 2010.

[234] Krieger, E., Joo, K., Lee, J., Lee, J., Raman, S., Thompson, J., Tyka, M., Baker, D., and Karplus, K.: Improving physical realism, stereochemistry, and side-chain accuracy in homology modeling: Four approaches that performed well in CASP8. *Proteins*, 77 Suppl 9(June):114–22, 2009.

[235] Qiu, J. and Elber, R.: SSALN: an alignment algorithm using structure-dependent substitution matrices and gap penalties learned from structurally aligned protein pairs. *Proteins*, 62(4):881–91, 2006.

[236] Jones, D. T.: Protein secondary structure prediction based on position-specific scoring matrices. *Journal of Molecular Biology*, 292(2):195–202, 1999.

Acknowledgements

I am grateful to all people who supported me during my time as a PhD student. First and foremost, I want to thank Gunter for supervising me on this exciting topic, for pushing my projects forward with great ideas, for challenging me, and for trusting in me. His way of working has shaped my own perception of science, life and deadlines a lot and I always enjoyed his positive and motivating attitude. Thanks, Gunter, for the opportunity to work with you!

I also want to thank Rainer who accompanied me as a mentor during all phases of my PhD thesis, provided great bioinformatic support during our collaborations and always had an open door for me.

I am grateful to Prof. Dr. Rainer Deutzmann, Eduard Hochmuth and Dr. Astrid Bruckmann who performed all mass-spectrometric measurements and contributed essentially to the establishment of Ago-APP and detection of phosphosites. Thanks Astrid, for the good collaboration and for being so patient with me!

I am especially thankful to Simone who introduced me to her projects and handed them over neatly organized and with a lot of preparatory work already done. I also owe lots of thanks to Janina who laid the foundation for Ago-APP during her PhD thesis and readily shared information and reagents. Many thanks to Leo for great help with protein purifications, thanks to Daniele and Anne for fruitful discussions, to Johannes for good collaboration on the phosphorylation project, and thanks to my great bachelor and master students Lukas and Daniela! Furthermore, Sigi, Corinna, Norbert and Gerhard eased my own workload a lot and I really appreciate their help. Many thanks go to all members of lab 2 for their warm reception, the great working atmosphere, and for not freezing everything at $-80\,^{\circ}\mathrm{C}$!

Finally, I wish to thank the people outside the lab, my friends and my fellow musicians, for taking my mind off the experiments and helping me find my balance. Many thanks to Birte without whom this thesis would not look like it looks. Zu guter Letzt ein besonderes Dankeschön meinen Eltern für ihre bedingungslose Unterstützung.